UNIVERSITY OF CALIFORNIA, SAN DIEGO

The role of Tmem2 in cardiac and skeletal muscle morphogenesis

A dissertation submitted in partial satisfaction of the
requirements for the degree Doctor of Philosophy

in

Biology

by

Lydia Esmeralda Hernandez

Committee in charge:

Professor Deborah Yelon, Chair
Professor Steven Briggs
Professor Andrew Chisholm
Professor Robert Ross
Professor David Traver

2017

The Dissertation of Lydia Esmeralda Hernandez is approved, and it is acceptable in quality and form for publication on microfilm and electronically:

_____

_____

_____

_____

_____

Chair

University of California, San Diego
2017

DEDICATION

To my Grandmother,
Thank you for teaching me strength and persistence.

To my Mother and my Aunt,
Thank you for your unconditional love and support.

TABLE OF CONTENTS

LIST OF FIGURES

LIST OF TABLES

ACKNOWLEDGEMENTS

I would like to thank Debbie for the opportunity to train in her lab and for her tireless assistance and guidance as my graduate advisor. Debbie embodies excellence in both science and mentoring. Debbie, thank you for being one of my most influential teachers.

I would like to thank my committee members for their feedback and contributions to my academic development.

Thank you to my friends and colleagues in the Yelon Lab.

Chapter 2, in full, is a reprint of the material as it appears in: Lucile Ryckebusch, Lydia Hernandez, Carole Wang, Jenny Phan, Deborah Yelon. (2016). Tmem2 regulates cell-matrix interactions that are essential for muscle fiber attachment. *Development* 143(16): p.2965-2972. Lydia Hernandez is a primary researcher/author on this paper. Lydia Hernandez contributed to designing the experiments, conducting research, interpreting results, and writing the manuscript presented in Chapter 2. Lucile Rycebusch contributed to designing the experiments, conducting research, interpreting results, and writing the manuscript presented in Chapter 2. Deborah Yelon contributed to designing the experiments, interpreting results, and writing the manuscript presented in Chapter 2. Carole Wang and Jenny Phan performed experiments and analyzed data presented in Chapter 2.

A modified version of Chapter 3 will be submitted for publication (Hernandez, Lydia; Ryckebüsch, Lucile; Wang, Carole; Ling, Rachel; Yelon,

Deborah. “Tmem2 restricts atrioventricular canal differentiation by regulating degradation of hyaluronic acid”). Lydia Hernandez is the primary researcher/author on this paper. Lydia Hernandez will be the first author of this manuscript and she contributed to designing the experiments, conducting research, interpreting results, and writing the manuscript presented in Chapter 3. Lucile Ryckebüsch contributed to designing the experiments, conducting research, interpreting results, and writing the manuscript presented in Chapter 3. Deborah Yelon contributed to designing the experiments, interpreting results, and writing the manuscript presented in Chapter 3. Carole Wang and Rachel Ling designed and created plasmid constructs used in Chapter 3.

Preliminary experiments described in Chapter 4 were designed and performed primarily by Lydia Hernandez. Lucile Ryckebüsch performed genetic reduction of Fn in *MZtmem2* mutants. Parthiv Sheth assisted with cell culture and western blots. Arjana Pradhan and Prae Pongtornpipat examined pharmacological inhibition of EGFR in zebrafish embryos. Mass spectrometry analysis of Tmem2 pulldowns was performed in collaboration with Zhouxin Shen of the Briggs laboratory.

VITA

1997 – 2000 Bachelor of Arts, University of California, Berkeley

2007 – 2010 Bachelor of Science, Portland State University, Portland

2010 – 2017 Doctor of Philosophy, University of California, San Diego

ABSTRACT OF THE DISSERTATION

The role of Tmem2 in cardiac and skeletal muscle morphogenesis

by

Lydia Esmeralda Hernandez

Doctor of Philosophy in Biology

University of California, San Diego, 2017

Professor Deborah Yelon, Chair

Cardiac morphogenesis and skeletal muscle morphogenesis are critical developmental processes that require ongoing coordination and signaling between cells and the matrix of their surrounding environment. The extracellular matrix (ECM) itself is a complex and dynamic structure whose regulation is of the utmost importance to cell behavior. While it is well characterized that the ECM is essential for organogenesis, it is less known how ECM composition informs development. Here, we show that the transmembrane protein Tmem2 is an essential regulator of ECM organization during cardiac and skeletal muscle morphogenesis. In zebrafish, maternal and zygotic depletion of *tmem2* renders embryos unable to form primitive heart tubes, whereas in muscle tissue this same loss results in destabilization of muscle fibers. In contrast, zygotic loss of *tmem2* results in ectopic atrioventricular canal (AVC) differentiation. All three of these striking phenotypes are accompanied by disorganized and defective ECM deposition, reflecting an important role for Tmem2 in regulation of the extracellular environments that impact development. The molecular mechanism of Tmem2 function, however, is unclear. Our results identify the structural requirements for Tmem2 activity across multiple developmental roles. Further, our studies characterize disorganization of the ECM in *tmem2* mutants. Finally, our findings support the model that Tmem2 directly influences ECM structure and composition in a context-dependent manner, while maintaining the possibility that Tmem2 can have additional mechanisms of activity.

Chapter 1: Mechanisms of cardiac and skeletal muscle morphogenesis

Overview: The role of Tmem2 in cardiac and skeletal muscle morphogenesis

In this chapter, I will summarize the morphogenetic processes that form the heart and skeletal muscle. I will also discuss what is known about how the extracellular matrix (ECM) influences each tissue during its development. Finally, I will examine the role of Tmem2 in each context. I have chosen to present these processes in the order in which they occur during development. First, I will discuss formation of the primitive heart tube. Next, I will review muscle fiber formation and attachment. After that, I will discuss the formation of the atrioventricular canal (AVC) within the heart. Last, I will discuss what is known about Tmem2 function, as well as a more detailed analysis of Tmem2 structure.

The primitive heart tube forms through cardiac fusion

In all vertebrates, cardiac morphogenesis occurs through the dynamic, collaborative motion of a community of cells (Brade et al., 2013; Brand, 2003; Fishman and Chien, 1997; Glickman and Yelon, 2002; Harvey, 2002; Miquerol and Kelly, 2013; Moorman and Christoffels, 2003; Moreno-Rodriguez et al., 2006; Schleich et al., 2013). First, bilateral populations of cardiomyocytes migrate toward the embryonic midline (Fig. 1.1A) (Bakkers et al., 2009; Dunwoodie, 2007; Glickman and Yelon, 2002; Harvey, 2002; Moorman and Christoffels, 2003). There, the two groups of cardiomyocytes meet and merge

through a process called cardiac fusion and assemble a myocardial cylinder (Fig. 1.1B,C) (Bussmann et al., 2007; Evans et al., 2010; Holtzman et al., 2007; Moreno-Rodriguez et al., 2006). The primitive heart tube is remodeled into two morphologically distinct chambers at later stages (Fig. 1.1D). While the stages of cardiac morphogenesis have been well described, the precise mechanisms driving these events remain poorly understood. Thus, the process of cardiac fusion provides a tractable opportunity to investigate the genetic pathways regulating cardiac cell behavior.

Mutations that disrupt cardiac fusion have revealed that the environment surrounding the cardiomyocytes has a significant influence on these processes. In particular, interaction between the myocardium and the adjacent endoderm influences cell movement. Mutations in both mouse and zebrafish that impact endoderm specification or integrity likewise inhibit cardiac fusion (Alexander et al., 1999; Holtzman et al., 2007; Kawahara et al., 2009; Kikuchi et al., 2001; Kupperman et al., 2000; Li et al., 2004; Mendelson et al., 2015; Molkentin et al., 1997; Osborne et al., 2008; Ragkousi et al., 2011; Ye and Lin, 2013; Yelon et al., 1999). Although studies in chick suggest that endodermal contraction physically pulls myocardial cells medially (Aleksandrova et al., 2015; Cui et al., 2009; Varner and Taber, 2012), the force exerted by endodermal tissue seems insufficient for the entirety of myocardial displacement during cardiac fusion (Aleksandrova et al., 2015; Cui et al., 2009; Varner and Taber, 2012; Xie et al., 2016; Ye et al., 2015). Recent

work from our lab has revealed the importance of PDGF signaling between the endoderm and myocardium in directing cardiomyocyte migration toward the embryonic midline (Bloomekatz et al., 2017). In zebrafish, mutation of *pdgfra*, a gene encoding the PDGF receptor, results in misdirection of cardiomyocyte trajectories during cardiac fusion. Importantly, it was also shown that *pdgfaa*, a PDGF ligand, is expressed in the endoderm and that ectopic expression of *pdgfaa* interfered with cardiac fusion. Thus, these results suggest an instructive role for PDGF signaling between the endoderm and the myocardium that promotes cardiac fusion.

While it is clear that the endoderm plays a critical role in cardiac cell movement, there are additional factors influencing the cell behaviors that initiate heart tube formation. Studies of zebrafish mutations that disrupt cardiac fusion have revealed the extracellular matrix (ECM) as another key regulator of cardiomyocyte movement (Arrington and Yost, 2009; Garavito-Aguilar et al., 2010; George et al., 1997; Linask and Lash, 1988; Trinh and Stainier, 2004; Trinh et al., 2005). Either excessive or depleted ECM deposition impacts myocardial movement toward the midline. For instance, excessive fibronectin (Fn) in zebrafish *hand2* (*han*) mutants and deficient Fn deposition in zebrafish *fn1/natter* (*nat*) mutants have both been shown to impede cardiac fusion (Fig. 1.2) (Garavito-Aguilar et al., 2010; Trinh and Stainier, 2004; Trinh et al., 2005). Further, the fusion defect in *han* mutants can be rescued through *nat* loss-of-function, suggesting that a precise

composition of ECM is necessary for optimal cardiomyocyte motility (Fig. 1.2F) (Garavito-Aguilar et al., 2010). Although correct ECM deposition is thought to be integral for cardiac fusion, the factors that insure appropriate ECM organization in this context remain unknown.

Tmem2 promotes cardiac fusion

Our studies of Tmem2 originated with an intriguing mutation that emerged from our laboratory's ongoing forward genetic screens (Auman et al., 2007). This zygotic recessive lethal mutation was first identified because of its effects on ventricular morphology and atrioventricular canal formation (Totong et al., 2011). Interestingly, generation of maternal-zygotic *tmem2* (*MZtmem2*) mutants, in which both maternal and zygotic supplies of *tmem2* are depleted, revealed an additional, earlier function of *tmem2* during cardiac fusion (Totong et al., 2011). In contrast to maternal *tmem2* (*Mtmem2*) mutants, which are indistinguishable from wild-type embryos, the cardiomyocytes in *MZtmem2* mutants do not migrate normally and instead remain bilateral to the midline (Fig. 1.3A,B), ultimately forming separate hearts in lateral positions, a condition known as cardia bifida (Fig. 1.3E, F). In addition, endocardial cells that build the vascular lining of the heart tube fail to fuse in *MZtmem2* mutants (Fig. 1.3C,D) (Totong et al., 2011). Thus, Tmem2 plays a crucial role in promoting both myocardial and endocardial fusion.

Does Tmem2 function within cardiomyocytes, the environment through which these cells travel, or both? Transgenic tissue-specific rescue experiments in *MZtmem2* mutant embryos yielded some insight into this question. Transgenic overexpression of *tmem2* in the myocardium is sufficient to induce cardiomyocyte movement in *MZtmem2* mutants (Fig. 1.4A-D) (Totong et al., 2011). Although morphogenesis is somewhat delayed in rescued embryos, cardiomyocytes complete cardiac fusion and initiate heart tube extension by 26 hours post fertilization (hpf). Interestingly, *tmem2* overexpression also impacts the endocardium. Similar to its rescue of myocardial fusion, myocardial expression of *tmem2* is sufficient to rescue endocardial fusion and tube formation in *MZtmem2* mutants (Fig. 1.4E-F) (Totong et al., 2011). These data suggest that Tmem2 influences the extracellular environment through which both myocardial and endocardial cells move as they undergo cardiac fusion. In Chapter 2, we interrogate this model of Tmem2 function by examining deposition of ECM components surrounding *MZtmem2* mutant cardiomyocytyes. In Chapter 3, we evaluate which regions of the Tmem2 protein are critical for promotion of cardiomyocyte movement.

Skeletal muscle morphogenesis requires cell-matrix interactions

Skeletal muscle morphogenesis involves multiple developmental processes that all require adhesion to the ECM (Goody et al., 2015). In vertebrates, muscle precursors originate within somites, the repeating

segments of paraxial mesoderm that flank the embryonic notochord and comprise the embryonic myotome (Bryson-Richardson and Currie, 2008; Buckingham and Vincent, 2009). These muscle cells elongate across each somite segment and attach to ECM at the somite boundaries (Gros et al., 2004; Snow et al., 2008a). Cell-ECM adhesions link muscles to tendons at the myotendinous junction (MTJ) (Fig. 1.5A,B) (Gillies and Lieber, 2011), which is, in turn, needed to transmit force to the skeletal system (Charvet et al., 2012). Not surprisingly, disruption of muscle adhesion to the basement membrane (BM) can lead to congenital muscular dystrophies (Bertini et al., 2011; Kirschner, 2013). Clearly, adhesion of muscle cells to the BM is critical for the normal progression of muscle morphogenesis and for muscle function. The adhesion of muscle fibers relies on two principal components: cell-matrix adhesion complexes (CMACs) and ECM composition.

Several transmembrane receptors concentrate at somite boundaries as part of cell-matrix adhesion complexes (CMACs) (Fig. 1.5A,B) (Bajanca et al., 2006; Julich et al., 2005; Lunardi and Dente, 2002; Moreau et al., 2003; Parsons et al., 2002a; Schofield et al., 1995; Song et al., 1992). Two major protein complexes involved in cell-matrix attachments are integrin heterodimers and the dystrophin-associated glycoprotein complex (DGC). Integrin adhesion complexes organize at somite boundaries and bind the ECM protein fibronectin, coordinating fibronectin polymerization (Julich et al., 2009; Lackner et al., 2013). Dystroglycan is a main component of the DGC and is

initially expressed as a single precursor protein, encoded by *dag1*, which is then cleaved into α and β subunits (Holt et al., 2000; Ibraghimov-Beskrovnaya et al., 1992). β-dystroglycan (βDG) is the transmembrane subunit and links the DGC to the cytoskeleton, whereas α-dystroglycan (αDG) binds to laminin, a major component of the BM (Ervasti and Campbell, 1993; Yamada et al., 1994).

In zebrafish, *dag1* morphants and mutants exhibit disorganized and apoptotic muscle cells as well as destabilization of myofiber attachments to somite boundaries (Gupta et al., 2012; Parsons et al., 2002a). Further, glycosylation of αDG is critical for it to bind ligands within the BM (Gee et al., 1994; Inamori et al., 2012; Moore and Winder, 2012; Sciandra et al., 2013). Mutations in genes required for glycosylation of αDG result in muscle diseases referred to as dystroglycanopathies (Godfrey et al., 2011; Kawahara et al., 2009). Thus, not only do CMACs have to be present at somite boundaries, but they also have to be appropriately modified in order to enable muscle fiber adhesion to the BM.

In addition to CMACs, the connection between muscle fibers and somite boundaries during skeletal muscle morphogenesis also relies upon appropriate deposition of the ECM components fibronectin and laminin (Fig. 1.5C). For example, zebrafish fibronectin morphants have aberrant fast-twitch muscle patterning and exhibit disorganized muscle fibers (Snow et al., 2008b). Meanwhile, failed polymerization of laminin at the MTJ results in excessively

long muscle fibers crossing over somite boundaries (Goody et al., 2010), and zebrafish *candyfloss* mutants, deficient in *laminin α2*, exhibit retraction of fibers from the MTJ following muscle contraction (Hall et al., 2007). Clearly, adhesion complexes and matrix proteins are critical players in the maintenance of muscle fiber integrity and function. Taken together, these studies reveal a fascinating dynamic between the ECM and CMACs during myoskeletal morphogenesis and homeostasis.

While cell-matrix attachments are clearly essential for muscle development, the way in which these interactions are regulated is less well defined. Intriguingly, our initial observations of *MZtmem2* mutants revealed defects in somite morphology (Totong et al., 2011). Namely, *MZtmem2* mutants exhibit slightly curved somites that are U-shaped rather than chevron-shaped. Closer investigation of this phenotype uncovered underlying issues with muscle fiber attachments. In Chapter 2 of this thesis, we demonstrate that Tmem2 influences both matrix organization and cell adhesion complexes at the MTJ and discuss the role of Tmem2 in regulating cell-matrix interactions that are essential for muscle fiber stabilization during morphogenesis.

The atrioventricular canal: a distinct subunit of the heart

The primitive heart begins as a linear tube comprised of two layers: an inner, vascular layer, the endocardium, and an outer layer of muscle, the myocardium. Between these two layers is a lining of ECM known as the

cardiac jelly. During development, signaling between the endocardium and myocardium at the boundary between the ventricle and the atrium triggers the formation of endocardial cushions (Fig. 1.7) (Eisenberg and Markwald, 1995). These cushions are eventually remodeled into valve flaps that prevent retrograde blood flow (Hu et al., 2000). The tightly defined region of the heart in which endocardial cushions develop is called the atrioventricular canal (AVC).

Cells within the AVC must differentiate and undergo specific structural changes for correct endocardial cushion formation to occur (Fig. 1.7). For example, endocardial AVC cells change shape from squamous to cuboidal (Beis et al., 2005) and specifically express *notch1b* and *has2* (Hurlstone et al., 2003) as well as cell adhesion molecule Dm-grasp/Alcam (Beis et al., 2005). A subset of endocardial cells transdifferentiate from epithelial to mesenchymal cells, a process called epithelial to mesenchymal transition (EMT). After EMT, they invade the cardiac jelly where they proliferate and contribute to the swelling of the EC (Markwald et al., 1977). These AVC-specific changes in cell shape and gene expression are accompanied by an increase in the AVC cardiac jelly (Moorman and Christoffels, 2003). In contrast, cells directly adjacent to the AVC do not undergo these changes and maintain their identity as ventricular or atrial cells.

Although the mechanism for coordination of atrioventricular differentiation is unclear, we do understand that signaling between the

endocardium and the myocardium is crucial for endocardial cushion development. *Ex vivo* cushion explant systems have shown the necessity for myocardial signaling in epithelial to mesenchymal transdifferentiation (EMT) of endocardial cells. In these experiments, myocardial explants were shown to promote seeding of endocardial cushion tissue cells into a three-dimensional collagen lattice (Runyan and Markwald, 1983). Further, these experiments elucidated the regional specificity of cell signaling control, showing that endocardium from the cushion-forming region is solely capable of responding to myocardial differentiation signals.

Evidence suggests that at least one of the relevant AVC differentiation signals being communicated between the endocardium and the myocardium is Wnt. During canonical Wnt signaling (Fig. 1.8), Wnt ligand binds to a frizzled (FZ) family transmembrane receptor (Mao et al., 2001a; Mao et al., 2001b; Tamai et al., 2000) and the ensuing signal prevents β-catenin from being tagged for degradation by the axin-containing destruction complex (Fig. 1.8A) (Nelson and Nusse, 2004). β-catenin then translocates to the nucleus where it activates downstream transcription factors (Fig. 1.8B) (Fodde et al., 2001). The adenomatous polyposis coli (Apc) protein is part of the axin-containing destruction complex and its loss of function results in constitutively active Wnt signaling. Zebrafish *apc* mutants with increased Wnt signaling exhibit several AVC defects including hyperplastic endocardial cushions and expansion of AVC molecular markers such as *bmp4* (Hurlstone et al., 2003). Conversely,

inhibition of Wnt signaling through over-expression of Axin1 led to reduced *bmp4* expression in the AVC (Verhoeven et al., 2011), thus revealing that *bmp4* is regulated downstream of canonical Wnt signaling.

This same work also placed *tbx2* as a downstream mediator of *bmp4* in the pathway patterning AVC differentiation (Verhoeven et al., 2011). *Tbx2* null mutant mice exhibit abnormally small endocardial cushions as well as aberrant expression of chamber markers within what is typically the AVC (Habets et al., 2002; Harrelson et al., 2004). On the other hand, over-expression of *tbx2* resulted in expansion of ECs (Shirai et al., 2009). Additional studies in mice highlighted the role of *Tbx2* as a transactivator of *Hyaluranon synthase 2* (*Has2*), which encodes the major enzyme responsible for the synthesis of hyaluronic acid (HA) (Shirai et al., 2009). The glycosaminoglycan HA is a major constituent of the cardiac jelly (Schroeder et al., 2003). Over-expression of *Tbx2* induces ectopic HA deposition in the cardiac jelly of both ventricular and atrial chambers (Shirai et al., 2009). Taken together, it is clear that the Wnt signaling pathway, along with its downstream effectors, are crucial to the proper differentiation of the AVC. How Wnt signaling is itself regulated, however, is less clear. Importantly, the ECM could be a potential regulator of the Wnt signaling pathway.

Between the endocardium and the myocardium is a dynamic layer of ECM consisting of proteoglycans and glycosaminoglycans (Valiente-Alandi et al., 2016). Correspondingly, mutations affecting synthesis of several ECM

components cause defective AVC formation. For example, the zebrafish mutant *jekyll* fails to form endocardial cushions and exhibits no constriction of the AVC region. This phenotype is caused by disruption of the gene that encodes UDP-glucose dehydrogenase, one of the enzymes responsible for HA synthesis (Walsh and Stainier, 2001).

Another enzyme required for HA synthesis is hyaluronan synthase, encoded by the gene *has2*. *Has2* mutant mice display a complete absence of cardiac jelly (Camenisch et al., 2000). Without cardiac jelly, endocardial cells of the AVC region fail to transdifferentiate and endocardial cushions are not formed. Adding back HA, however, rescues endocardial cushion formation in the *Has2* knockout mice. Conversely, zebrafish *dicer* mutants display both excessive HA deposition and ectopic endocardial cushion differentiation (Lagendijk et al., 2011). Knockdown of *has2* is able to rescue this phenotype and results in proper AVC restriction.

Like HA, CS has been shown to be critical for the appropriate development of the AVC. In zebrafish embryos, chemical inhibition of CS synthesis results in loss of AVC constriction, causing a phenotype much like the *jekyll* mutant (Peal et al., 2009). Taken together, these studies reveal that ECM composition is critical for appropriate AVC development. However, the means by which ECM deposition is spatially regulated remains poorly understood. Mutations in the zebrafish gene *tmem2* provide a valuable entry point for addressing these open questions.

Tmem2 restricts atrioventricular canal differentiation

In wild-type embryos, expression of the endocardial AVC marker, *notch1b,* and myocardial AVC markers, *bmp4* and *versican,* is restricted to the AVC region by 48 hpf. In contrast, *tmem2* mutants fail to restrict these AVC markers by 48 hpf (Fig. 1.9A-F). These mutants also fail to restrict endocardial localization of the AVC molecular marker, Dm-grasp, (Totong et al., 2011). In *tmem2* mutants, DM-grasp staining is expanded throughout the ventricular endocardium as well as the AVC (Fig. 1.9G-L) (Totong et al., 2011). Taken together, these data show that *tmem2* mutants exhibit ectopic atrioventricular differentiation.

Interestingly, in addition to AVC restriction defects, *tmem2* mutants also exhibit aberrant hyaluronic acid deposition. Whereas wild-type embryos have localized accumulation of hyaluronic acid at the AVC, *tmem2* mutant hearts display grossly expanded HA deposition throughout the ventricle (Smith et al., 2011). Overall, these data suggest that Tmem2 could function to restrict atrioventricular differentiation through regulation of HA deposition. In Chapter 3, we present our findings supporting a model for Tmem2 function through HA regulation.

Tmem2 structure and function

Clearly, Tmem2 plays multiple roles in cardiac and skeletal muscle morphogenesis: Tmem2 functions to promote cardiac fusion, stabilize muscle fiber attachments, and restrict AVC differentiation. Further, these functions of Tmem2 most likely involve the regulation of ECM. What is less clear, however, is the precise mechanism by which Tmem2 executes its functions. The structure of the Tmem2 protein leaves open many options for its biochemical role. The goal of my thesis research has been to determine the mechanism through which Tmem2 accomplishes its various tasks. At the time that the studies presented in Chapters 2 and 3 were initiated, very little was known about the molecular mechanism of Tmem2 function. In this section, I will outline what was known about Tmem2 structure in the preliminary stages of our research, as well as review findings from recent studies that have provided new insight into Tmem2 activity.

Tmem2 is a predicted single-pass type II transmembrane protein with a short cytoplasmic portion and an extended extracellular region (Fig. 1.12) (Smith et al., 2011; Totong et al., 2011). Within the Tmem2 extracellular region, there are four recognized domains – the G8 domain, several PbH1 repeats, and two Pander-like domains. PbH1 repeats typically form pectin lyase folds with enzymatic activity capable of degrading polysaccharides (Henrissat et al., 1995; Mayans et al., 1997). Although their precise function remains unclear, Pander-like domains have been shown to be present in

proteins involved in apoptosis and metastasis and glycosylation (Cao et al., 2003; Johansson et al., 2013; Pereira et al., 2014; Yoshida et al., 2013). The G8 domain of the human PKHD1 protein has been associated with polycystic kidney disease (He et al., 2006) and mutations within the G8 region of the KIAA1199 protein are associated with non-syndromic hearing loss (Abe et al., 2003).

Although there are several identified domains within Tmem2, they are poorly characterized and do not immediately suggest a biochemical role for Tmem2 during cardiac and muscle morphogenesis. Despite this, the structure of Tmem2 does closely resemble that of the KIAA1199 protein, also known as cell migration-inducing and hyaluranon binding protein (CEMIP). KIAA1199 is a soluble rather than transmembrane protein; however, it contains a G8, PLT, and PL domain as well as three conserved PbH1 repeats (Yoshida et al., 2013). KIAA1199 has been shown to bind the EGF receptor and activate EGF signaling in cervical cancer cells (Shostak et al., 2014). Additionally, KIAA1199 promotes cell migration in cultured fibroblast cells (Evensen et al., 2013). Most interestingly, KIAA1199 has been identified as a hyaluronidase in synovial fibroblasts whose activity relies on the clathrin-coated pit pathway (Yoshida et al., 2013). Research illustrating the ability of KIAA1199 to bind and depolymerize HA yielded key support toward the hypothesis that Tmem2 could function through regulation of HA.

Building upon this, recent work in mammalian cell culture has demonstrated that Tmem2 can function as a cell-surface hyaluronidase. HEK 293T cells transiently transfected with FLAG-tagged full-length TMEM2 cDNA gained the ability to depolymerize HA molecules within the range of 20-1500 kDa, into fragments of ~5 kDa (Yamamoto et al., 2017). In Tmem2, amino acid residue 265 positionally corresponds to site of the deafness mutation (residue 187) in human KIAA1199 (Abe et al., 2003; Yoshida et al., 2013). A similar point mutation of residue 265 in Tmem2 abolished its ability to degrade HA (Yamamoto et al., 2017), confirming that this region within the PLT domain is critical for Tmem2 activity in HA catabolism.

Importantly, the ability of Tmem2 to depolymerize HA was recently shown to be essential for the role of Tmem2 in promoting angiogenesis. Zebrafish *tmem2* mutants exhibit intersegmental vessel (ISV) sprouting defects as well as excess HA deposition surrounding stunted ISVs (De Angelis et al., 2017). Degradation of HA with hyaluronidase treatment rescued ISV sprouting in *tmem2* mutants. These findings support a model wherein Tmem2 promotes angiogenesis through regulating local HA levels. Interestingly, overexpression of partially degraded HA was also able to efficiently rescue ISV sprouting in mutants, suggesting that Tmem2 regulates these processes through HA depolymerization specifically (De Angelis et al., 2017). Does Tmem2 act in a similar way in order to restrict AVC differentiation? In Chapter 3, I will examine the link between Tmem2, HA regulation, and AVC patterning.

Summary

Prior studies provide substantial evidence that regulation of the ECM is frequently a crucial component of cardiac and skeletal muscle morphogenesis. However, we have an incomplete understanding of the way in which ECM organization is controlled and how ECM organization, in turn, informs morphogenetic programs. We speculate that the transmembrane protein Tmem2 coordinates ECM organization in multiple embryonic tissues. In Chapter 2, I will present studies that demonstrate the role of Tmem2 in regulating cell-matrix interactions that are essential for muscle fiber attachment. In Chapter 3, I will examine how Tmem2 structure influences its function within multiple developmental contexts as well as link Tmem2 regulation of HA to the process of AVC differentiation. Finally, in Chapter 4, I will integrate these ideas and present future directions toward elucidating the mechanisms through which ECM influences embryonic development.

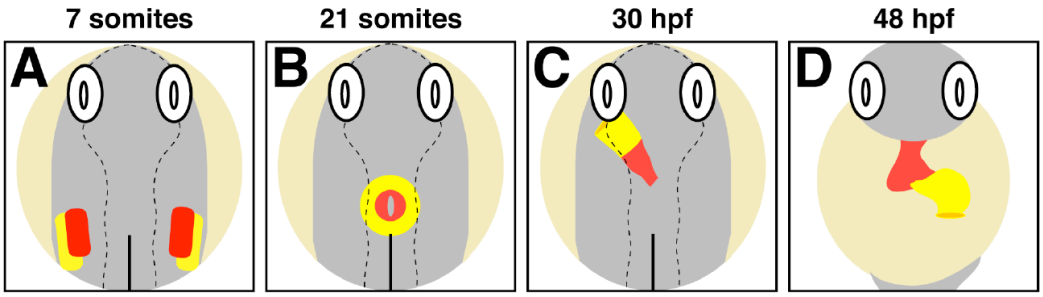

Figure 1.1. Schematic view of heart development in zebrafish
Dorsal (A-C) and frontal (D) views of zebrafish cardiac development. (A) Atrial (yellow) and ventricular (red) myocardial progenitors cluster into bilateral groups. (B) Cardiomyocytes then migrate toward the embryonic midline and fuse, forming a ring (Berdougo et al., 2003; Yelon et al., 1999). (C) This ring then elongates into to the primitive heart tube. (D) By 48 hours post fertilization (hpf), the heart has undergone looping, and restriction at the atrioventricular canal (AVC) separates the ventricular and atrial chambers. Adapted from (Schoenebeck and Yelon, 2007).

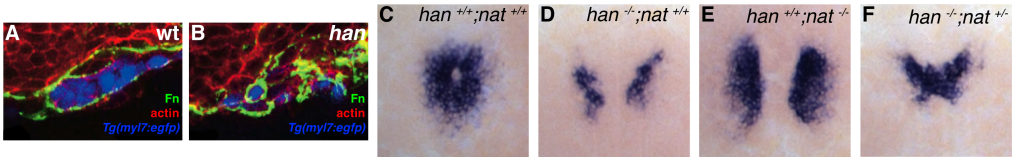

Figure 1.2. Both loss of fibronectin (FN) and excessive FN can hinder cardiomyocyte movement

(A,B) Transverse sections of the right side of the lateral plate mesoderm at 20 somites (som), dorsal up. Adapted from (Trinh et al. 2005). (A) In wild-type (wt) cardiomyocytes (pseudocolored blue), Fn (green) is deposited basally. (B) In *hand2* (*han*) mutants, Fn is widely and irregularly distributed. (C-G) Expression of *myl7* at 22 som; dorsal views, anterior up, Adapted from (Garavito-Aguilar et al., 2010). (C, D) At this stage, a ring of cardiomyocytes has formed in wt embryos (C), but *han* mutants (D) never exhibit cardiac fusion (Yelon et al., 2000). (E) The *nat* mutation in the zebrafish *fn1* gene causes cardia bifida (Trinh and Stainier, 2004). (F) Heterozygosity for *nat* in *han* mutants rescues cardiac fusion, indicating that excess Fn is responsible for hindering cardiomyocyte movement in *han* mutants.

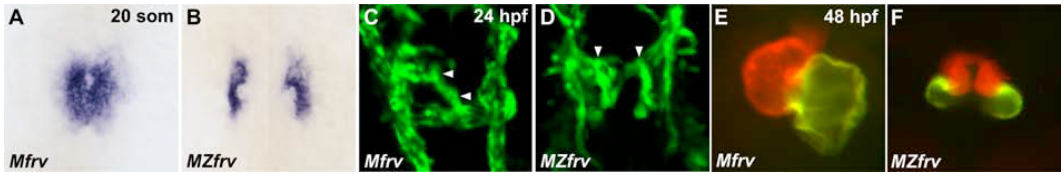

Figure 1.3. *MZtmem2* mutants exhibit defects in both myocardial and endocardial medial movement

(A,B) Expression of *myl7* at 20 somites (som) and (C,D) *Tg(vegfr2:g-rcfp)* at 24 hpf; dorsal views, anterior up. Arrows indicate endocardium. Note that *frv* is the original allele designation for this specific mutation in *tmem2*. Myocardial and endocardial medial movement are normal in *Mtmem2* (A,C) and zygotic *tmem2* mutants and are hindered in *MZtmem2* (B,D) mutants. (E,F) Immunofluorescence employing the MF20 and S46 antibodies demonstrates that *Mtmem2* (E) mutant embryos develop normally looped hearts with a distinct ventricle (red) and atrium (green). (F) In *MZtmem2* mutant embryos, the heart remains bifurcated with subdivided ventricular (red) and atrial (green) chambers. Adapted from (Totong et al., 2011).

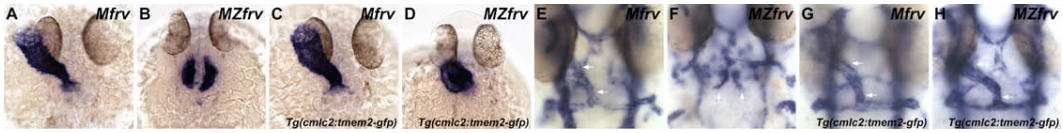

Figure 1.4. *MZtmem2* mutant myocardial and endocardial fusion defects are rescued by myocardial *tmem2* expression

(A-D) Expression of *myl7* at 26 hpf and (E-H) the endothelial cadherin gene *cdh5* (Larson et al., 2004) at 32 hpf; dorsal views, anterior up. Arrows in E-H indicate the endocardium. Note that *frv* is the original allele designation for this specific mutation in *tmem2*. The transgene *Tg(cmlc2:tmem2-gfp)* (C,D,G,H) drives expression of a Tmem2-Gfp fusion protein in the myocardium. Whereas transgene expression has no effect on *Mtmem2* embryos (A,C,E,G), it rescues both myocardial movement (B,D) and endocardial movement (F, H) in *MZtmem2* embryos. Adapted from (Totong et al., 2011).

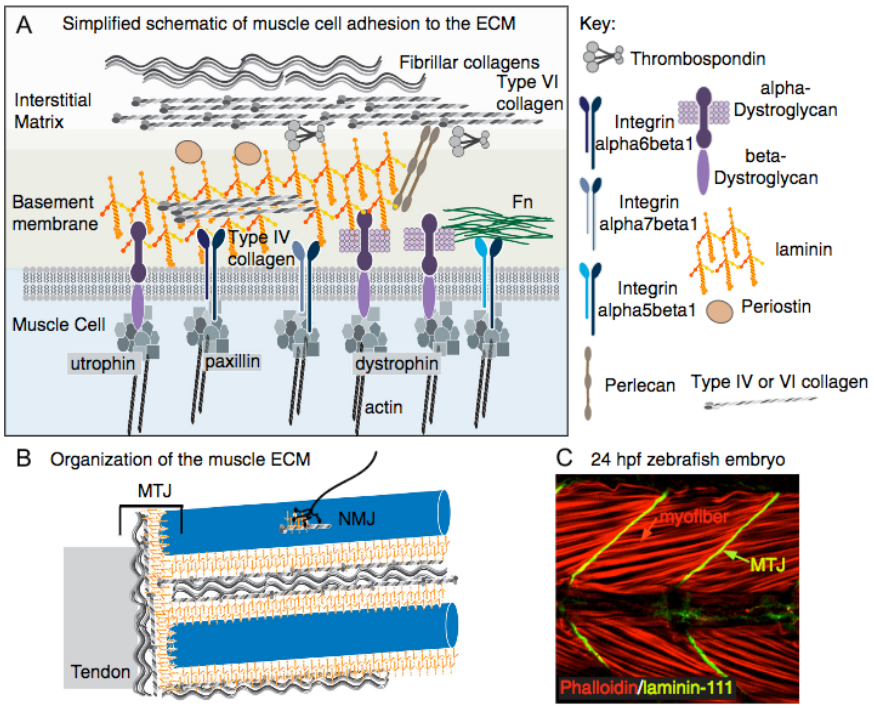

Figure 1.5. Extracellular matrix is crucial for attachment of muscle cells to the myotendinous junction

(A) Cartoon schematizes adhesive interactions between muscle cells and the extracellular matrix (ECM). Cell-matrix adhesion complexes (CMACs) link the ECM to the actin cytoskeleton within muscle cells. (B) ECM surrounds individual muscle fibers and is also organized at the myotendinous junction (MTJ). (C) Fluorescence depicts phalloidin (red) and laminin-111 (green) in a 24 hpf zebrafish embryo. Side view, anterior left, dorsal top. Muscle cells elongate and attach to laminin-rich somite boundaries that develop into MTJs. Reproduced from (Goody et al., 2015).

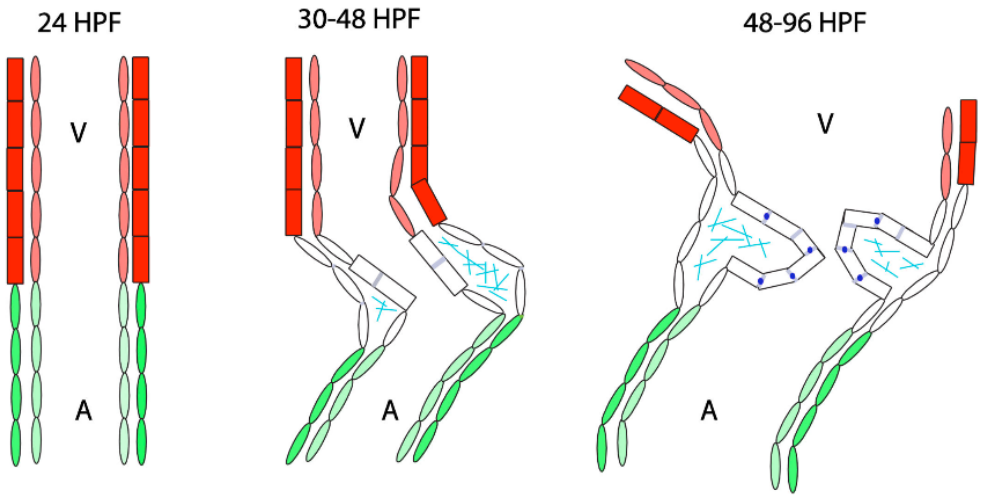

Figure 1.6. Schematic of the morphological changes in the zebrafish atrioventricular canal (AVC) between 24 and 96 hpf
Ventricle, red. Atrium, green. At 24 hpf, the primitive heart tube consists of an outer myocardial layer and an inner endocardial layer separated by a thin layer of extracellular matrix (ECM). Between 30-48 hpf, endocardial cells within the AVC (white) undergo structural changes and become cuboidal in shape. In addition, cardiac jelly deposition (sky blue) becomes enriched within endocardial cushions by 48 hpf. Reproduced from (Peal et al., 2009).

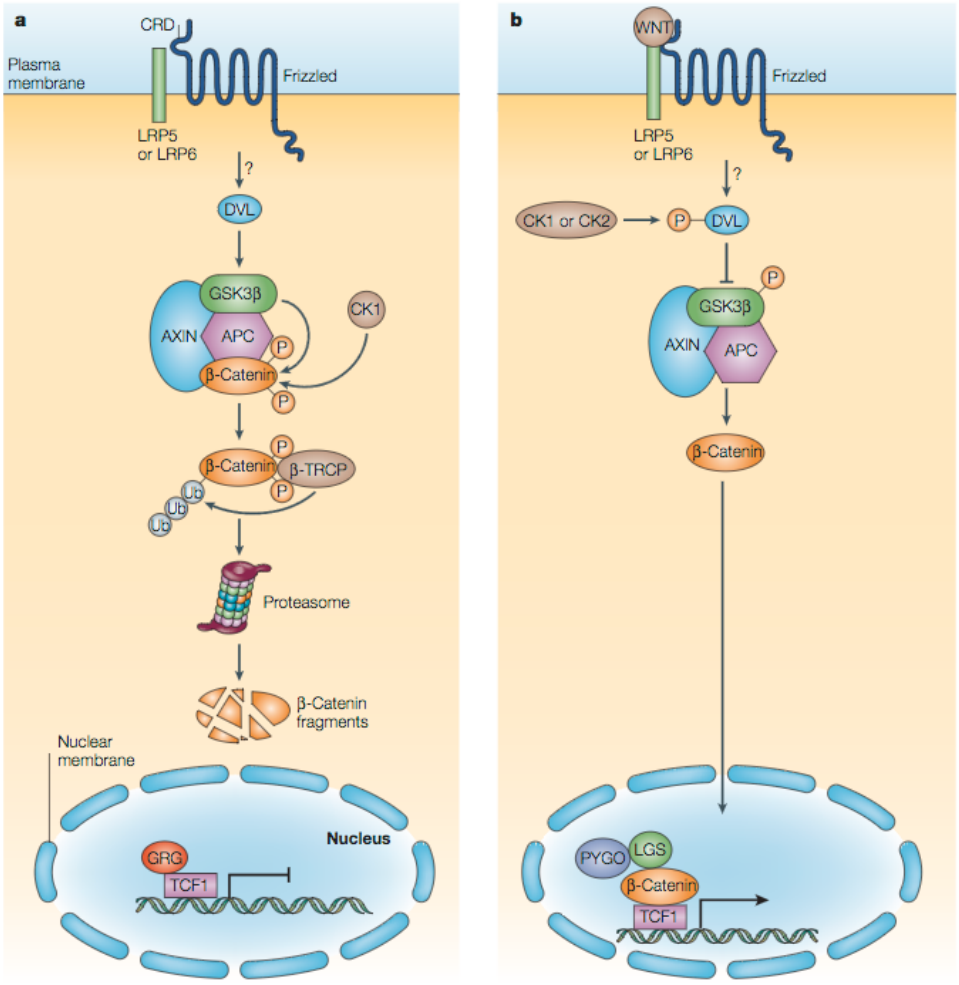

Figure 1.7. Schematic of the canonical Wnt signaling pathway
(A) In the absence of Wnt ligands, β-catenin associates with the axin destruction complex, which includes the tumor suppressor Adenomatous polyposis coli (APC). This association targets β-catenin for phosphorylation and subsequent ubiquitylation, ultimately leading to the degradation of β-catenin by the proteasome. (B) When Wnt ligands are available, they bind to the Frizzled transmembrane receptor and its co-receptors. Wnt ligand-receptor engagement prevents ubiquitylation of β-catenin and results in the translocation of β-catenin to the nucleus, where it binds to TCF transcription factors and activates downstream target genes. Reproduced from (Staal and Clevers, 2005).

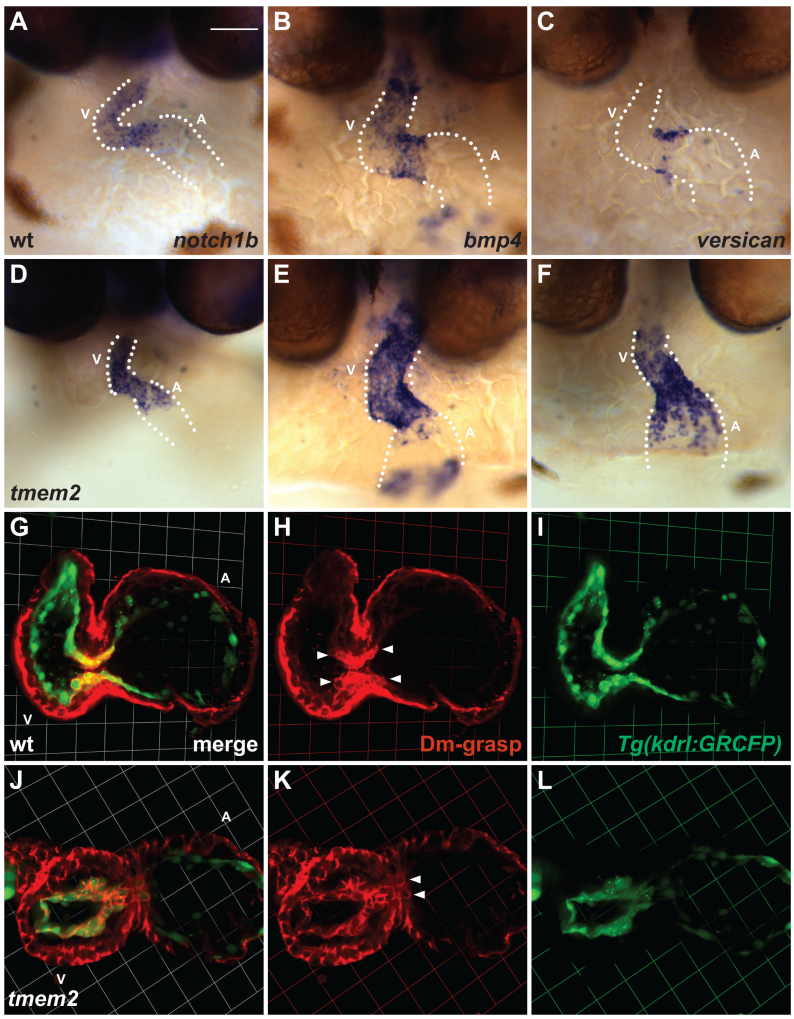

Figure 1.8 *tmem2* mutants display ectopic localization of atrioventricular canal (AVC) markers.
(A-F) Frontal views showing expression of atrioventricular canal (AVC) markers in wild-type (wt) (A-C) and *tmem2* mutant embryos (D-F) at 48 hpf. Dotted lines outline the heart chambers. In wild-type embryos, expression of molecular markers such as *notch1b* (A), *bpm4* (B), and *versican* (C) are restricted to the AVC region. In contrast, *tmem2* mutants fail to restrict expression of these markers to the AVC (D-F). (G-L) Three-dimensional projections of confocal sections of wild-type (G-I) and *tmem2* mutant (J-L) hearts expressing *Tg(kdrl:GRCFP)* (green) in the endocardium at 57 hpf. Immunofluorescence depicts Dm-grasp (red) throughout the myocardium and in the endocardium of the AVC (arrowheads). In *tmem2* mutants, Dm-grasp is ectopically localized in the ventricular endocardium. A, atrium; V, ventricle. Adapted from (Totong et al., 2011).

Figure 1.9. Predicted structure of the Tmem2 protein
The Tmem2 protein is predicted to encode a type II transmembrane protein, containing a single transmembrane domain (TM) and a small cytoplasmic region (C). In its extracellular portion, Tmem2 contains a G8 domain, a Pander-like Tmem2 domain (PLT), three parallel beta helix repeats (PbH1), and a Pander-like domain (PL).

Chapter 2: Tmem2 regulates cell-matrix interactions that are essential for muscle fiber attachment

Reprinted from:

Lucile Ryckebusch, Lydia Hernandez, Carole Wang, Jenny Phan, Deborah Yelon, “Tmem2 regulates cell-matrix interactions that are essential for muscle fiber attachment.” Development, 2016. 143(16): p.2965-2972.

Summary Statement

The transmembrane protein Tmem2 facilitates muscle fiber attachment by influencing both the organization of the extracellular matrix and the glycosylation of α-dystroglycan.

Abstract

Skeletal muscle morphogenesis depends upon interactions between developing muscle fibers and the extracellular matrix (ECM) that anchors fibers to the myotendinous junction (MTJ). The pathways that organize the ECM and regulate its engagement by cell-matrix adhesion complexes (CMACs) are therefore essential for muscle integrity. Here, we demonstrate the impact of transmembrane protein 2 (tmem2) on cell-matrix interactions during muscle morphogenesis in zebrafish. Maternal-zygotic *tmem2* (*MZtmem2*) mutants exhibit muscle fiber detachment, in association with impaired laminin organization and ineffective fibronectin degradation at the MTJ. Similarly, disorganized laminin and fibronectin surround *MZtmem2* cardiomyocytes, which could account for their hindered movement during cardiac morphogenesis. In addition to ECM defects, *MZtmem2* mutants display hypoglycosylation of α-dystroglycan within the CMAC, which could contribute to the observed fiber detachment. Expression of the Tmem2 ectodomain can rescue aspects of the *MZtmem2* phenotype, consistent with a possible extracellular function of Tmem2. Together, our results suggest that

Tmem2 regulates cell-matrix interactions by affecting both ECM organization and CMAC activity. These findings evoke possible connections between the functions of Tmem2 and the etiologies of congenital muscular dystrophies, particularly dystroglycanopathies.

INTRODUCTION

In vertebrates, most skeletal muscles derive from precursors found within the somites, repetitive segments of paraxial mesoderm that flank the embryonic notochord (Bryson-Richardson and Currie, 2008; Buckingham and Vincent, 2009). As muscle precursors mature, they elongate to form fibers that span each segment and attach to the somite boundaries (Goody et al., 2015). Attachments are created through direct interactions of muscle fibers with the extracellular matrix (ECM), and sites of attachment develop into the myotendinous junction (MTJ), which transmits muscular forces to the skeletal system (Charvet et al., 2012). Thus, cell-matrix connections facilitate the morphology, integrity, and function of developing muscles. In contrast, failure to maintain fiber attachments can lead to the progressive tissue degeneration that underlies muscular dystrophy. Although numerous causative mutations have been associated with congenital muscular dystrophies (Bertini et al., 2011; Kirschner, 2013), our understanding of the molecular mechanisms that regulate muscle fiber attachment remains incomplete.

Several protein complexes are known to play primary roles in connecting muscle cells to the MTJ (Charvet et al., 2012; Goody et al., 2015; Thorsteinsdottir et al., 2011). Within the ECM, deposition of both fibrillar fibronectin and polymerized laminin is crucial for successful anchoring of muscle fibers. These ECM molecules are engaged by a variety of transmembrane receptors at fiber termini, including integrin heterodimers and the dystrophin-associated glycoprotein complex (DGC). In collaboration with cytoplasmic proteins like focal adhesion kinase (FAK) and paxillin, these receptors form cell-matrix adhesion complexes (CMACs) that link the extracellular environment to the cytoskeleton and thereby facilitate both force transmission and signaling. Whereas the importance of ECM and CMAC components is well documented, it is less clear how deposition of the ECM is controlled or how CMAC assembly is regulated in order to insure appropriate cell-matrix interactions.

The use of the zebrafish as a model organism provides valuable opportunities for interrogating the functions of genes involved in muscle fiber attachment (Berger and Currie, 2012; Gibbs et al., 2013). Here, we show that the zebrafish gene *transmembrane protein 2* (*tmem2*) plays an important and previously unappreciated role in regulating cell-matrix interactions at the MTJ. Tmem2 is a type II transmembrane protein with a small cytoplasmic domain, a single-pass transmembrane domain, and a large ectodomain (Smith et al., 2011; Totong et al., 2011). Prior studies have demonstrated that *tmem2*

regulates the regional restriction of the cardiac atrioventricular canal (Smith et al., 2011; Totong et al., 2011). In addition, embryos lacking both maternal and zygotic supplies of *tmem2* (*MZtmem2*) exhibit earlier defects in multiple tissues, including aberrantly shaped somites (Totong et al., 2011). Through analysis of the somite defects in *MZtmem2* mutants, we find that loss of *tmem2* function leads to muscle fiber detachment. Our results indicate that *tmem2* is required for appropriate ECM deposition during skeletal muscle morphogenesis, as well as for deposition of the ECM that surrounds cardiomyocytes during heart tube formation. In addition, *tmem2* promotes the glycosylation of α-dystroglycan within the DGC at the MTJ. Thus, our studies suggest that Tmem2 impacts cell-matrix interactions by influencing both ECM organization and CMAC post-translational modification.

RESULTS AND DISCUSSION

Loss of *tmem2* function leads to muscle fiber detachment

Our prior studies indicated that embryos lacking both maternal and zygotic supplies of *tmem2* (*MZtmem2*) exhibit abnormal somite morphology, whereas embryos lacking only maternal supplies of *tmem2* (*Mtmem2*) are indistinguishable from wild-type (Fig. 2.1A,D) (Totong et al., 2011). Notably, instead of the chevron-shaped somites seen in *Mtmem2* embryos, *MZtmem2* mutants display U-shaped somites (Fig. 2.1B,E). Formation of chevron-shaped somites requires Hedgehog signaling from the notochord (Barresi et

al., 2000; Blagden et al., 1997; Henry and Amacher, 2004); however, the morphology, integrity, and differentiation of the *MZtmem2* notochord appear relatively normal (Figs. 2.1C,F, 2.S1B,D). Moreover, the *MZtmem2* somite shape does not seem to result from defective Hedgehog signaling, since *ptc1* expression appears intact in *MZtmem2* mutants (Fig. 2.S1A,C).

We investigated whether defects in muscle fiber morphogenesis could underlie the aberrant somite shape in *MZtmem2* mutants. *MZtmem2* embryos exhibit a normal number of somites (Fig. 2.1A,D) and have no apparent defects in initial somite boundary formation (Fig. 2.S2A,B). However, muscle fiber attachment defects are prevalent in *MZtmem2* mutants (Fig. 2.1G,H). Both fast and slow fibers exhibit detachment from the MTJ (Figs. 2.1H, 2.S3); in addition, some muscle fibers aberrantly cross the MTJ (Fig. 2.1H). Fiber detachment becomes more widespread as development proceeds (Figs. 2.1J,K, 2.S4A,B), indicating failure to properly maintain attachments. Consistent with this, although zygotic *tmem2* (*Ztmem2*) mutants exhibit normal somite morphology at early stages, defects in somite shape and muscle fiber integrity emerge in some *Ztmem2* mutants over time (Fig. 2.S4C-G), presumably as maternal supplies of *tmem2* are depleted. Together, these results provide the first demonstration that *tmem2* plays an important role in preserving muscle fiber attachment to the MTJ.

Tmem2 regulates organization of basement membrane components

Establishment and maintenance of muscle fiber attachment at the MTJ require successful interactions with the ECM molecules that compose the basement membrane (Goody et al., 2015; Snow and Henry, 2009). Moreover, the *MZtmem2* phenotype shares some characteristics with the phenotypes of laminin-deficient and fibronectin-deficient embryos, including the presence of fibers that cross the MTJ (Snow et al., 2008a; Snow et al., 2008b), prompting us to investigate the ECM in *MZtmem2* mutants. Instead of the normally concentrated deposition of laminin at the MTJ in *Mtmem2* embryos (Fig. 2.2A,C), we observed diminished and poorly organized laminin in *MZtmem2* mutants (Fig. 2.2B,D), particularly in locations where fibers were detached (Fig. 2.2D). In contrast, fibronectin deposition appears relatively robust, albeit somewhat disorganized, in *MZtmem2* mutants (Figs. 2.S2A-F, 2.2E,F). During the usual progression of muscle morphogenesis (Jenkins et al., 2016; Snow and Henry, 2009), fibronectin levels degrade at the MTJ over time (Fig. 2.2E,G), in conjunction with accumulation of laminin (Fig. 2.2A,C). However, in *MZtmem2* mutants, fiber attachment defects are accompanied by aberrantly increased fibronectin localization (Fig. 2.2F,H). This may represent a secondary consequence of laminin deficiency, since organized laminin has been shown to play an indirect role in facilitating fibronectin degradation at the MTJ (Jenkins et al., 2016); alternatively, increased fibronectin could be a secondary response to muscle fiber detachment, akin to the increased

fibronectin fibrillogenesis seen in association with some myopathies (Hori et al., 2011; Rampoldi et al., 1986; Zacharias et al., 2011).

The deficient and disorganized ECM at the *MZtmem2* MTJ made us wonder whether ECM defects could account for other aspects of the *MZtmem2* mutant phenotype. *MZtmem2* mutants exhibit cardia bifida, reflecting an early failure of cardiac morphogenesis (Totong et al., 2011). In wild-type embryos, bilateral populations of cardiomyocytes move toward the midline, where they meet and merge to assemble the heart tube through a process called cardiac fusion. *MZtmem2* mutants fail to execute cardiac fusion and instead display two separated groups of cardiomyocytes in bilateral positions (Fig. 2.3F,G) (Totong et al., 2011). The composition of the basement membrane has a potent influence on cardiac fusion: either diminished or excessive ECM deposition can inhibit cardiomyocyte movement (Arrington and Yost, 2009; Garavito-Aguilar et al., 2010; Trinh and Stainier, 2004). Interestingly, the ECM adjacent to the *MZtmem2* myocardium exhibits irregular and disorganized deposition of both laminin and fibronectin (Fig. 2.3A-E), which could account for the failure of cardiac fusion in *MZtmem2* mutants. Thus, our data suggest that Tmem2 regulates both cardiac and skeletal muscle morphogenesis via modulation of the ECM.

The Tmem2 ectodomain can enact aspects of Tmem2 function

Since the biochemical function of Tmem2 is currently unknown, it remains unclear whether this protein could exert its influence on the basement membrane through direct interaction with ECM components. To evaluate whether the Tmem2 ectodomain is sufficient to execute its functions, we replaced the transmembrane and cytoplasmic domains of Tmem2 with a signal peptide and tested whether this modified version of Tmem2 can rescue the *MZtmem2* mutant phenotype. Injection of wild-type *tmem2* mRNA into *MZtmem2* mutants can rescue both muscle fiber attachment (Fig. 2.1I,L; Table 2.S1) and cardiac fusion (Fig. 2.3F-K; Table 2.S2). Similarly, we found that the Tmem2 ectodomain can also ameliorate both of these features of the *MZtmem2* phenotype, although less efficiently than full-length Tmem2 (Fig. 2.1L; Tables 2.S1, 2.S2). Therefore, the Tmem2 ectodomain can mediate at least some of the molecular functions of Tmem2, consistent with a model in which Tmem2 functions within the extracellular environment.

Tmem2 influences glycosylation of alpha-dystroglycan

Our results suggest that the muscle fiber detachments in *MZtmem2* mutants could be a direct consequence of faulty ECM organization. Since fiber attachment also relies upon effective CMAC assembly (Goody et al., 2010; Goody et al., 2015; Jackson and Ingham, 2013), we investigated whether the MTJ defects in *MZtmem2* mutants are restricted to the basement

membrane or are also reflected in the localization of CMAC components. Examination of three components of the DGC – the scaffolding protein paxillin, a phosphorylated form of FAK (pFAK), and the core complex component β-dystroglycan (βDG) – demonstrated that each was localized to the MTJ in *MZtmem2* mutants (Fig. 2.4A-F). However, the distribution of each component was affected: paxillin was not properly concentrated (Fig. 2.4A,B), pFAK levels appeared reduced (Fig. 2.4C,D), and some gaps in bDG localization were observed (Fig. 2.4E,F). These aberrations could reflect ineffective CMAC assembly due to poor ECM engagement, or they could represent CMAC displacements that are secondary to fiber detachment (Bassett et al., 2003; Jacoby et al., 2009). Together, these observations suggest that recruitment of CMAC components to the MTJ does not require Tmem2, but that Tmem2 influences CMAC organization and integrity.

Our analysis of dystroglycan localization at the *MZtmem2* MTJ also revealed a significant defect in the glycosylation of α-dystroglycan (αDG) (Fig. 2.4E,F). Dystroglycan is post-translationally cleaved into two subunits, αDG and βDG (Moore and Winder, 2012). αDG functions as a laminin receptor, and its affinity for laminin depends upon its proper glycosylation (Sciandra et al., 2013). Strikingly, the glycosylated form of αDG is barely detectable at the *MZtmem2* MTJ, even though βDG localization is robust (Figs. 2.4F,H, 2.S5C; Table 2.S3). The influence of Tmem2 on αDG glycosylation may require its transmembrane and/or cytoplasmic domains: whereas full-length Tmem2 can

rescue glycosylation in *MZtmem2* mutants, the Tmem2 ectodomain cannot (Figs. 2.4G,H, 2.S5C; Table 2.S3). Thus, in addition to its effects on ECM organization, Tmem2 promotes αDG glycosylation and, presumably, DGC activity, and this function of Tmem2 may employ a mechanism distinct from its other roles.

Tmem2 promotes cell-matrix interactions by influencing ECM organization and DGC modification

Together, our data establish Tmem2 as a previously unappreciated player in the cell-matrix interactions that control muscle morphogenesis. Tmem2 influences two distinct elements that enforce muscle fiber attachment: ECM deposition and CMAC composition. Since reduced laminin deposition interferes with fiber attachment (Goody et al., 2010; Hall et al., 2007; Jacoby et al., 2009; Snow et al., 2008b), it is likely that the ECM disruption in *MZtmem2* mutants contributes to their muscle defects. The onset of fiber detachment in *MZtmem2* mutants corresponds to the timeframe when laminin enrichment normally begins at the somite boundary (Crawford et al., 2003). Furthermore, ECM disorganization could explain the cardia bifida in *MZtmem2* mutants (Arrington and Yost, 2009; Garavito-Aguilar et al., 2010; Trinh and Stainier, 2004). In addition, since DGC glycosylation promotes its engagement of the ECM (Sciandra et al., 2013), hypoglycosylation of αDG could also contribute to the fiber detachments in *MZtmem2* mutants, as seen in embryos with reduced

glycosyltransferase activity (Kawahara et al., 2010; Lin et al., 2011).

Do the ECM and CMAC features of the *MZtmem2* phenotype represent two separate functions of Tmem2, or are these roles of Tmem2 interrelated? Although ECM composition is not likely to have a direct impact on αDG glycosylation, prior studies have found that laminin organization can be influenced by DGC glycosylation state (Kanagawa et al., 2005; Michele et al., 2002). Alternatively, Tmem2 could influence the ECM and DGC through two independent mechanisms. In this regard, it is intriguing that the Tmem2 ectodomain can fulfill some, but not all, aspects of Tmem2 function: although the ectodomain can improve fiber attachment in *MZtmem2* mutants, it seems less effective than full-length Tmem2, and it cannot rescue αDG glycosylation. Thus, our data suggest that Tmem2 can function in the extracellular environment, consistent with our prior finding that myocardial expression of *tmem2* can non-autonomously rescue *MZtmem2* endocardial phenotypes (Totong et al., 2011). At the same time, our results suggest that distinct subcellular locations of Tmem2 function are relevant to its influence on posttranslational modification of αDG. We therefore favor a model in which independent activities of Tmem2, affecting ECM organization and αDG glycosylation, collaborate to enforce muscle fiber attachment.

The influence of Tmem2 on muscle fiber attachment suggests an interesting link to the etiology of muscular dystrophy. In particular, Tmem2 may be relevant to the set of congenital muscular dystrophies known as

dystroglycanopathies, which feature aberrant glycosylation of αDG (Muntoni et al., 2008; Wells, 2013). Mutations in 18 genes have been shown to cause dystroglycanopathies, and several of these genes encode characterized or putative glycosyltransferases (Bouchet-Séraphin et al., 2015; Godfrey et al., 2011). However, as many as half of the dystroglycanopathy patients examined do not present mutations in known genes, and the process of post-translational modification of the DGC is not fully understood. Future elucidation of the molecular mechanisms of Tmem2 function is likely to provide valuable perspective on its relationship to dystroglycanopathy, as well as further insight into how ECM organization and CMAC composition both contribute to the stability of cell-matrix interactions during muscle development.

MATERIALS AND METHODS

Zebrafish

To obtain *MZtmem2* mutant embryos, we used germline replacement to generate chimeric female fish with a *tmem2*^{sk38} mutant germline, and we bred these females to male *tmem2* heterozygotes, as previously described (Totong et al., 2011). *MZtmem2* mutants were distinguished from their *Mtmem2* siblings by morphological criteria and PCR genotyping (Totong et al., 2011).

All zebrafish work followed IACUC-approved protocols.

Immunofluorescence

Wholemount immunofluorescence was performed as previously described (Goody et al., 2012), using rhodamine phalloidin (Invitrogen, R415) and antibodies listed in Table 2.S4. For cryosections, embryos were fixed overnight in 4% paraformaldehyde at 4°C, followed by cryoprotection, mounting, sectioning, staining, and treatment with SlowFade Gold with DAPI (Invitrogen), as described previously (Garavito-Aguilar et al., 2010).

In situ hybridization

In situ hybridization for *ptc1* (ZDB-GENE-980526-196), *ehh* (ZDB-GENE-980526-135), and *myl7* (ZDB-GENE-991019-3) was performed as previously described (Yelon et al., 1999).

Injection

Embryos were injected at the one-cell stage with 200 pg mRNA encoding either full-length Tmem2 (Totong et al., 2011) or a modified version of the Tmem2 ectodomain. In this fusion protein, we replaced the first 103 amino acids of Tmem2, corresponding to its cytoplasmic and transmembrane domains, with the first 23 amino acids of zebrafish Sonic Hedgehog (Ekker et al., 1995), which serve as a signal to target the ectodomain for secretion.

Imaging

Fluorescent images are maximal intensity projections of confocal reconstructions, with the exception of the single optical slices shown in Fig. 2.3A-E. Z-stacks containing 120-140 slices (0.5 micron thick) were acquired with a 25x water objective on a Leica SP5 microscope and analyzed with Imaris software (Bitplane). Additional images were captured using Zeiss Axiozoom and Axioimager microscopes with a Zeiss AxioCam and processed using Zeiss AxioVision and Adobe Creative Suite.

ACKNOWLEDGMENTS

We thank L. Pandolfo and K. Garske for expert zebrafish care, C. Henry for helpful input, and members of the Yelon lab for constructive discussions.

COMPETING INTERESTS

No competing interests declared.

AUTHOR CONTRIBUTIONS

LR, LH, and DY designed these studies; LR, LH, CW, and JP performed experiments and analyzed data; and LR and DY wrote the manuscript with input from all authors.

FUNDING

This work was supported by grants to DY from the National Institutes of Health (NIH) [R01HL069594; R01HL133166] and the March of Dimes [1-FY08-589], fellowship support to LR from the Association Française contre les Myopathies [MNM1 2013–16528] and the American Heart Association and The Children's Heart Foundation [13POST16870010, 15POST25080308], and by fellowship support to LH from the UCSD Cell and Molecular Genetics Training Program [NIH T32GM007240] and the American Heart Association [15PRE22480001].

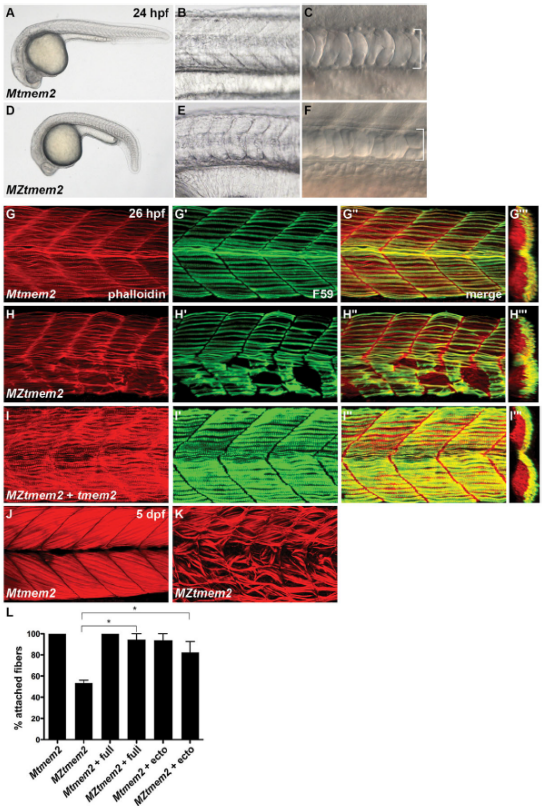

Figure 2.1. Disrupted muscle fiber attachment in *MZtmem2* mutants
(**A-F**) Lateral views display somite and notochord morphology at 24 hours post-fertilization (hpf). *Mtmem2* (A-C) control siblings are indistinguishable from wild-type, and *MZtmem2* mutants (D-F) exhibit a normal number of somites (32 somites in A,D). However, *MZtmem2* mutants (D-F) have U-shaped (E), rather than chevron-shaped (B), somites, and a slightly narrow notochord (bracket, F). (**G-K**) Immunofluorescence reveals muscle fiber organization, using phalloidin (red) to recognize both fast and slow fibers and F59 (green) to recognize slow fibers; lateral views with dorsal up (except for transverse views in G4-I4) at 26 hpf (G-I) or 5 days post-fertilization (dpf) (J,K). *MZtmem2* mutants display muscle fiber detachment (H1-H3), whereas *Mtmem2* siblings exhibit normal fiber attachment (G1-G3). Attachment can be rescued in *MZtmem2* mutants by injection of wild-type *tmem2* mRNA (I1-I3; n=6/7). The severity of detachment in *MZtmem2* mutants increases over time (K), indicating the importance of *tmem2* for the maintenance of muscle fiber attachment. (**L**) Bar graph compares average prevalence of fiber attachment in somites at 48 hpf; error bars indicate s.e.m. $F59^{+}$ fibers were counted within 11 somites of multiple embryos (*Mtmem2*, n=6; *MZtmem2*, n=4; *Mtmem2* expressing full-length *tmem2* ("+full"), n=6; *MZtmem2*+full, n=8; *Mtmem2* expressing *tmem2* ectodomain ("+ecto"), n=2; *MZtmem2*+ecto, n=5). Introduction of either full-length Tmem2 or the Tmem2 ectodomain into *MZtmem2* mutants caused improvement in fiber attachment. Asterisks indicate significant differences from *MZtmem2* (Student's t-test; $p<0.001$ for full, $p<0.05$ for ecto). See also Table 2.S1.

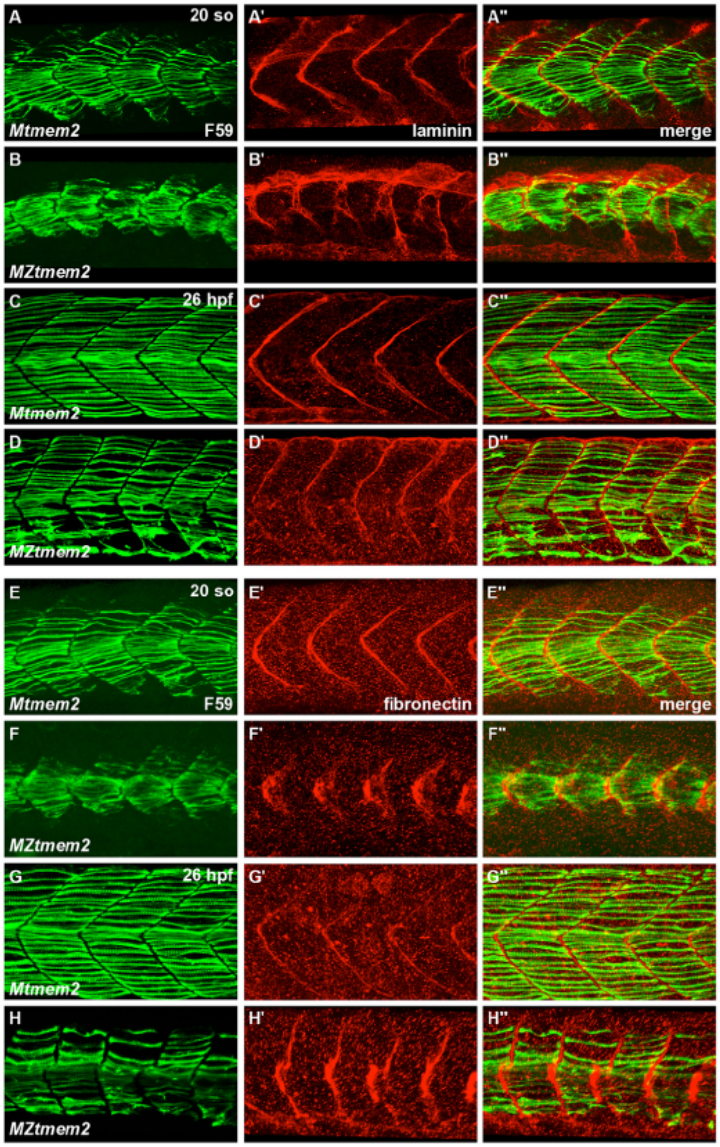

Figure 2.2. Aberrant ECM organization at the MTJ in *MZtmem2* mutants
(**A-H**) Immunofluorescence indicates localization of laminin (red, A-D) and fibronectin (red, E-H) relative to slow muscle fibers, labeled with F59 (green, A-H); lateral views, dorsal up, at 20 so (A,B,E,F), and 26 hpf (C,D,G,H). (A-D) Laminin is present at the *MZtmem2* MTJ by 20 so (B), although it appears disorganized compared to what is seen in *Mtmem2* siblings (A). By 26 hpf, laminin deposition appears diminished at the *MZtmem2* MTJ (D). (E-H) Fibronectin fibrillogenesis is evident at the *MZtmem2* MTJ at 20 so (F), albeit in an aberrant pattern that echoes the morphology of the *MZtmem2* somites. By 26 hpf, when much of the fibronectin has been degraded at the *Mtmem2* MTJ (G), fibronectin levels appear increased in *MZtmem2* mutants (H), particularly where fibers are detached. However, nearly all of this fibronectin degrades in *MZtmem2* mutants by 40 hpf (data not shown).

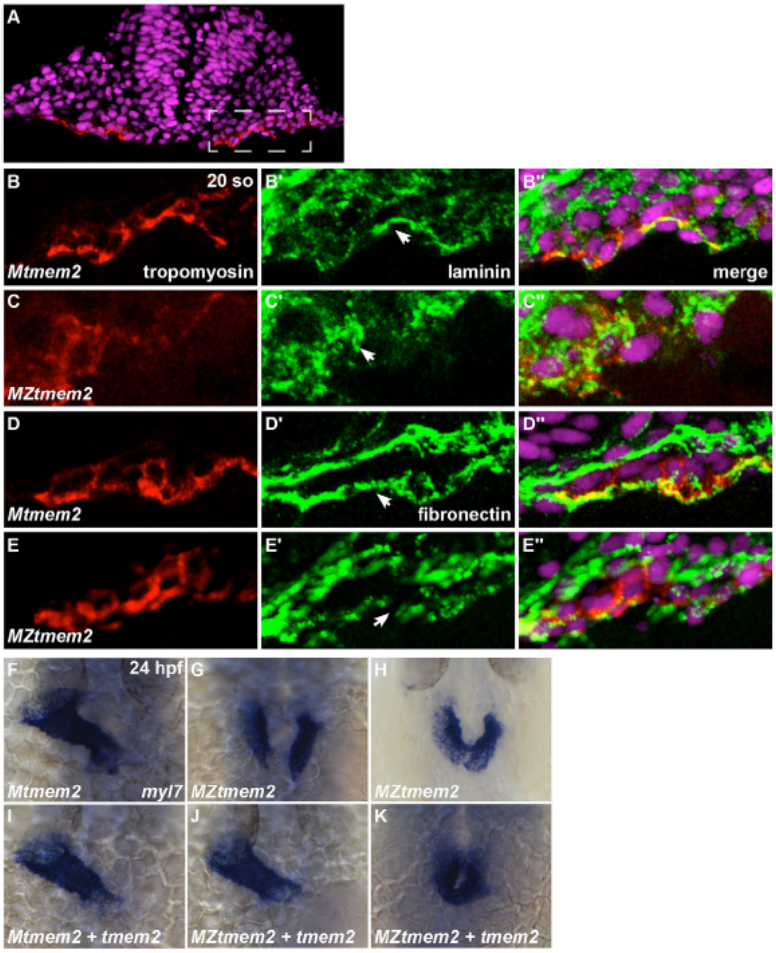

Figure 2.3. ECM disorganization accompanies cardia bifida in *MZtmem2* mutants

(**A-E**) Immunofluorescence illustrates laminin (green; B,C) and fibronectin (green, D,E) localization near the myocardium (marked by tropomyosin (red)); transverse sections, dorsal up, at 20 so, with DAPI (magenta). Dashed rectangle in A indicates the right cardiac primordium, closer views of which are shown in B-E. (B) During cardiac fusion, laminin deposition is normally evident on the basal side of the myocardium (arrowhead, B2) (Arrington and Yost, 2009). (C) In *MZtmem2* mutants, laminin organization appears severely compromised (arrowhead, C2), and a discrete basal layer does not form. (D,E) Fibronectin fibrils normally underlie the myocardium during cardiac fusion (arrowhead, D2) (Trinh and Stainier, 2004), but fibronectin deposition appears irregular and disorganized in *MZtmem2* mutants (arrowhead, E2). (**F-K**) Expression of *myl7* at 24 hpf in *Mtmem2* (F,I) and *MZtmem2* (G,H,J,K) siblings; dorsal views, rostral up. By 24 hpf, the heart tube assembles normally in *Mtmem2* siblings (F), but *MZtmem2* mutants typically exhibit cardia bifida (G). Occasionally, *MZtmem2* mutants display partial cardiac fusion (H, Table 2.S2). Injection of *tmem2* mRNA rescues cardiac fusion (K) in *MZtmem2* mutants and can even restore heart tube formation (J; Table 2.S2), but does not affect heart formation in *Mtmem2* siblings (I; Table 2.S2).

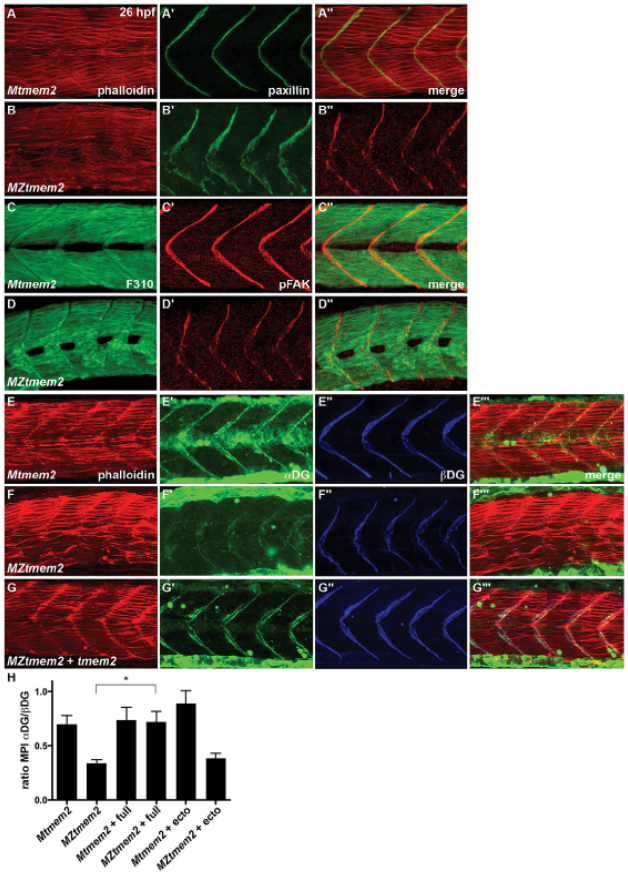

Figure 2.4. Abnormal distribution and glycosylation of CMAC components in *MZtmem2* mutants

(A-G) Immunofluorescence shows localization of paxillin (green; A,B), pFAK [pY^{397}] (red; C,D), βDG (blue; E-G), and glycosylated αDG (green; E-G) relative to muscle fibers, marked with phalloidin (red; A,B,E-G) or the antibody F310 (green; C,D); lateral views, dorsal up, at 26 hpf. (A-D) Both paxillin (B2) and pFAK (D2) are recruited to the *MZtmem2* MTJ. However, compared to the concentrated and robust localization in *Mtmem2* siblings (A2,C2), paxillin appears disorganized (B2), and pFAK levels are diminished (D2). (E-G) The antibody IIH6, which recognizes a glycosylated epitope of αDG within its laminin-binding site (Ervasti and Campbell, 1993), detects αDG at the MTJ in *Mtmem2* siblings (E2), but detects only trace amounts of glycosylated αDG at the *MZtmem2* MTJ (F2, Table 2.S3). In contrast, βDG is readily detectable at the *MZtmem2* MTJ (F3). αDG glycosylation can be rescued in *MZtmem2* mutants by injection of *tmem2* mRNA (G2, Table 2.S3). (**H**) Bar graph compares immunostaining intensity for glycosylated αDG, relative to levels of βDG, at the MTJ at 26 hpf; error bars indicate s.e.m. For each condition, we measured the mean pixel intensity (MPI) of immunostaining at 5 different MTJs in each of 3 representative embryos; see also Fig. 2.S5. Introduction of full-length Tmem2, but not the Tmem2 ectodomain, caused improvement in αDG glycosylation in *MZtmem2* mutants. Asterisk indicates significant difference from *MZtmem2* (Student's t-test; $p<0.005$).

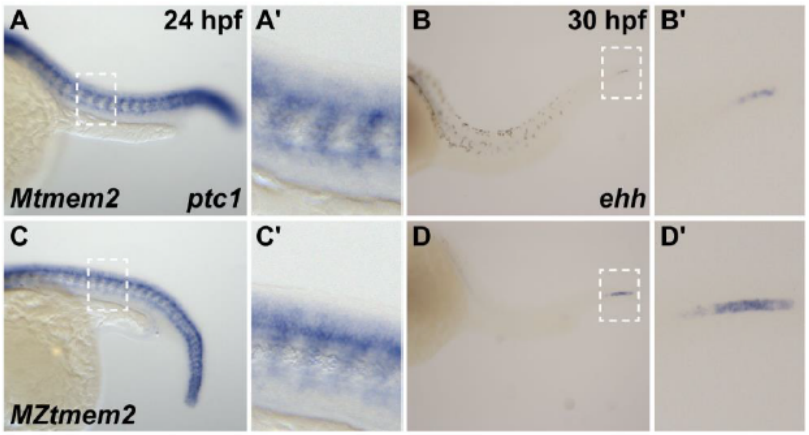

Figure 2.S1. Hedgehog signaling and notochord differentiation are intact in *MZtmem2* mutants

(**A-D**) In situ hybridization depicts expression of *ptc1* at 24 hpf (A,C) or *ehh* at 30 hpf (B,D) in *Mtmem2* (A,B) and *MZtmem2* (C,D) siblings, lateral views, anterior at left. A2-D2 show closer views of regions outlined by white rectangles in A1-D1. (A,C) Expression of *ptc1* serves as a reporter of Hedgehog signaling. Loss of Hedgehog signaling causes formation of U-shaped somites (Lewis et al., 1999; Schauerte et al., 1998; van Eeden et al., 1996), but Hedgehog signal transduction seems relatively robust in *MZtmem2* mutants. (B,D) Notochord maturation is accompanied by loss of expression of *ehh*, a chordamesoderm marker (Parsons et al., 2002b; Stemple, 2005). As notochord differentiation proceeds from anterior to posterior, *ehh* is visible only at the caudal end of the notochord by 30 hpf (B). The progression of differentiation is relatively normal in *MZtmem2* mutants (D), although the slightly increased extent of *ehh* expression that remains at 30 hpf suggests a slight delay.

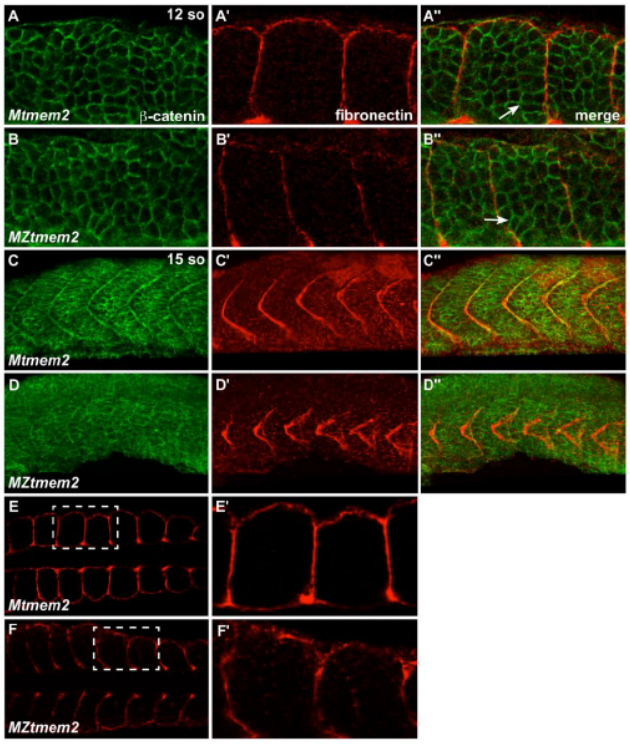

Figure 2.S2. Initial formation of somite borders appears normal in *MZtmem2* mutants

(**A-F**) Immunofluorescence indicates localization of fibronectin (red) relative to β-catenin (green) at 12 so (A,B) and 15 so (C-F). (A,B) Dorsal views, anterior to the left, of the right myotome show fibronectin localization at somite boundaries. In *MZtmem2* mutants (B2), fibronectin is deposited at each somite boundary, in a pattern comparable to that seen in *Mtmem2* siblings (A2). Additionally, muscle precursor cells at the borders of *MZtmem2* somites exhibit characteristic elongation indicative of the formation of epithelial somite boundaries (Henry et al., 2005) (B3, arrow), just as in *Mtmem2* siblings (A3, arrow). These results suggest that the initial formation of somite boundaries proceeds normally in *MZtmem2* mutants. (C,D) Lateral views, dorsal up, display fibronectin localization at somite boundaries at 15 so, when the earliest aberrations in fibronectin organization appear in *MZtmem2* mutants. In *MZtmem2* mutants (D), fibronectin is present at somite boundaries, but seems disorganized, in contrast to the sharply defined fibronectin deposition present in *Mtmem2* siblings (C). (E,F) Dorsal views, anterior to the left, indicate that fibronectin is present at somite boundaries at 15 so in *MZtmem2* mutants (F), as it is in *Mtmem2* siblings (E). E2 and F2 show closer views of regions outlined by white rectangles in E1 and F1.

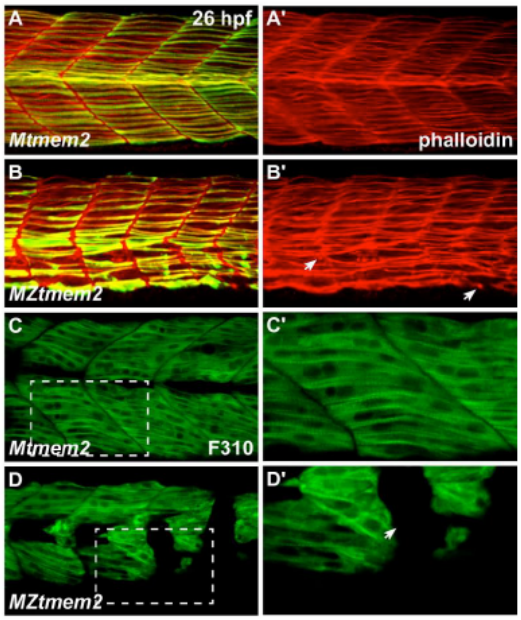

Figure 2.S3. Disruption of fast muscle fiber attachment in *MZtmem2* mutants
(**A-D**) Immunofluorescence reveals muscle fiber organization, using phalloidin (red in A,B) to recognize both fast and slow fibers, F59 (green in A,B) to recognize slow fibers (Devoto et al., 1996), and F310 (green in C,D) to recognize fast fibers (Nord et al., 2014); lateral views, dorsal up, at 26 hpf. (A,B) In addition to exhibiting detachment of $F59^{+}$ slow muscle fibers (B1; see also Fig. 2.1H), *MZtmem2* mutants display detachment of $F59^{-}$ fast muscle fibers (arrows, B2), in contrast to the attached fibers observed in *Mtmem2* siblings (A). (C,D) Similarly, *MZtmem2* mutants (D) display detachment of $F310^{+}$ fast muscle fibers (arrow, D2), in contrast to the attachment seen in *Mtmem2* siblings (C). C2 and D2 show closer views of regions outlined by white rectangles in C1 and D1.

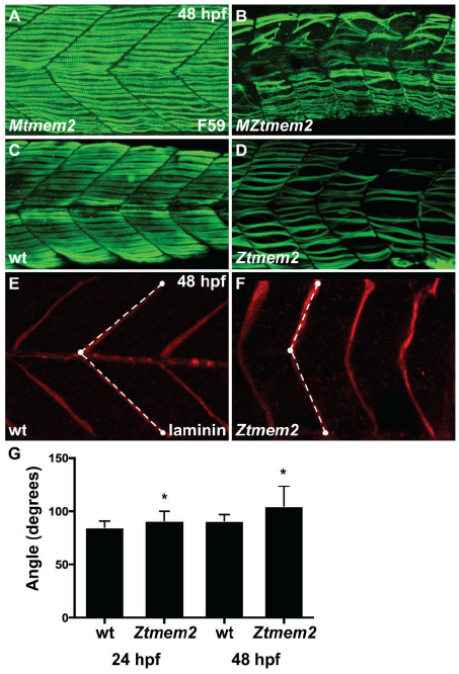

Figure 2.S4. Impairment of muscle fiber organization in zygotic *tmem2* mutants (**A-D**) Immunofluorescence with F59 (green) reveals slow muscle fiber organization; lateral views with dorsal up at 48 hpf. At this stage, *MZtmem2* mutants (B) exhibit detachment and disorganization of slow muscle fibers, in contrast to the normal attachment seen in their *Mtmem2* siblings (A). Although we have not observed muscle fiber detachment in zygotic *tmem2* (*Ztmem2*) mutants at 24 hpf (data not shown), we have found fiber detachment and disorganization in some *Ztmem2* mutants (D) by 48 hpf (n=4 out of 33 *Ztmem2* mutants examined). (**E,F**) Immunofluorescence detecting laminin (red) deposition at the MTJ reveals somite shape defects in *Ztmem2* mutants. In wild-type (E) and *Ztmem2* (F) sibling embryos, somite shape was evaluated by measuring the angle formed at the MTJ. White dots represent examples of the reference points chosen at the horizontal myoseptum, the dorsal edge of the MTJ, and the ventral edge of the MTJ; dashed lines represent the angle measured using ImageJ software. (**G**) Bar graph compares average angles formed at the MTJ in wild-type and *Ztmem2* embryos at 24 hpf and 48 hpf (in wild-type, n=85 at 24 hpf and n=75 at 48 hpf; in *Ztmem2*, n=52 at 24 hpf and n=154 at 48 hpf). Error bars indicate s.d., and asterisks indicate a significant difference from wild-type (Student's t-test; $p<0.0001$). Somite shapes in *Ztmem2* mutants become less chevron-shaped and more U-shaped over time, presumably as maternal supplies of *tmem2* are depleted and muscle fiber defects accumulate.

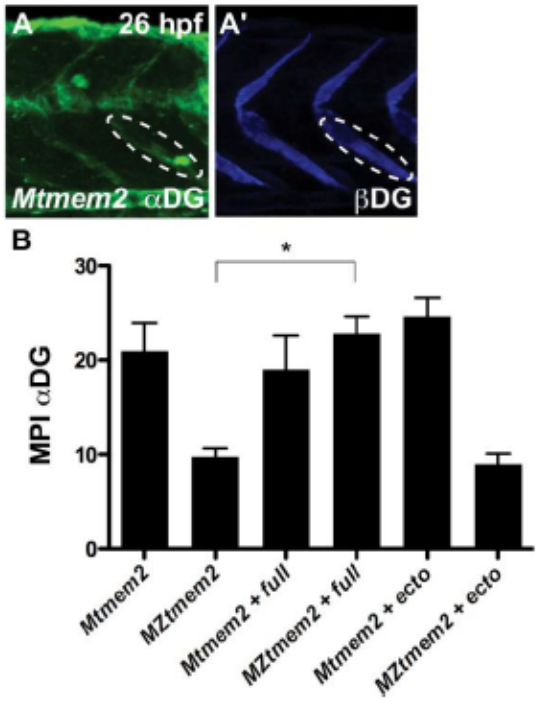

Figure 2.S5. Quantification of intensity of immunostaining for dystroglycan at the MTJ

(**A**) Confocal reconstruction depicts immunostaining for glycosylated αDG (A1) and βDG (A2) in a *Mtmem2* embryo at 26 hpf; lateral view, dorsal up. To quantify the intensity of immunostaining through the entire depth of the confocal stack, we used Imaris software to rotate each reconstruction 30 degrees toward the right and then used ImageJ software to measure the mean pixel intensity (MPI) within an oval-shaped region of interest positioned at the MTJ. Ovals of the same size and in the same position were used to measure MPI for both glycosylated αDG and βDG (ovals in A1,A2). (**B**) Bar graph compares MPI of immunostaining for glycosylated αDG at the MTJ at 26 hpf; error bars indicate s.e.m. For each condition, we measured the MPI at 5 different MTJs in each of 3 representative embryos (*Mtmem2*: 2 embryos presenting normal staining and 1 embryo presenting traces of staining; *MZtmem2*: 2 embryos presenting traces of staining and 1 embryo presenting no staining; *Mtmem2* + full: 2 embryos presenting normal staining and 1 embryo presenting traces of staining; *MZtmem2* + full: 3 embryos presenting normal staining; *Mtmem2* + ecto: 3 embryos presenting normal staining; *MZtmem2* + ecto: 2 embryos presenting traces of staining and 1 embryo presenting no staining). Introduction of full-length Tmem2, but not the Tmem2 ectodomain, caused evident improvement in aDG glycosylation in *MZtmem2* mutants. Asterisk indicates significant difference from *MZtmem2* (Student's t-test; $p<0.01$). See also Fig. 2.4H and Table 2.S3.

Table 2.S1. Rescue of muscle fiber attachment by injection of *tmem2* mRNA

		Muscle fiber phenotype at 48 hpf		
		many detached	few detached	all attached
Mtmem2	uninjected			8/8 (100%)
MZtmem2	uninjected	9/9 (100%)		
Mtmem2	full-length			7/7 (100%)
MZtmem2	full-length	1/17 (6%)	1/17 (6%)	15/17 (88%)
Mtmem2	ectodomain		1/2 (50%)	1/2 (50%)
MZtmem2	ectodomain	2/8 (25%)	3/8 (25%)	3/8 (37.5%)

Summary of 3 independent experiments evaluating whether injection of mRNA encoding either full-length Tmem2 or the Tmem2 ectodomain can rescue the muscle fiber detachment defects in *MZtmem2* mutants. Genotype (*Mtmem2* and *MZtmem2*) and mRNA injected (uninjected, full-length, or ectodomain) are provided for each set of embryos. Data indicate the fraction of examined embryos displaying severe muscle fiber detachment, a small number of detached fibers, or normal fiber attachment. For each embryo, we examined 11 somites on the left side of the myotome, using immunofluorescence with F59 and phalloidin to reveal muscle fiber organization. Embryos were classified as "many detached" if fiber detachment was evident in all 11 somites examined and as "few detached" if fiber detachment was evident in 5 or fewer somites. In a subset of these embryos, we counted the numbers of attached and detached $F59^{+}$ fibers within the 11 somites examined, and this quantification is presented in Fig. 2.1L. Full-length Tmem2 and the Tmem2 ectodomain are both capable of rescuing muscle fiber attachment in *MZtmem2* mutants, although full-length Tmem2 seems to rescue more efficiently.

Table 2.S2. Rescue of cardiac fusion by injection of *tmem2* mRNA

		Cardiac fusion phenotype at 24 hpf			
		Cardia Bifida	partial fusion	cardiac ring	heart tube
Mtmem2	uninjected				8/8 (100%)
MZtmem2	uninjected	19/23 (83%)	4/23 (17%)		
Mtmem2	full-length				27/27 (100%)
MZtmem2	full-length			4/18 (22%)	14/18 (78%)
Mtmem2	ectodomain		1/13 (8%)		12/13 (92%)
MZtmem2	ectodomain	2/28 (7%)	7/28 (25%)	17/28 (61%)	2/28 (7%)

Summary of 4 independent experiments evaluating whether injection of mRNA encoding either full-length Tmem2 or the Tmem2 ectodomain can rescue the cardiac fusion defects in *MZtmem2* mutants. Genotype (*Mtmem2* and *MZtmem2*) and mRNA injected (uninjected, full-length, or ectodomain) are provided for each set of embryos. Cardiac phenotypes were assessed through in situ hybridization for *myl7*, as in Fig. 2.3F-K. Data indicate the fraction of examined embryos displaying cardia bifida (as in Fig. 2.3G), partial fusion at the posterior end of the cardiac primordia (as in Fig. 2.3H), fusion to form a ring of cardiomyocytes (as in Fig. 2.3K), or normal heart tube assembly (as in Fig. 2.3J). Full-length Tmem2 and the Tmem2 ectodomain are both capable of rescuing cardiac fusion in *MZtmem2* mutants, although full-length Tmem2 seems to rescue more efficiently.

Table 2.S3. Rescue of αDG glycosylation by injection of *tmem2* mRNA

		IIH6 staining at 26 hpf		
		no staining	traces of staining	normal staining
Mtmem2	uninjected		4/26 (15%)	22/26 (85%)
MZtmem2	uninjected	18/32 (56%)	14/32 (44%)	
Mtmem2	full-length		1/9 (11%)	8/9 (89%)
MZtmem2	full-length		2/13 (15%)	11/13 (85%)
Mtmem2	ectodomain			5/5 (100%)
MZtmem2	ectodomain	1/7 (14%)	6/7 (86%)	

Summary of 3 independent experiments evaluating whether injection of mRNA encoding either full-length Tmem2 or the Tmem2 ectodomain can rescue αDG glycosylation at the MTJ in *MZtmem2* mutants. Genotype (*Mtmem2* and *MZtmem2*) and mRNA injected (uninjected, full-length, or ectodomain) are provided for each set of embryos. αDG glycosylation was assessed through immunostaining of with the antibody IIH6, as in Fig. 2.4E'-G'. Data indicate the fraction of examined embryos displaying no IIH6 staining at the MTJ, trace amounts of IIH6 staining at the MTJ (as in Fig. 2.4F'), or normal IIH6 staining at the MTJ (as in Fig. 2.4E' and 2.4G'). In a subset of these embryos, we measured the intensity of IIH6 staining at 5 different MTJs in each of 3 representative embryos; the results of this quantitative analysis are presented in Figs. 2.4H and 2.S5. Full-length Tmem2 is capable of rescuing αDG glycosylation at the MTJ in *MZtmem2* mutants, whereas introduction of the Tmem2 ectodomain is not sufficient to rescue normal levels of glycosylated amutants, whereas introduction of the Tmem2 ectodomain is not sufficient to rescue normal levels of glycosylated αDG in this context.

Table 2.S4. Antibodies used for immunofluorescence

	Antigen	Reagent	Vendor	Dilution
Primary antibodies	Myosin heavy chain	Mouse monoclonal (F59)	Developmental Studies Hybridoma Bank (supernatant)	1:10
	Laminin	Rabbit polyclonal	Sigma (#L9393)	1:100
	Fibronectin	Rabbit polyclonal	Sigma (#F3648)	1:100
	b-catenin	Mouse monoclonal (15B8)	Sigma (#C7207)	1:500
	Tropomyosin	Mouse monoclonal (CH1)	Developmental Studies Hybridoma Bank (supernatant)	1:10
	Paxillin	Mouse monoclonal (349)	BD Biosciences (#612405)	1:50
	FAK [pY^{397}]	Rabbit polyclonal	Invitrogen (#44-624G)	1:50
	Myosin heavy chain	Mouse monoclonal (F310)	Developmental Studies Hybridoma Bank (supernatant)	1:10
	a-dystroglycan	Mouse monoclonal (IIH6-C4)	Santa Cruz Biotechnology (#sc-73586)	1:50
	b-dystroglycan	Mouse monoclonal (43DAG1/8D5)	Novocastra (#NCL-b-DG)	1:50
Secondary antibodies	Rabbit IgG	Goat polyclonal; Alexa Fluor 594	Molecular Probes (#A11012)	1:200
	Rabbit IgG	Goat polyclonal; Alexa Fluor 647	Molecular Probes (#A21245)	1:200
	Mouse IgG1	Goat polyclonal; FITC	Southern Biotechnology (#1070-02)	1:100

Chapter 2, in full, is a reprint of the material as it appears in: Lucile Ryckebusch, Lydia Hernandez, Carole Wang, Jenny Phan, Deborah Yelon. (2016). Tmem2 regulates cell-matrix interactions that are essential for muscle fiber attachment. *Development* 143(16): p.2965-2972. Lydia Hernandez is a primary researcher/author on this paper. Lydia Hernandez contributed to designing the experiments, conducting research, interpreting results, and writing the manuscript presented in Chapter 2. Lucile Rycebusch contributed to designing the experiments, conducting research, interpreting results, and writing the manuscript presented in Chapter 2. Deborah Yelon contributed to designing the experiments, interpreting results, and writing the manuscript presented in Chapter 2. Carole Wang and Jenny Phan performed experiments and analyzed data presented in Chapter 2.

Chapter 3: Tmem2 restricts atrioventricular canal differentiation by regulating degradation of hyaluronic acid

ABSTRACT

Atrioventricular valve development relies upon the precisely defined dimensions of the atrioventricular canal (AVC). Transmembrane protein 2 (Tmem2) is a key player in this process: in zebrafish, zygotic *tmem2* (*Ztmem2*) mutants display ectopic AVC characteristics alongside excess hyaluronic acid (HA) deposition. However, the molecular mechanisms of Tmem2 function during AVC differentiation remain unclear. To address this, we performed a structure-function analysis and determined that the extracellular domains of Tmem2 are crucial for its role in restricting AVC boundaries. These same domains are also essential for an earlier function of Tmem2 in promoting cardiomyocyte movement during cardiac fusion. Tmem2 has recently been shown to act as a hyaluronidase, and degradation of HA can restore the restriction of AVC differentiation in *Ztmem2* mutants. Furthermore, a residue vital for Tmem2 hyaluronidase activity is also critical for delimiting AVC differentiation but is not essential during cardiac fusion. Overall, these data support a model in which Tmem2 regulates AVC differentiation by controlling the degradation of HA and suggest that this mechanism for Tmem2 function could be context-dependent.

INTRODUCTION

Atrioventricular valves divide the cardiac chambers and must be precisely patterned and spatially defined in order to insure proper blood flow. Atrioventricular valve development occurs after the onset of cardiac function and within an environment of ongoing morphological changes in the heart. The primitive heart begins as a linear tube comprised of two layers: an inner, vascular layer, the endocardium, and an outer layer of muscle, the myocardium. Between these two layers is a lining of extracellular matrix (ECM) known as the cardiac jelly. At the junction between the ventricle and the atrium, characteristic morphological changes distinguish a region referred to as the atrioventricular canal (AVC). Cells within the AVC must differentiate and undergo specific structural changes, ultimately forming swellings of tissue known as endocardial cushions (Markwald et al., 1977). Eventually, through extensive tissue remodeling, endocardial cushions give rise to the valve leaflets of the mature atrioventricular valve (Armstrong and Bischoff, 2004).

Although the precise mechanisms for coordination of AVC differentiation are unclear, we do understand that appropriately confined Wnt signaling is required to trigger specific changes in the AVC myocardium and endocardium. In zebrafish, a defined region of Wnt signaling activity delineates the AVC (Moro et al., 2012), and aberrant expansion of Wnt signaling leads to ectopic AVC differentiation. For example, in zebrafish *apc* mutants, which exhibit constitutively active Wnt signaling due to persistent nuclear presence of β-catenin, expression of AVC molecular markers, such as

bmp4, is expanded and excess endocardial cushion formation occurs (Hurlstone et al., 2003). Conversely, attenuation of Wnt signaling, either through overexpression of *apc* or the Wnt antagonist Dkk1, reduces expression of *bmp4* in the AVC (Verhoeven et al., 2011) and inhibits formation of endocardial cushions (Hurlstone et al., 2003). These findings suggest that Wnt signaling is essential for AVC differentiation and demonstrate that *bmp4* expression is induced downstream of Wnt signaling. The upstream factors that regulate Wnt signaling, however, remain undefined.

Our earlier work has identified *tmem2* as a key player in the process of delimiting AVC differentiation. Zebrafish *tmem2* mutants display expansion of AVC molecular markers as well as a failure to appropriately restrict formation of endocardial cushions (Smith et al., 2011; Totong et al., 2011). These defects are accompanied by increased deposition of the glycosaminoglycan hyaluronic acid (HA), a major component of the cardiac ECM, between the endocardium and the myocardium (Smith et al., 2011). In addition to its role in restricting AVC differentiation, *tmem2* has been implicated in vessel sprouting (De Angelis et al., 2017), promoting cardiac fusion (Totong et al., 2011), and stabilizing muscle fiber attachments (Ryckebusch et al., 2016), and aberrant ECM deposition has been observed in each of these contexts in *tmem2* mutants. Taken together, these observations prompt the hypothesis that *tmem2* may control cardiovascular and muscle morphogenesis through regulation of the ECM.

Despite recent work examining the various activities of Tmem2, relatively little is known about how Tmem2 structure informs its various physiological functions. Tmem2 is a single-pass type II transmembrane protein with a short cytoplasmic portion and an extended extracellular region (Smith et al., 2011; Totong et al., 2011). Within the extracellular region, there are four recognized domains – a G8 domain, a Pander-like Tmem2 domain (PLT), a series of parallel beta helix (PbH1) repeats, and a second Pander-like (PL) domain. The functions of these types of domains have been defined in the context of other proteins. For example, Pander-like domains have been identified in proteins involved in glycosylation, apoptosis, and metastasis (Cao et al., 2003; Johansson et al., 2013; Pereira et al., 2014; Yoshida et al., 2013). The G8 domain of KIAA1199, a protein with structural similarities to Tmem2, can bind the EGF receptor and activate EGF signaling (Shostak et al., 2014). PbH1 repeats typically form pectin lyase folds with enzymatic activity capable of degrading polysaccharides (Henrissat et al., 1995; Mayans et al., 1997). At the onset of our studies, it was unknown whether or how any of these domains were relevant to the activities of Tmem2.

Recently, mammalian cell culture studies have identified Tmem2 as a cell surface hyaluronidase capable of depolymerizing large HA molecules down to ~5 kDa fragments (Yamamoto et al., 2017). Moreover, the hyaluronidase activity of Tmem2 appears to be important to its function in the context of angiogenesis. Zebrafish *tmem2* mutants exhibit decreased

intersegmental vessel (ISV) sprouting as well as increased HA deposition surrounding these vessels, and reduction of HA levels in *tmem2* mutants via treatment with exogenous hyaluronidase improved their ISV sprouting (De Angelis et al., 2017). Together, these findings support the idea that Tmem2 can control morphogenetic processes by regulating degradation of HA.

Does the ability of Tmem2 to function as a hyaluronidase also underlie its influence on the restriction of AVC differentiation? This seems like a promising model in light of the excess HA deposition observed in the *tmem2* mutant heart (Smith et al., 2011). In addition, mutations affecting HA synthesis are known to result in defective AVC formation. In mice, loss of function of Hyaluronan Synthase 2 (Has2), which synthesizes HA, inhibits formation of endocardial cushions (Camenisch et al., 2000). Conversely, zebrafish *dicer* mutants have increased *has2* expression, resulting in excess HA deposition and ectopic endocardial cushion differentiation (Lagendijk et al., 2011). Knockdown of *has2* is able to rescue this phenotype and results in proper AVC restriction (Lagendijk et al., 2011). While it is clear that the levels of HA deposition are important for appropriate AVC development, the functional relationship between Tmem2, AVC differentiation, and HA catabolism has remained unexamined.

Here, we show that the four identified domains within the Tmem2 extracellular region are critical for its roles in AVC restriction, cardiac fusion, and muscle fiber maintenance. Examination of the subcellular localization of

Tmem2 suggests that these domains are likewise important for correct trafficking of Tmem2 to the plasma membrane. Finally, our results show that the activity of Tmem2 as a hyaluronidase is critical for restricting AVC differentiation. Intriguingly, however, we demonstrate that this same activity is inessential to the role of Tmem2 in promoting cardiac fusion. Overall, through structure-function analysis of Tmem2, we identify Tmem2 as a regulator of HA degradation in the context of AVC development and suggest that this mechanism for Tmem2 function could be context-dependent.

RESULTS

Extracellular domains of Tmem2 are critical for proper AVC differentiation

To gain insight into the molecular mechanism by which Tmem2 restricts AVC differentiation, we sought to identify which domains of Tmem2 are critical for its function. For this structure-function analysis, we have examined whether altered forms of Tmem2 – variants either replacing or lacking identified domains (Fig. 3.1) – could rescue aspects of the *tmem2* mutant phenotype. All constructs used here are fusion proteins with Gfp attached to the C-terminus, since in prior studies, we have shown that expression of *tmem2-gfp* rescues *tmem2* mutant defects as effectively as expression of *tmem2* without a C-terminal tag (Totong et al., 2011). Using these constructs,

we have examined which domains of Tmem2 are required for regulating the expression pattern of *bmp4*, a molecular marker of the AVC myocardium (Hurlstone et al., 2003). In wild-type embryos at 48 hours post fertilization (hpf), concentrated expression of *bmp4* is evident in a confined territory at the AVC (Fig. 3.2A). In contrast, zygotic *tmem2* (*Ztmem2*) mutants fail to appropriately delimit *bmp4* expression and instead exhibit *bmp4* expression broadly throughout the ventricle (Totong et al., 2011) (Fig. 3.2B). Injection of mRNA encoding full-length *tmem2-gfp* at the one-cell stage is able to rescue the *bmp4* expression pattern in *Ztmem2* mutants (Fig. 3.2D; Table 3.1). We therefore examined whether expression of *tmem2* variants could rescue mutant defects as effectively as expression of full-length *tmem2*.

We wondered whether the cytoplasmic and transmembrane domains of Tmem2 were required for its activity, perhaps enabling Tmem2 to function as a signaling molecule. To address this question, we created the variant *htrc-tmem2*, in which the cytoplasmic and transmembrane domains of Tmem2 have been replaced with those from the human transferrin receptor, another type II transmembrane protein (Fig. 3.1). Expression of *htrc-tmem2* can rescue the *bmp4* expression pattern in *Ztmem2* mutants, albeit not as robustly as full-length *tmem2* does (Table 3.1). This result indicated that the Tmem2 cytoplasmic domain is not essential for its activity during AVC differentiation and suggested that the primary function of Tmem2 might take place outside of the cell. To test this idea, we examined the effectiveness of a secreted

version of the Tmem2 ectodomain, *sc-tmem2* (Fig. 3.1). Expression of *sc-tmem2* in *tmem2* mutants could rescue the *bmp4* expression pattern, but not as effectively as *htrc-tmem2* or full-length *tmem2* (Table 3.1). These findings suggest that membrane localization of Tmem2 is valuable, although not absolutely required, for its function in AVC restriction. Having demonstrated that the Tmem2 ectodomain is functional, we focused more closely on the extracellular region and examined variants of Tmem2 that lack individual extracellular domains. Notably, Tmem2 variants lacking the G8, PLT, PbH1, or PL domains (Fig. 3.1) could not rescue the *bmp4* phenotype in *Ztmem2* mutants (Fig. 3.2F; Table 3.1). Taken together, these data suggest that the extracellular domains of Tmem2 are critical for its function to delimit AVC differentiation.

Extracellular domains of Tmem2 are critical for promoting cardiac fusion

Next, we wondered whether the extracellular domains that are important for the role of Tmem2 during AVC differentiation are also important for the activity of Tmem2 in other developmental contexts. Strikingly, maternal-zygotic *tmem2* (*MZtmem2*) mutants do not complete cardiac fusion (Ryckebusch et al., 2016; Totong et al., 2011): cardiomyocytes are significantly hindered in their movement toward the midline and instead remain in bilateral clusters (Fig. 3.3B) or only partially fuse at the midline by 24 hpf (Fig. 3.3C). In contrast, maternal *tmem2* (*Mtmem2*) mutants form primitive

heart tubes (Fig. 3.3A) and are indistinguishable from wild-type embryos. Similar to what we observed with AVC differentiation, expression of full-length *tmem2* rescues the cardiac fusion defects in *MZtmem2* mutants (Fig. 3.2E,F; Table 3.2). Expression of *htrc-tmem2* similarly rescues cardiac fusion (Fig. 3.3H; Table 3.2), suggesting that the specific cytoplasmic and transmembrane domains of Tmem2 are not essential for its role in promoting cardiomyocyte movement. Expression of *sc-tmem2* can also rescue cell movement in *MZtmem2* mutants, albeit not as efficiently as full-length *tmem2* (Table 3.2). Consistent with what we observed in the context of AVC formation, these findings support the idea that membrane localization could be important for optimal Tmem2 activity. Finally, none of the variants that include extracellular domain deletions were able to rescue the *MZtmem2* cardiac fusion defects in *MZtmem2* mutants (Fig. 3.3J; Table 3.2), indicating that the G8, PLT, PbH1, and PL domains are important for Tmem2 function during cardiac fusion, as well as during AVC differentiation.

Having seen that the extracellular domains of Tmem2 are critical for its function during multiple aspects of cardiac morphogenesis, we next wondered whether these same regions are important for Tmem2 activity during skeletal muscle morphogenesis. In addition to cardiac fusion defects, *MZtmem2* mutants exhibit detachment of muscle fibers from somite boundaries (Ryckebusch et al., 2016). We have previously shown that full-length *tmem2* and the secreted version of the Tmem2 ectodomain (*sc-tmem2*) can rescue

muscle fiber detachment in *MZtmem2* mutants (Ryckebusch et al., 2016) (Fig. 3.S1G). Given this, we next wanted to determine which portions of the ectodomain were important for the role of Tmem2 in stabilizing muscle fiber attachments. Interestingly, we found that expression of *tmem2* variants that are missing either the G8 or PL domain can rescue muscle fiber detachment in *MZtmem2* mutants, albeit not as effectively as full-length *tmem2* (Fig. 3.S1G). In contrast, *tmem2* variants lacking either the PLT or PbH1 domains fail to ameliorate *MZtmem2* muscle detachments (Fig. 3.S1D-F,G), suggesting that the PLT and PbH1 extracellular domains are the most essential for Tmem2 function in maintaining skeletal muscle integrity during morphogenesis.

Taken together, our results indicate that domains within the Tmem2 extracellular region are critical for its function during multiple developmental contexts. Further, our findings suggest that localization of Tmem2 to the plasma membrane enhances its function during both cardiac fusion and AVC differentiation.

Non-functional Tmem2 variants fail to localize to the plasma membrane

Having seen that localization of Tmem2 to the membrane appears to enhance its function, we next wanted to confirm the subcellular localization of our Tmem2 variants *in vivo*. Through visualization of Gfp localization in live embryos following injection with variant mRNA, we were able to confirm the presence and relative stability of all Tmem2 variants (Fig. 3.4). Consistent

with what we have observed in our prior work, full-length Tmem2 localized to the plasma membrane (Totong et al., 2011) (Fig. 3.4A). Likewise, Htrc-Tmem2 was also visible at the membrane (Fig. 3.4B). The secreted version of Tmem2, Sc-Tmem2, appeared to traffic to the extracellular region (Fig. 3.4C). Interestingly, none of the variants containing extracellular domain deletions localized to the plasma membrane (Fig. 3.4D-H), suggesting that all four of these domains influence Tmem2 localization. Keeping in mind that these constructs fail to rescue aspects of Tmem2 function, we surmise that correct subcellular localization of Tmem2 is a critical component of its activity.

Ztmem2 mutants exhibit excessive HA deposition

Several pieces of evidence point to a relationship between Tmem2 function and regulation of HA turnover. Recent work in mammalian cells has identified Tmem2 as a cell surface hyaluronidase (Yamamoto et al., 2017). Additional work investigating the function of Tmem2 during angiogenesis showed that increased levels of HA accompanied the vessel sprouting defects observed in *tmem2* mutants (De Angelis et al., 2017). Moreover, degradation of HA with exogenous hyaluronidase ameliorated the *tmem2* mutant angiogenesis defects, thus supporting the model that Tmem2 functions to regulate degradation of HA in *vivo*. Could increases in HA levels also underlie the *Ztmem2* cardiac defects?

Interestingly, a different mutant allele of *tmem2*, *wkm*^{hu5935} (Smith et al.,

2011), exhibits excess HA deposition between the endocardium and the myocardium. Consistent with this, we find that *Ztmem2*^{sk38} mutants display aberrant cardiac deposition of HA. By employing a HA binding protein (HABP) to visualize HA, we observed a layer of HA deposition between the endocardium and the myocardium of wild-type embryos at 48 hpf (Fig. 3.5A-C). In *Ztmem2* mutants, however, we observed a dramatic increase in the amount of HA deposition both at the AVC and throughout the ventricle (Fig. 3.5D-F). Thus, our data bolster earlier findings that Tmem2 indeed constrains HA levels within cardiac tissue. We also found that *Ztmem2* mutants display excess chondroitin sulfate (CS) deposition. Whereas CS localization is concentrated at the AVC in wild-type embryos (Fig. 3.S2B,C), *Ztmem2* mutants exhibit increased CS deposition at the AVC and throughout the ventricular chamber (Fig. 3.S2E,F). These data suggest that Tmem2 plays an important role in limiting deposition of multiple components of the cardiac jelly.

Tmem2 restricts AVC differentiation through HA regulation

Given that Tmem2 functions to regulate HA degradation in other developmental contexts, we wondered whether the influence of Tmem2 on AVC differentiation might be mediated via HA degradation as well. To test this, we injected hyaluronidase into the pericardial space of *Ztmem2* mutant and wild-type sibling embryos at 30 hpf, when deposition of the cardiac jelly first becomes visible (Peal et al., 2009). Control embryos were injected with

the same volume of PBS (Fig. 3.6A,B). We found that hyaluronidase treatment improved the spatial restriction of *bmp4* expression in the majority of mutant embryos examined (Fig. 3.6D; Table 3.3), whereas this treatment did not typically disrupt the *bmp4* expression pattern in wild-type embryos (Fig. 3.6C; Table 3.3). From these results, we surmise that Tmem2 restricts AVC differentiation by limiting HA levels.

Having seen this, we next wanted to determine whether Tmem2 function influences Wnt signaling upstream of *bmp4*. We used the transgenic zebrafish line *Tg(7xTCF-Xla.Siam:GFP)* (Moro et al., 2012) to visualize Wnt activity in both wild-type and *Ztmem2* mutant embryos. As previously reported, Wnt pathway activity is prominent within the wild-type AVC at 48 hpf (Fig. 3.7A, B) (Moro et al., 2012). Intriguingly, Wnt signaling appears to expand beyond the normal AVC region in *Ztmem2* mutants (Fig. 3.7C,D) (Table 3.4). Can manipulation of HA levels rescue the ectopic Wnt signaling in *Ztmem2* mutants? Indeed, hyaluronidase treatment noticeably restrained the expansion of Wnt signaling in the majority of *Ztmem2* mutants examined (Fig. 3.7G,H), whereas wild-type sibling embryos were mostly unaffected (Fig. 3.7E,F) (Table 3.4). Thus, our data suggest that constraint of HA levels by Tmem2 plays a critical role in appropriately restricting Wnt signaling activity to the AVC. Importantly, these results provide the first evidence that Tmem2 acts upstream of Wnt signaling to delimit AVC differentiation.

Tmem2 residue 267 is essential for its function in AVC restriction, but not for its role in cardiac fusion

If Tmem2 is restricting AVC differentiation through HA regulation, how does it accomplish this? One possibility is that Tmem2 can affect HA turnover directly. In human Tmem2, residue 265 in the PLT domain has been shown to be critical for its activity as a hyaluronidase (Yamamoto et al., 2017). In order to examine whether the ability of Tmem2 to degrade HA impacts its functions during cardiac morphogenesis, we altered the corresponding residue within zebrafish Tmem2 (R267H) (Fig. 3.1) and tested whether this variant could rescue *tmem2* mutant phenotypes. Strikingly, we found that expression of *R267H* did not restore a normal *bmp4* expression pattern in *Ztmem2* mutants (Fig. 3.8B, Table 3.1), nor did it seem to affect the *bmp4* expression pattern in wild-type siblings (Fig. 3.8A, Table 3.S1). These findings suggest that the ability of Tmem2 to depolymerize HA is essential for its function in spatially restricting AVC differentiation.

Next, we examined whether the R267H variant was functional in the context of cardiac fusion. Here, we were intrigued to see that expression of *R267H* efficiently rescues the *MZtmem2* cardiac fusion defect; mutant embryos expressing *R267H* assemble primitive heart tubes as frequently as those expressing full-length *tmem2* (Fig. 3.8D, Table 3.2). Thus, our data reveal that R267H is fully functional in the context of cardiac fusion, whereas it is non-functional in the context of AVC differentiation. Taken together, these

findings indicate that the requirements for Tmem2 activity are context-dependent.

Following this, we were curious to see whether R267H localizes normally to the plasma membrane. Interestingly, subcellular localization of R267H (Fig. 3.4I) does not appear similar to that of full-length Tmem2 (Fig. 3.4A). Rather than localize prominently to the plasma membrane, R267H clusters in foci within the cytoplasm. Putting this together with our observations of R267H function, one can extrapolate that having a critical amount of Tmem2 at the plasma membrane is more essential for restricting AVC differentiation than it is for promoting cardiac fusion. Overall, our findings support the possibility that Tmem2 has multiple mechanisms of activity.

DISCUSSION

Taken together, our studies shed new light on the mechanisms that spatially restrict AVC differentiation. We have demonstrated that Tmem2 is a key regulator of this process that functions to confine the distribution of Wnt signaling as well as the expression of *bmp4* to the AVC. Moreover, Tmem2 is needed to limit HA deposition, and it appears that this function of Tmem2 mediates its influence over Wnt signaling and *bmp4* expression. Our results presented here support a model whereby Tmem2 acts at the cell surface as a hyaluronidase that delimits HA distribution in the cardiac ECM, thereby

confining both Wnt and Bmp signaling, and the consequent AVC differentiation, to the atrioventricular canal.

Overall, our findings highlight the importance of appropriate HA regulation for correctly establishing AVC boundaries. It remains unresolved, however, the precise mechanism by which Tmem2 governs HA modulation and, in turn, how HA influences AVC development on the molecular level. One intriguing possibility is that Tmem2 promotes HA depolymerization, perhaps so that the smaller molecular weight HA may function as a bioactive signaling molecule. Indeed, it has been demonstrated that specific sizes of HA can induce different signaling pathways (De Angelis et al., 2017; Itano, 2008; Jiang et al., 2005; Termeer et al., 2002). For example, *tmem2* mutant zebrafish exhibit VEGF signaling defects that are rescued by introduction of HA oligomers (o-HA) (De Angelis et al., 2017). Additional research will be needed in order to determine whether it is HA deposition level or HA fragment size that informs AVC differentiation.

We do note that HA is only one of several ECM components influenced by *tmem2* function. For instance, our previous findings revealed that *MZtmem2* mutants display aberrant fibronectin and laminin organization surrounding cardiomyocytes and at myotendinous junctions (Ryckebusch et al., 2016). Additionally, we see excesses of both HA and CS deposition in *tmem2* mutant hearts. In light of these observations, it is interesting to consider that Tmem2 may have parallel roles in regulating organization of the

ECM within multiple developmental contexts. In future investigations, it will be interesting to determine precisely how Tmem2 regulates organization of these additional ECM components. Perhaps these findings could reveal alternative molecular mechanisms of Tmem2 that may be critical to its other developmental roles.

With that possibility in mind, we find it intriguing that the R267H variant of Tmem2 does not rescue AVC expansion in *Ztmem2* mutants but is adequately functional to rescue cardiac fusion in *MZtmem2* mutants. Cell culture studies have shown that this amino acid residue is critical for degradation of HA (Yamamoto et al., 2017; Yoshida et al., 2013). One interpretation of these results is that the hyaluronidase activity of Tmem2 is critical for spatial restriction of the AVC but is not essential for promoting cardiac fusion. If Tmem2 does not influence cardiac fusion through HA degradation, what is the mechanism of Tmem2 activity in this context? Perhaps Tmem2 influences ECM composition through some other means or plays another role entirely. The possibility that Tmem2 has multiple modes of function appears even more probable when we consider work investigating KIAA1199, also known as cell migration-inducing and hyaluranon binding protein (CEMIP). Although it is not a transmembrane protein, KIAA1199 is otherwise structurally very similar to Tmem2. KIAA1199 contains a G8, PLT, and PL domain as well as three conserved PbH1 repeats (Yoshida et al., 2013). Likewise, KIAA1199 has been identified as a hyaluronidase, whose

enzymatic activity relies on the corresponding amino acid residue identified as essential in Tmem2. Importantly, KIAA1199 has been shown to have multiple mechanisms of activity beyond its role as a hyaluronidase, including activation of EGF signaling and regulation of calcium release from the endoplasmic reticulum (Evensen et al., 2013; Shostak et al., 2014). Combined with the differential function we observe in Tmem2 variants across developmental contexts, the evidence suggests that Tmem2, like KIAA1199, most likely functions via multiple modes of activity that are context-dependent.

We also note that the R267H variant does not localize correctly to the plasma membrane. It may be that the aberrant subcellular localization of R267H is what accounts for its inability to restrict AVC differentiation effectively. The studies that have shown the importance of this residue for HA degradation (Yamamoto et al., 2017; Yoshida et al., 2013) have not examined whether there is a corresponding localization defect, and so it is unclear exactly why this altered residue causes the loss of hyaluronidase activity. Perhaps altering this residue disrupts key protein interactions that both traffic Tmem2 to the plasma membrane and enable it to depolymerize HA. Regardless, despite not knowing the precise mechanism by which this key residue impacts HA catabolism, our findings suggest that Tmem2 delimits differentiation of the AVC through HA regulation. Further, our findings indicate that this is likely not the sole function of Tmem2, and that Tmem2 may act in a variety of ways depending upon the developmental context.

Overall, our work investigating the role of Tmem2 in cardiac morphogenesis yields several key findings. First, we have gained new insight into the physiological relevance of identified protein domains within Tmem2. Finally, we have established Tmem2 as an essential regulator of HA in the context of AVC patterning, a finding that may prove helpful in elucidating the broader pathway of how HA influences early cardiac valve development. Although it is interesting to consider the activities of Tmem2 as a key regulator of ECM composition during developmental and disease processes, it nonetheless remains undefined whether these roles of Tmem2 are conserved in mouse and human. Future examination of the conservation of these roles will be important to assess the broader relevance of our findings.

MATERIALS AND METHODS

Zebrafish

We used the zebrafish strains *Tg(7xTCF-Xla.Siam:GFP)*^{ia4} (Moro et al., 2012) and *tmem2*^{sk38} (Totong et al., 2011). *Ztmem2* mutant embryos were generated by intercrossing *tmem2*^{sk38} heterozygotes. *MZtmem2* mutant embryos were obtained by breeding male *tmem2* heterozygotes to chimeric female fish with a *tmem2*^{sk38} mutant germline, created via germline replacement as previously described (Totong et al., 2011). *Ztmem2* and *MZtmem2* mutants were distinguished from their siblings by morphological criteria and by PCR genotyping (Totong et al., 2011). All zebrafish work followed protocols approved by the University of California, San Diego Institutional Animal Care and Use Committee (IACUC).

Immunofluorescence

Whole-mount immunofluorescence was performed as previously described (Alexander et al., 1999; Peal et al., 2009), using Rhodamine Phalloidin (Invitrogen, R415) and antibodies listed in Table 3.S3. For visualization of HA localization, staining was performed as previously described (Alexander et al., 1999) using biotinylated hyaluranon-binding protein (HABP) (EMD Millipore, Billerica, MA; 1:10) and Streptavidin 488 (Thermo Fisher Scientific, Waltham, MA; 1:500).

In situ hybridization

In situ hybridization for *myl7* (ZDB-GENE-991019-3) and *bmp4* (ZDB-GENE-980528-2059) was performed as previously described (Yelon et al., 1999).

Injection

Embryos were injected at the one-cell stage with 150 pg of mRNA encoding either full-length *tmem2* or *tmem2* variants. For live imaging of subcellular localization (Fig. 3.4), embryos were injected at the one-cell stage with only 50 pg of mRNA. Capped mRNA was synthesized using the mMessage mMachine Sp6 kit (Ambion, Foster City, CA).

For hyaluronidase treatment, embryos were injected within the pericardial sac at 30 hpf with 1 nl (~50 units) of hyaluronidase from *Streptomyces hyalurolyticus* (H1136; Sigma, St. Louis, MO). PBS was injected as a control.

Imaging

Fluorescent images are maximal intensity projections of confocal reconstructions of 0.5 micron thick slices acquired using a 25x water objective on a Leica SP5 microscope and analyzed using Imaris software (Bitplane). For Fig. 3.4. Z-stacks contain 14 slices each. For Fig. 3.5. Z-stacks contain 4 slices each. For Figs. 3.7, 3.S1, and 3.S2, Z-stacks contain between 120-150

slices. Additional images were captured using a Zeiss Axiozoom microscope with a Zeiss AxioCam and processed using Zeiss AxioVision and Adobe Creative Suite.

Tmem2 constructs

Coding sequences for all constructs, including *tmem2* and *tmem2* variants, were inserted into a pCS2 vector with an in-frame C-terminal Gfp tag. Variants *sc-tmem2*, *htrc-tmem2*, and *ΔC-term* were generated using standard subcloning procedures. Variants *ΔG8*, *ΔPLT*, *ΔPbH1*, *ΔPL*, and *R267H* were generated using Gibson Assembly cloning (New England Biolabs, Ipswich, MA). Details of primer sequences used for making constructs are available upon request.

Sc-tmem2 includes the secretory signal sequence (the first 33 amino acids) from the zebrafish *sonic hedgehog* (*shh*) gene (Ekker et al., 1995), cloned into a version of *tmem2-gfp* (Totong et al., 2011) that is missing the Tmem2 cytoplasmic and transmembrane domains (amino acids 1-103). Htrc-tmem2 includes the cytoplasmic and transmembrane domains of the type II transmembrane protein human transferrin receptor (amino acids 1-96) (Jing et al., 1990), cloned into a version of *sc-tmem2* vector that is missing the *shh* secretory signal sequence. ΔC-term includes the first 875 amino acids of Tmem2, followed by a Gfp tag. ΔG8 lacks amino acids 122-246 of Tmem2-Gfp**.** ΔPLT lacks amino acids 222-389 of Tmem2-Gfp. ΔPbH1 lacks amino

acids 672-815 of Tmem2-Gfp. ΔPL lacks amino acids 1239-1327 of Tmem2-Gfp. R267H incorporates an arginine to histidine change at residue 267 of Tmem2-Gfp.

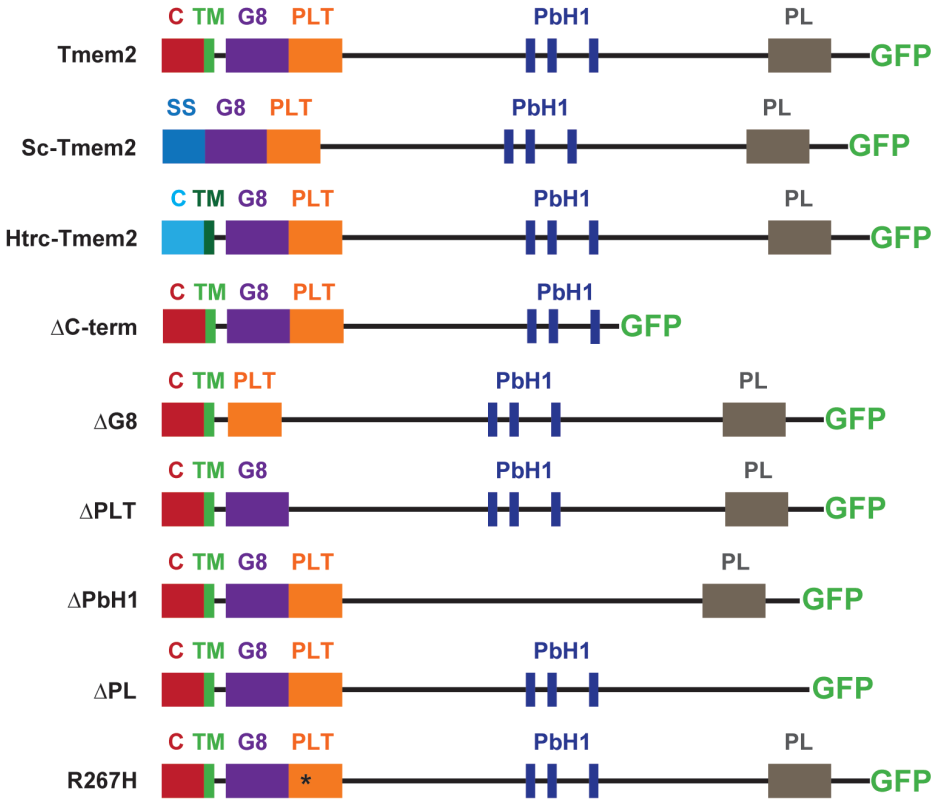

Figure 3.1. Tmem2 variants employed in this study
We constructed a series of Tmem2-derived variants and examined the ability of each to rescue the *tmem2* mutant phenotype, relative to the degree of rescue provided by expression of a full-length Tmem2-Gfp fusion protein (top), in which Gfp is fused to the C-terminus of Tmem2. Tmem2 is predicted to be a type II transmembrane protein and contains a cytoplasmic (C) and transmembrane (TM) domain, a G8 domain, a Pander-like Tmem2 (PLT) domain, three conserved parallel beta-helix repeats (PbH1), and a Pander-like (PL) domain (Smith et al., 2011; Totong et al., 2011). The Sc-Tmem2 variant replaces the cytoplasmic and transmembrane domains of Tmem2-Gfp with a secretory signal sequence. In the Htrc-Tmem2 variant, the cytoplasmic and transmembrane domains of Tmem2-Gfp are replaced by the cytoplasmic and transmembrane domains of the human transferrin receptor, a type II transmembrane protein. In the ΔC-term variant, a truncated version of Tmem2, missing the portion of the C-terminus that would be absent in the protein encoded by the *tmem2*^{sk38} mutant allele (Totong et al., 2011), is fused to Gfp. Additional Tmem2 variants include deletions of the G8 domain, the PLT domain, the PbH1 repeats, and the PL domain. Finally, the R267H variant contains a missense mutation that changes residue 267, within the PLT domain, from arginine to histidine.

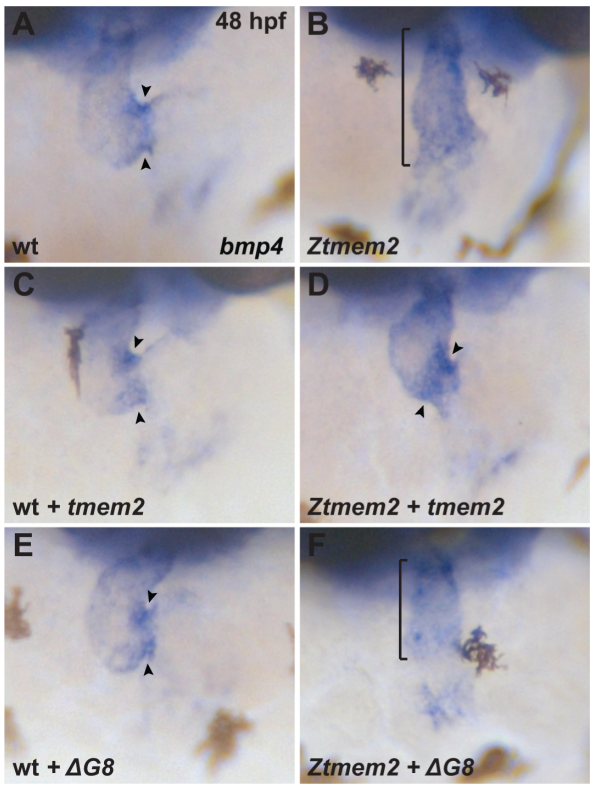

Figure 3.2. Extracellular domains of Tmem2 are critical for proper AVC differentiation

In situ hybridization indicates expression of *bmp4* in wild-type (A,C,E) embryos and *Ztmem2* (B,D,F) mutant siblings at 48 hours post fertilization (hpf); frontal views. In wild-type (wt) embryos, concentrated expression of *bmp4* is restricted to the AVC (A, arrowheads), whereas *bmp4* is more broadly expressed throughout the ventricle in *Ztmem2* mutants (B, bracket). Expression of full-length *tmem2* can restore the concentrated expression of *bmp4* in the AVC of *Ztmem2* mutants (D, arrowheads, Table 1), but does not affect *bmp4* expression in wt siblings (C, arrowheads, Table 3.S1). As with *ΔC-term* and all other extracellular domain deletion variants, expression of the *ΔG8* variant does not affect *bmp4* expression in wt embryos (E, arrowheads, Table 3.S1) and provides no evident rescue of the *bmp4* expression pattern in *Ztmem2* mutants (F, bracket, Table 3.1).

Table 3.1. Rescue of *bmp4* expression pattern by expression of *tmem2* and variants

Genotype	Injected mRNA	Expanded *bmp4*	Restricted *bmp4*
wild-type	uninjected	-	71/71 (100%)
Ztmem2	uninjected	38/38 (100%)	-
Ztmem2	*tmem2*	8/28 (29%)	20/28 (71%)
Ztmem2	*sc-tmem2*	16/20 (80%)	4/20 (20%)
Ztmem2	*htrc-tmem2*	23/37 (62%)	14/37 (38%)
Ztmem2	*ΔC-term*	20/20 (100%)	-
Ztmem2	*ΔG8*	21/21 (100%)	-
Ztmem2	*ΔPLT*	22/22 (100%)	-
Ztmem2	*ΔPbH1*	13/13 (100%)	-
Ztmem2	*ΔPL*	12/12 (100%)	-
Ztmem2	*R267H*	32/32 (100%)	-

Summary of experiments evaluating whether expression of *tmem2* or *tmem2* variants can rescue the *bmp4* expression pattern in *Ztmem2* mutants. Genotype (wild-type or *Ztmem2*) and the injected mRNA are listed for each set of embryos. Phenotypes were assessed through in situ hybridization for *bmp4*, as in Fig. 3.2. Data indicate the fraction of embryos displaying expanded *bmp4* expression throughout the ventricle (as in Fig. 3.2B,F) or restricted *bmp4* expression, concentrated within the AVC (as in Fig. 3.2A,C,D,E). Full-length *tmem2* and *htrc-tmem2* can rescue the *bmp4* expression pattern in *Ztmem2* mutants. The *sc-tmem2* variant can also rescue the *bmp4* expression pattern, albeit less efficiently than *tmem2* and *htrc-tmem2*. (Significant differences from uninjected *Ztmem2* were calculated using Fisher's exact test; $p<0.00001$ for *tmem2* and *htrc-tmem2*, $p=0.01$ for *sc-tmem2*). In contrast, the *ΔC-term*, *ΔG8, ΔPLT, ΔPbh1, ΔPL*, and *R267H* variants do not provide notable rescue of the *bmp4* expression pattern defects in *Ztmem2* mutants. For each mRNA, wild-type siblings were injected as controls; see Table 3.S1 for these additional data.

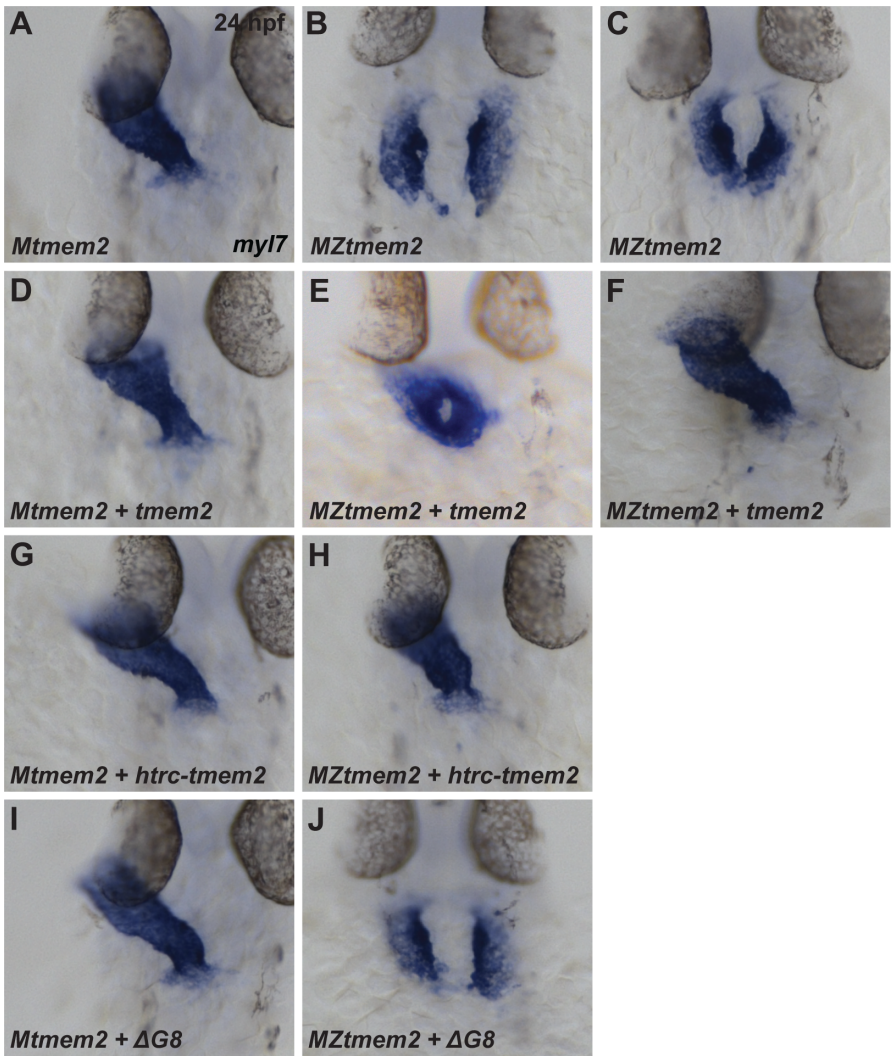

Figure 3.3. Extracellular domains of Tmem2 are critical for promoting cardiac fusion

In situ hybridization indicates expression of *myl7* in *Mtmem2* (A,D,G,I) and *MZtmem2* (B,C,E,F,H,J) embryos at 24 hpf; dorsal views, anterior up. The heart tube assembles normally in *Mtmem2* embryos by 24 hpf (A). *MZtmem2* mutant siblings, however, display either cardia bifida (B) or, less frequently, partial cardiac fusion (C) (Table 3.2). Expression of full-length *tmem2* in *MZtmem2* mutants can facilitate cardiomyocyte movement to the midline (E) and frequently restores heart tube formation (F) (Table 3.2). Expression of *htrc-tmem2* in *MZtmem2* mutants can also rescue their cardiac fusion defects (H, Table 3.2). As with *ΔC-term* and all other extracellular domain deletion variants, expression of the *ΔG8* variant does not rescue cardiac fusion in *MZtmem2* mutants (J, Table 3.2). *Mtmem2* sibling embryos appear unaffected by expression of *tmem2* (D) or *tmem2* variants (G, I, Table 3.S2).

Table 3.2. Rescue of cardiac fusion by expression of *tmem2* and variants

Genotype	Injected mRNA	Not fused	Ring	Tube
Mtmem2	uninjected	-	-	38/38 (100%)
MZtmem2	uninjected	35/35 (100%)	-	-
MZtmem2	*tmem2*	3/32 (9%)	8/32 (25%)	21/32 (66%)
MZtmem2	*sc-tmem2*	9/28 (32%)	17/28 (61%)	2/28 (7%)
MZtmem2	*htrc-tmem2*	5/41 (12%)	11/41 (27%)	25/41 (61%)
MZtmem2	*ΔC-term*	16/17 (94%)	1/17 (6%)	-
MZtmem2	*ΔG8*	31/31 (100%)	-	-
MZtmem2	*ΔPLT*	31/31 (100%)	-	-
MZtmem2	*ΔPbH1*	36/36 (100%)	-	-
MZtmem2	*ΔPL*	29/29 (100%)	-	-
MZtmem2	*R267H*	-	19/53 (36%)	34/53 (64%)

Summary of experiments evaluating whether expression of *tmem2* or *tmem2* variants can rescue the cardiac fusion defects in *MZtmem2* mutants. Genotype (*Mtmem2* or *MZtmem2*) and and the injected mRNA are listed for each set of embryos. Phenotypes were assessed through in situ hybridization for *myl7*, as in Fig. 3.3. Embryos displaying two distinct, bilateral populations of cardiomyocytes (as in Fig. 3.3B,J) or two groups of cardiomyocytes joined only at the posterior (as in Fig. 3.3C) were categorized as “not fused”. Embryos displaying a fused ring of cardiomyocytes, but not a heart tube, were categorized as “ring” (as in Fig. 3.3E). Embryos displaying a heart tube were categorized as “tube” (as in Fig. 3.3A,D,F,G,H,I). Data indicate the fraction of embryos within each category. Full-length *tmem2*, *sc-tmem2*, *htrc-tmem2*, and *R267H* can rescue cardiac fusion in *MZtmem2* mutants. (Significant differences from uninjected *MZtmem2* were calculated using Fisher’s exact test; $p<0.001$ for *tmem2*, *htrc-tmem2*, *sc-tmem2*, and *R267H*). In contrast, *ΔC-term* and the *tmem2* variants lacking either the G8, PLT, PbH1, or PL domains do not provide notable rescue of the *MZtmem2* cardiac fusion defects. Expression of *tmem2* or *tmem2* variants does not appear to affect cardiac fusion in *Mtmem2* siblings; see Table 3.S2 for these additional data.

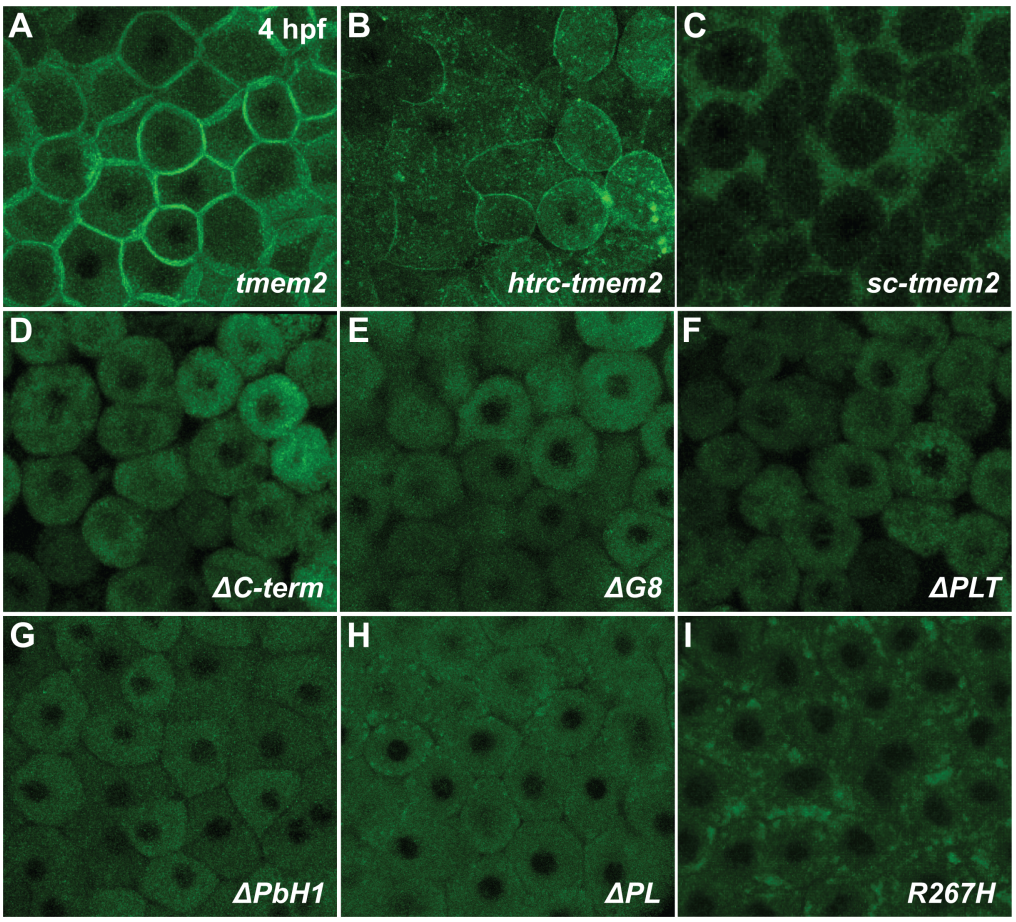

Figure 3.4. Subcellular localization of *tmem2* and *tmem2* variants in zebrafish blastomeres

Confocal reconstruction visualizes Gfp localization in a lateral portion of the blastula at 4 hpf, following injection with mRNA encoding Tmem2-Gfp (A) or its variants (B-I). Both full-length Tmem2 and Htrc-Tmem2 localize to the plasma membrane (A,B). Sc-Tmem2 appears to traffic to the extracellular environment (C). All variants lacking extracellular domains display broad cytoplasmic localization (D-H). R267H does not appear to localize to the plasma membrane like full-length Tmem2, nor does it exhibit the same broad localization as the variants with deletions of extracellular domains deletions. Instead, R267H seems to localize to particular foci within the cytoplasm (I). For *tmem2*, n=12; for *htrc-tmem2*, n=11; for *sc-tmem2*, n=9; for *ΔC-term*, n=10; for *ΔG8*, n=8; for *ΔPLT*, n=9; for *ΔPbH1*, n=10; for *ΔPL*, n=8; for *R267H*, n=16.

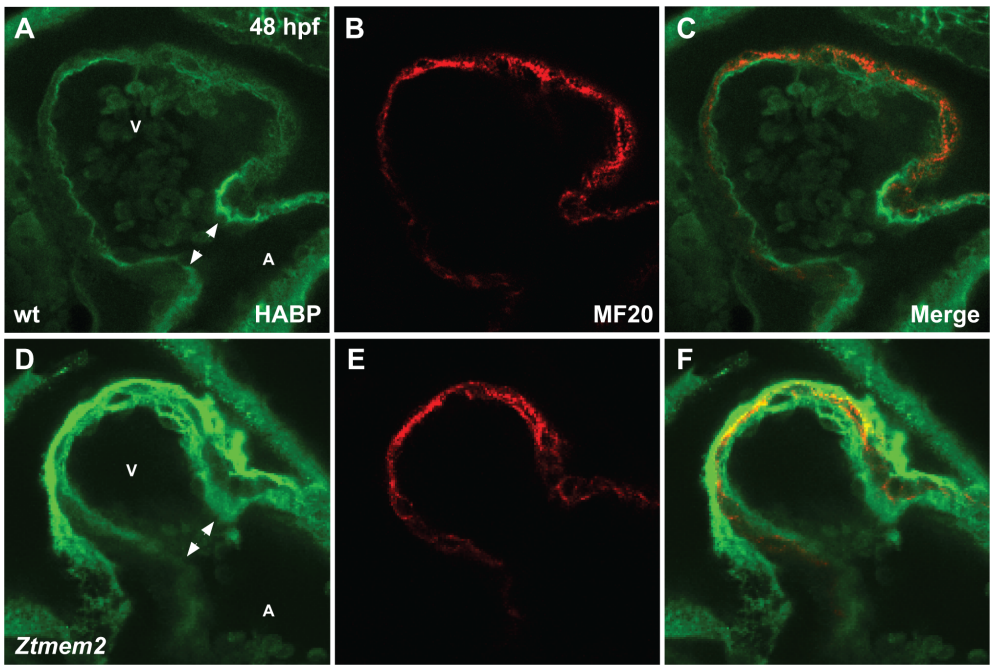

Figure 3.5. *Ztmem2* mutants exhibit aberrant HA deposition
Fluorescence depicts MF20 (red) and HABP (green) localization in wt (A-C) and *Ztmem2* mutant (D-F) embryos at 48 hpf. Three-dimensional reconstructions of selected optical sections through the ventricle (V) and the atrium (A), showing both channels (C,F), red only (B,E) or green only (A,D). In wt embryos, a thin layer of HA is visible throughout the ventricular cardiac jelly with increased concentration within the AVC (A, arrowheads). In contrast, *Ztmem2* mutants exhibit grossly increased levels of HABP throughout the ventricular cardiac jelly and at the AVC (D, arrowheads).

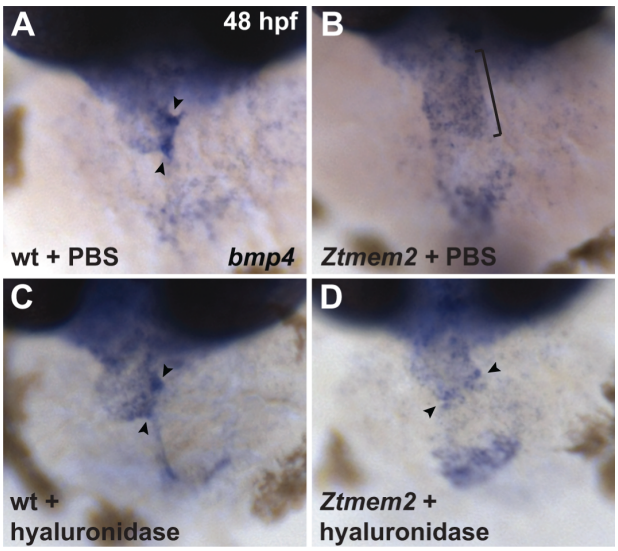

Figure 3.6. Hyaluronidase treatment rescues *bmp4* expression pattern defects in *Ztmem2* mutants

Expression of *bmp4* in wt (A, C) and *Ztmem2* (B, D) mutant embryos at 48 hpf, as in Fig. 3.2. Pericardial injections of PBS do not disrupt the *bmp4* expression pattern in wt (A) or Ztmem2 mutant (B) embryos; compare to Fig. 3.2A,B. In contrast, pericardial injection of hyaluronidase rescues the concentrated expression of *bmp4* in the AVC of a majority of *Ztmem2* mutants (D, arrowheads, Table 3.3), but does not affect the *bmp4* expression pattern in the majority of wt siblings (C, arrowheads, Table 3.3).

Table 3.3. Rescue of *bmp4* expression pattern by hyaluronidase treatment

Genotype	Injection	Expanded *bmp4*	Restricted *bmp4*
wild-type	PBS	-	11/11 (100%)
Ztmem2	PBS	22/22 (100%)	-
wild-type	Hyaluronidase	5/58 (9%)	53/58 (91%)
Ztmem2	Hyaluronidase	4/22 (18%)	18/22 (82%)

Summary of experiments evaluating whether hylauronidase treatment can rescue the *bmp4* expression pattern in *Ztmem2* mutants. Genotype (wild-type or *Ztmem2*) and the material injected are listed for each set of embryos. Phenotypes were assessed through in situ hybridization for *bmp4*, as in Figs. 3.2 and 3.6 and in Table 3.1. Data indicate the fraction of embryos displaying expanded *bmp4* expression throughout the ventricle (as in Fig. 3.6B) or restricted *bmp4* expression, concentrated within the AVC (as in Fig. 3.6A,C,D). Hyaluronidase treatment is able to efficiently rescue the *bmp4* expression pattern in *Ztmem2* mutants (Significant difference from uninjected *Ztmem2* was calculated using Fisher's exact test; $p<0.00001$).

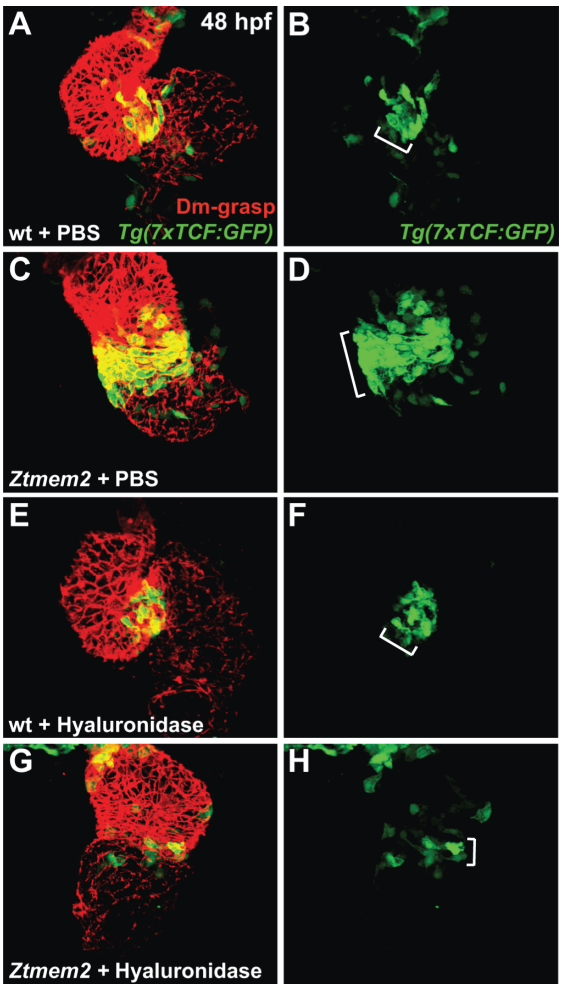

Figure 3.7. Hyaluronidase treatment rescues distribution of Wnt signaling in *Ztmem2* mutants

Immunofluorescence depicts localization of Dm-grasp (red) and Gfp (green), driven by the Wnt signaling reporter *Tg(7xTCF:GFP)* (Moro et al., 2012), in wt (A,B,E,F) and *Ztmem2* (C,D,G,H) mutant embryos at 48 hpf. Images shown are three-dimensional reconstructions showing both channels (A,C,E,G) or green only (B,D,F,H). In PBS-injected wt embryos (A,B), Wnt signaling activity is restricted to the AVC (bracket in B). In PBS-injected *Ztmem2* mutants (C,D), the distribution of Wnt signaling activity is expanded beyond its normal restriction (bracket in D). Hyaluronidase treatment restricts the distribution of Wnt signaling activity in the majority of *Ztmem2* mutants (G, bracket in H, Table 3.4), but does not affect the Wnt signaling distribution in most wt siblings (E, bracket in F, Table 3.4).

Table 3.4. Rescue of Wnt signaling distribution by hyaluronidase treatment

Genotype	Injection	Expanded TCF	Restricted TCF
wild-type	PBS	-	5/5 (100%)
Ztmem2	PBS	5/5 (100%)	-
wild-type	Hyaluronidase	3/25 (14%)	22/25 (84%)
Ztmem2	Hyaluronidase	4/16 (25%)	12/16 (75%)

Summary of experiments evaluating whether hylauronidase treatment can rescue the restriction of Wnt signaling activity in *Ztmem2* mutants. Genotype (wild-type or *Ztmem2*) and the material injected are listed for each set of embryos. Phenotypes were assessed through immunofluorescence for Dm-grasp and Gfp, as in Fig. 3.7. Data indicate the fraction of embryos displaying expanded Wnt reporter expression (as in Fig. 3.7D) or restricted Wnt reporter expression (as in Fig. 3.7B,F,H). Hyaluronidase treatment is able to efficiently restrict the distribution of Wnt signaling activity in *Ztmem2* mutants. (Significant difference from uninjected *Ztmem2* was calculated using Fisher's exact test; p=0.006).

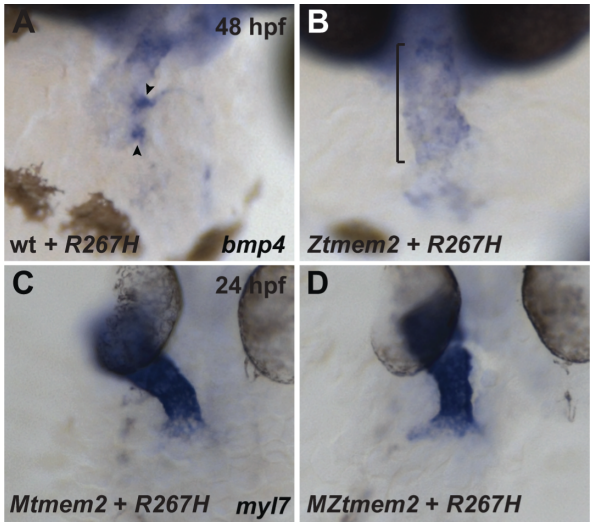

Figure 3.8. The R267H variant fails to restore AVC restriction in *Zmem2* mutants, but efficiently rescues cardiac fusion in *MZtmem2* mutants
Expression of *bmp4* in wt (A) and *Ztmem2* (B) mutant embryos, as in Fig. 3.2. Expression of *R267H* does not rescue the *bmp4* expression pattern in *Ztmem2* embryos (B, bracket, Table 3.1) and does not affect the *bmp4* expression pattern in wt siblings (A, arrowheads, Table 3.S1); compare to wt and *Ztmem2* embryos shown in Fig. 3.2A,B. Expression of *myl7* in *Mtmem2* (C) and *MZtmem2* (D) embryos at 24 hpf, as in Fig. 3.3. Expression of *R267H* efficiently rescues cardiac fusion defects in *MZtmem2* mutants (D, Table 2) (Significant difference from uninjected *MZtmem2* was calculated using Fisher's exact test; $p<0.001$ for *R267H*), but does not seem to alter cardiac fusion in *Mtmem2* siblings (C, Table 3.S2); compared to wt and *MZtmem2* embryos shown in Fig. 3.3A,B.

Table 3.S1. Rescue of *bmp4* expression pattern by expression of *tmem2* and variants

Genotype	Injected mRNA	Expanded *bmp4*	Restricted *bmp4*
wild-type	uninjected	-	71/71 (100%)
Ztmem2	uninjected	38/38 (100%)	-
wild-type	*tmem2*	-	81/81 (100%)
Ztmem2	*tmem2*	8/28 (29%)	20/28 (71%)
wild-type	*sc-tmem2*	-	73/73 (100%)
Ztmem2	*sc-tmem2*	16/20 (80%)	4/20 (20%)
wild-type	*htrc-tmem2*	-	50/50 (100%)
Ztmem2	*htrc-tmem2*	23/37 (62%)	14/37 (38%)
wild-type	*ΔC-term*	-	64/64 (100%)
Ztmem2	*ΔC-term*	20/20 (100%)	-
wild-type	*ΔG8*	-	84/84 (100%)
Ztmem2	*ΔG8*	21/21 (100%)	-
wild-type	*ΔPLT*	-	63/63 (100%)
Ztmem2	*ΔPLT*	22/22 (100%)	-
wild-type	*ΔPbH1*	-	75/75 (100%)
Ztmem2	*ΔPbH1*	13/13 (100%)	-
wild-type	*ΔPL*	-	82/82 (100%)
Ztmem2	*ΔPL*	12/12 (100%)	-
wild-type	*R267H*	-	64/64 (100%)
Ztmem2	*R267H*	32/32 (100%)	-

This table restates all of the data from Table 3.1, with the additional inclusion of data from wild-type sibling embryos injected with each mRNA.

Table 3.S2. Rescue of cardiac fusion by expression of *tmem2* and variants

Genotype	Injected mRNA	Not fused	Ring	Tube
Mtmem2	uninjected	-	-	38/38 (100%)
MZtmem2	uninjected	35/35 (100%)	-	-
Mtmem2	*tmem2*	-	-	28/28 (100%)
MZtmem2	*tmem2*	3/32 (9%)	8/32 (25%)	21/32 (66%)
Mtmem2	*sc-tmem2*	-	-	34/34 (100%)
MZtmem2	*sc-tmem2*	9/28 (32%)	17/28 (61%)	2/28 (7%)
Mtmem2	*htrc-tmem2*	-	-	47/47 (100%)
MZtmem2	*htrc-tmem2*	5/41 (12%)	11/41 (27%)	25/41 (61%)
Mtmem2	*ΔC-term*	-	-	15/15 (100%)
MZtmem2	*ΔC-term*	16/17 (94%)	1/17 (6%)	-
Mtmem2	*ΔG8*	-	-	37/37 (100%)
MZtmem2	*ΔG8*	31/31 (100%)	-	-
Mtmem2	*ΔPLT*	-	-	27/27 (100%)
MZtmem2	*ΔPLT*	31/31 (100%)	-	-
Mtmem2	*ΔPbH1*	-	-	36/36 (100%)
MZtmem2	*ΔPbH1*	36/36 (100%)	-	-
Mtmem2	*ΔPL*	-	-	42/42 (100%)
MZtmem2	*ΔPL*	29/29 (100%)	-	-
Mtmem2	*R267H*	-	-	54/54 (100%)
MZtmem2	*R267H*	-	19/53 (36%)	34/53 (64%)

This table restates all of the data from Table 3.2, with the additional inclusion of data from *Mtmem2* sibling embryos injected with each mRNA.

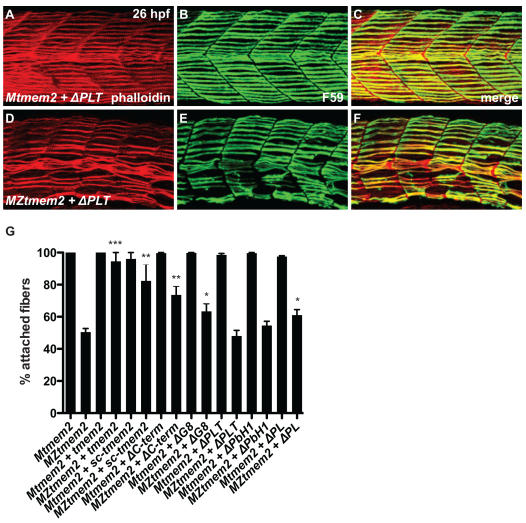

Figure 3.S1. Rescue of muscle fiber attachment by expression of *tmem2* and variants

(A-F) Immunofluorescence depicts muscle fiber organization, using phalloidin (red) to recognize both fast and slow muscle fibers and F59 (green) to recognize slow fibers; lateral views with dorsal up at 26 hpf. Somite morphology of *Mtmem2* siblings is indistinguishable from wild-type embryos, whereas *MZtmem2* mutants display muscle fiber detachment (Ryckebusch et al., 2016). Expression of full-length *tmem2* improves the *MZtmem2* phenotype (Ryckebusch et al., 2016). *MZtmem2* mutants overexpressing *ΔPLT* still display muscle fiber detachment (D-F), whereas *Mtmem2* siblings overexpressing *ΔPLT* exhibit normal fiber attachment (A-C). (G) Bar graph compares average prevalence of fiber attachment in somites at 26 hpf; error bars indicate s.e.m. For each embryo, we examined the left side of the myotome. F59+ fibers were counted in each of 10 somites of multiple embryos. Asterisks indicate significant differences from un-injected *MZtmem2*. Full-length *tmem2*, *sc-tmem2*, *ΔC-term*, *ΔG8, ΔPL* provide significant rescue of muscle fiber attachment in *MZtmem2* mutants. (Student's t-test; $p<0.0001$ for *tmem2*, $p=0.0056$ for *sc-tmem2*, $p=0.0014$ for *ΔC-term*, $p=0.0234$ for *ΔG8*, $p=0.0235$ for *ΔPL*). Although the percent of attached fibers in *MZtmem2* embryos expressing *ΔC-term*, *ΔG8, ΔPL* is significantly higher than in uninjected *MZtmem2* mutants, it is also significantly different than the efficiency of rescue seen with full-length *tmem2*. In contrast, *ΔPLT* and *ΔPbH1* expression does not appear to rescue muscle fiber attachment in *MZtmem2* embryos. Finally, expression of *tmem2* and *tmem2* variants does not appear to affect wild-type siblings. This graph re-states published data on *sc-tmem2* data (also referred to as "ectodomain") (Ryckebusch et al., 2016). For *Mtmem2*, n=4; for *MZtmem2*, n=7; for *Mtmem2* expressing *tmem2*, n=6; for *MZtmem2* expressing *tmem2*, n=8; for *Mtmem2* expressing *sc-tmem2*, n=2; for *MZtmem2* expressing *sc-tmem2*, n=5; for *Mtmem2* expressing *ΔC-term*, n=3; for *MZtmem2* expressing *ΔC-term*, n=5; for *Mtmem2* expressing *ΔG8*, n=4; for *MZtmem2* expressing *ΔG8*, n=5; for *Mtmem2* expressing *ΔPLT*, n=4; for *MZtmem2* expressing *ΔPLT*, n=7; for *Mtmem2* expressing *ΔPbH1*, n=3; for *MZtmem2* expressing *ΔPbH1*, n=4; for *Mtmem2* expressing *ΔPL*, n=2; for *MZtmem2* expressing *ΔPL*, n=5.

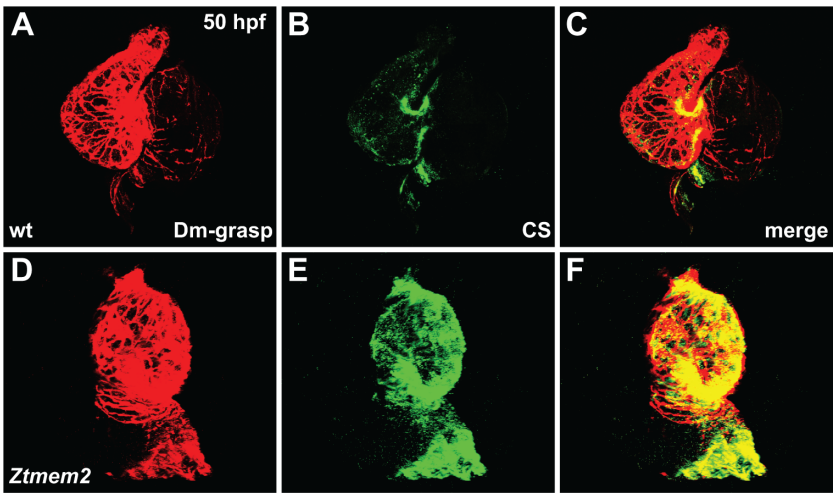

Figure 3.S2. Chondroitin sulfate localization is expanded in *Ztmem2* mutants
Immunofluorescence depicts localization of Dm-grasp (red) and chondroitin sulfate (CS, green) in wild-type (wt) (A-C) and *Ztmem2* mutant (D-F) hearts at 50 hpf. Images shown are three-dimensional reconstructions showing red only (A,D), green only (B,E), or both channels (C,F). In wt hearts, CS deposition is concentrated within the AVC (B). In contrast, *Ztmem2* mutants display broad and heightened CS localization throughout the ventricle (E).

Table 3.S3. Antibodies used for immunofluorescence

	Antigen	Reagent	Vendor	Dilution
Primary Antibodies	Chondroitin sulfate	Mouse monoclonal (CS-56)	Sigma (#C8035)	1:200
	Dm-grasp	Mouse monoclonal (Zn-5)	Zebrafish International Resource Center	1:10
	Gfp	Rabbit polyclonal	Invitrogen (#A11122)	1:100
	MF20	Mouse monoclonal	Developmental Studies Hybridoma Bank (supernatant)	1:10
	Myosin heavy chain	Mouse monoclonal (F59)	Developmental Studies Hybridoma Bank (supernatant)	1:10
Secondary Antibodies	Mouse IgG	Goat polyclonal; Alexa 488	Invitrogen (#A11001)	1:100
	Mouse IgG	Goat polyclonal; Alexa 594	Invitrogen (#A11005)	1:100
	Mouse IgG2b	Goat polyclonal; TRITC	SouthernBiotech (#1090-03)	1:100
	Rabbit IgG	Goat polyclonal: Alexa 488	Invitrogen (#A11008)	1:100
	Rabbit IgG	Goat polyclonal: Alexa Fluor 594	Molecular Probes (#A11012)	1:400

A modified version of Chapter 3 will be submitted for publication (Hernandez, Lydia; Ryckebüsch, Lucile; Wang, Carole; Ling, Rachel; Yelon, Deborah. “Tmem2 restricts atrioventricular canal differentiation by regulating degradation of hyaluronic acid”). Lydia Hernandez is the primary researcher/author on this paper. Lydia Hernandez will be the first author of this manuscript and she contributed to designing the experiments, conducting research, interpreting results, and writing the manuscript presented in Chapter 3. Lucile Ryckebüsch contributed to designing the experiments, conducting research, interpreting results, and writing the manuscript presented in Chapter 3. Deborah Yelon contributed to designing the experiments, interpreting results, and writing the manuscript presented in Chapter 3. Carole Wang and Rachel Ling designed and created plasmid constructs used in Chapter 3.

Chapter 4: Future directions toward understanding mechanisms of extracellular matrix regulation during cardiac development

In this thesis, we have shown that Tmem2 influences the deposition and composition of the extracellular matrix (ECM) during both cardiac and skeletal muscle development. Moreover, our results suggest that the coordination of ECM organization by Tmem2 is instrumental for the stability of muscle fiber attachments, for facilitating cardiomyocyte movement, and for the restriction of AVC differentiation. In addition, our findings indicate that these functions of Tmem2 rely upon the four identified domains contained within its extracellular portion. Together, these data reiterate the importance of the extracellular milieu during cardiac and muscle morphogenesis. At the same time, it is clear that many open questions related to this topic remain to be examined. In this chapter, I will discuss several key areas for future investigations that will expand our understanding of the dynamic interactions between cells and their environment during embryonic cardiogenesis. For instance, what is the precise mechanism for HA regulation by Tmem2? Following this, how exactly does the ECM inform cardiac development? Then, if Tmem2 has multiple modes of activity during development, what could these alternative activities be and what protein interactions are involved? Finally, I will discuss the broader significance of our work regarding Tmem2.

How does Tmem2 regulate hyaluronic acid turnover?

Several studies have shown that the appropriate pattern of HA deposition is required in order to correctly regulate differentiation of the AVC.

Excess HA deposition results in ectopic AVC differentiation outside of its normal boundaries, whereas decreased levels of HA inhibit endocardial cushion formation within the AVC (Camenisch et al., 2000; Lagendijk et al., 2011; Walsh and Stainier, 2001). In previous work, our lab has demonstrated that *tmem2* is a key player in restricting AVC differentiation (Totong et al., 2011). Moreover, in Chapter 3, we confirmed prior work demonstrating that *tmem2* mutants exhibit excess HA deposition between the endocardium and the myocardium (Smith et al., 2011), indicating a role for Tmem2 in limiting the levels of HA in the cardiac jelly. While our data strongly support a model whereby Tmem2 restricts AVC differentiation via regulation of HA, the precise mechanism by which Tmem2 influences the amount of HA remains unknown. Does Tmem2 influence HA levels directly, indirectly, or through some combination of approaches?

tmem2 mutants display expanded *has2* expression (Smith et al., 2011; Totong et al., 2011) that presumably results in excess HA synthesis. Thus, it is possible that Tmem2 could exert its influence on HA at the transcriptional level, upstream of *has2* expression. Very recent work, however, has identified Tmem2 as a hyaluronidase. When transfected with *tmem2* cDNA, HEK293 cells gained the ability to degrade HA from ~1500 kDa down to ~5 kDa molecules (Yamamoto et al., 2017). It is not clear, however, whether this activity of Tmem2 is physiologically relevant within the developing embryo.

Additional recent work investigating the role of Tmem2 in angiogenesis supports the notion that Tmem2 hyaluronidase activity is important for its function. Zebrafish *tmem2* mutants exhibit decreased intersegmental vessel (ISV) sprouting and increased HA levels surrounding ISVs (De Angelis et al., 2017). Injection of *tmem2* embryos with hyaluronidase degrades HA and improves angiogenesis. Thus, these results suggest that Tmem2 could indeed function through degrading HA in vivo.

While our data also support the hypothesis that Tmem2 works through depolymerization of HA, it remains unclear whether Tmem2 directly binds HA. KIAA199, a protein that is structurally very similar to Tmem2, has been shown to bind HA directly in cell culture (Yoshida et al., 2013). However, work investigating the ability of Tmem2 to promote HA degradation does not examine whether Tmem2 interacts directly with HA molecules (Yamamoto et al., 2017). Rather than depolymerize HA itself, it is still plausible that Tmem2 could induce the activity of other known hyaluronidases or matrix metalloproteinases (MMPs) in order to coordinate HA catabolism. In the future, it will be valuable to determine the precise physical nature of Tmem2-HA interaction through biochemical approaches in embryonic tissue.

If Tmem2 acts as a hyaluronidase in vivo, then we might imagine that overexpression of *tmem2* would result in deficient endocardial cushion formation, given that that embryos deficient in HA do not form endocardial cushions (Camenisch et al., 2000; Walsh and Stainier, 2001). We note,

however, that overexpression of *tmem2* in wild-type embryos does not appear to result in any noticeable defects in AVC differentiation (Totong et al., 2011) (Fig. 3.2B; Table 3.1). Considering how strictly the HA pathway is controlled, perhaps there are co-factors required for Tmem2 hyaluronidase function that serve to limit its activity. Clearly, additional work investigating the exact way in which Tmem2 regulates HA and what additional factors modulate Tmem2 activity will be beneficial in broadening our awareness of how the ECM is organized.

How does HA affect AVC formation?

It is understood that HA levels are tightly regulated and that this regulation plays a critical role in AVC development (Toole, 2004; Valiente-Alandi et al., 2016). What remains unknown is the precise way in which matrix composition informs cell behavior. How does HA deposition influence the differentiation of myocardial and endocardial cells in the AVC? One possibility is that HA size and deposition impact signaling by influencing the activity of various signaling pathways (De Angelis et al., 2017; Itano, 2008; Jiang et al., 2005; Termeer et al., 2002). For example, in the AVC of mice, HA activates phosphorylation of ErbB2 and ErbB3 heterodimers (Camenisch et al., 2000), an interaction critical for endocardial cushion formation (Erickson et al., 1997). Phosphorylation of these heterodimers induces the activity of β-catenin and downstream effectors of the Wnt signaling pathway (Bourguignon et al., 2007).

As described in Chapter 1, Wnt-driven β-catenin translocation is essential for endocardial cushion development (Hurlstone et al., 2003; Liebner et al., 2004). In addition, β-catenin activity also influences *has2* expression patterns (Hurlstone et al., 2003). This positive feedback loop of HA regulation is one striking example by which HA can impact both its own expression as well as signaling pathways that are crucial for AVC differentiation.

Additional work has shown the impact of low molecular weight HA fragments, also referred to as o-HA, on the VEGF signaling pathway. In forming endocardial cushions, endocardial cells at the AVC undergo an epithelial to mesenchymal transition (EMT). In avian studies, it has been demonstrated that o-HAs, inhibit EMT by activating VEGF signaling, an antagonist of EMT (Chang et al., 2004; Rodgers et al., 2006).

Research in zebrafish *tmem2* mutants also examined the impact of o-HA in the context of angiogenesis (De Angelis et al., 2017). As described above, *tmem2* mutants exhibit intersegmental vessel (ISV) sprouting defects that were ameliorated by depolymerization of HA. Intriguingly, treatment of *tmem2* mutants with exogenous o-HA also ameliorated their ISV sprouting defects (De Angelis et al., 2017). Thus, these findings suggest that HA fragment size, rather than HA levels, is a key component to angiogenesis.

Is HA fragment size similarly important for the regulation of AVC differentiation? To test this, we could perform a similar experiment and treat *tmem2* mutants with exogenous o-HA at 30 hpf. If we see rescue of the

restriction of AVC differentiation, then this would suggest that the role of Tmem2 in this context is to generate HA molecules of a specific size. On the other hand, if introduction of o-HAs fails to rescue AVC defects in *tmem2* mutants, we might conclude that Tmem2 regulation of HA levels or distribution could be more critical for the spatial restriction of AVC differentiation.

Nonetheless, it is entirely possible that multiple mechanisms of HA activity overlap to instruct AVC development. Understanding the full picture of the timing and mechanism of HA function would be beneficial to create a more thorough understanding of the processes that coordinate cell behavior during cardiac morphogenesis.

Does Tmem2 promote cardiac fusion through regulation of HA?

Early cardiac morphogenesis requires cardiomyocytes to move toward the embryonic midline, where they merge to give rise to the primitive heart tube (Bussmann et al., 2007; Holtzman et al., 2007; Moreno-Rodriguez et al., 2006; Schoenebeck and Yelon, 2007) (Fig 1.1), a process referred to as cardiac fusion. In zebrafish embryos lacking both maternal and zygotic sources of *tmem2* (*MZtmem2*), cardiomyocytes do not migrate medially and cardiac fusion does not occur (Ryckebusch et al., 2016; Totong et al., 2011) (Fig. 1.3B). In Chapters 2 and 3, we identified regions of the Tmem2 protein that are essential for its function in promoting cardiomyocyte migration. The reason why cardiac fusion fails in *MZtmem2* mutants, however, remains poorly

understood. Both correct endodermal specification and ECM composition are essential for cardiac fusion to occur (Arrington and Yost, 2009; Garavito-Aguilar et al., 2010; Holtzman et al., 2007; Kikuchi et al., 2001; Kupperman et al., 2000; Trinh and Stainier, 2004). However, our lab has observed normal endodermal specification and morphogenesis in *MZtmem2* mutant embryos (data not shown). Given that *MZtmem2* mutants exhibit aberrant ECM organization and deposition in multiple tissues (Ryckebusch et al., 2016), it seems probable that defective ECM composition could underlie the inhibition of cardiac fusion in these embryos. What are the requirements for ECM composition during cardiac fusion and does Tmem2 coordinate these conditions?

Our findings suggest that Tmem2 functions to delimit AVC differentiation through regulation of HA. Is regulation of HA by Tmem2 also essential for its function in promoting cardiac fusion? A first step in addressing this question would be to determine whether HA is present in the matrix that surrounds migrating cardiomyocytes during cardiac fusion. If HA is indeed present within this extracellular milieu, we could then examine whether *MZtmem2* mutants exhibit aberrant HA deposition. Based upon what we have observed in zygotic *tmem2* mutant hearts (Fig. 3.5D-F), we might observe similarly excessive HA deposition in *MZtmem2* mutants. If we detect aberrant HA deposition, we can then test whether modulating HA levels in *MZtmem2* mutants rescues their cardiac fusion defects. If we find that HA degradation

rescues cardiomyocyte mobility in MZtmem2 mutants, then these results would suggest a role for Tmem2 regulation of HA in this earlier developmental context. It is possible, however, that HA may not be a critical component of the ECM during this particular process. Alternatively, we may determine that HA is a component of the ECM that mediates cardiac fusion, but that HA remains appropriately deposited around the cardiomyocytes in *MZtmem2* mutants. Either of these results would suggest that the *MZtmem2* fusion defect is most likely not a consequence of erroneous HA turnover.

Although we cannot currently rule out HA as a key player in cardiac fusion, our findings to date do not support this model. R267H, the Tmem2 variant lacking hyaluronidase activity, is not able to rescue the *tmem2* mutant AVC restriction defect. In sharp contrast, this same variant seems fully functional in the context of cardiac fusion. Over-expression of R267H in *MZtmem2* mutants rescues cardiac fusion as effectively as full-length Tmem2 does (Fig. 3.8D) (Table 3.2). If we take the interpretation that the main functional defect of R267H is its inability to degrade HA, then we can surmise from these results that AVC restriction relies on depolymerization of HA by Tmem2, whereas cardiac fusion does not. However, as described in Chapter 3, R267H does not localize correctly to the plasma membrane (Fig. 3.4). Perhaps, as an alternative interpretation, the principal functional defect of R267H is that it simply can't traffic efficiently to the membrane. It could be that higher levels of Tmem2 protein are required for AVC differentiation than for

cardiac fusion and that there simply isn't enough R267H present at the membrane to function effectively. We could test this by increasing the level of R267H overexpression and assessing whether this improves the mutant AVC defects. We have performed a similar experiment where we doubled overexpression levels of the secreted Tmem2 ectodomain (Sc-tmem2). However, we failed to see any improvement in *tmem2* mutant AVC restriction. Thus, we might also see that increasing R267H overexpression similarly fails to rescue AVC differentiation. Alternatively, we could investigate how localization of Tmem2 affects function. To do this, we could attempt to create a version of R267H that is anchored to the outside of the plasma membrane - possibly via the addition of a glycosylphosphatidylinositol (GPI) linker - and assess its ability to rescue mutant AVC differentiation. In future studies, it will be essential to learn exactly why the R267H variant is not functional in AVC differentiation. By doing this, we will gain a clearer understanding of the physical mechanism of Tmem2 activity.

However, regardless of the precise reason for why R267H fails to rescue AVC expansion, its ability to rescue cardiac fusion defects in *MZtmem2* mutants strongly indicates that Tmem2 has multiple mechanisms of action. Assuming that Tmem2 restricts AVC differentiation by regulating HA depolymerization, the following question remains: how does Tmem2 promote cardiac fusion?

What could be additional mechanisms of Tmem2 activity?

One potential way for Tmem2 to promote cardiac fusion could be through the regulation of other ECM components besides HA. It is known that correct composition of the ECM is required for cardiac fusion to occur (Arrington and Yost, 2009; Trinh and Stainier, 2004; Trinh et al., 2005) and our laboratory's analyses of *hand2* mutants have shown that an excess of Fn can inhibit cardiomyocyte movement (Garavito-Aguilar et al., 2010) (Fig. 1.2D). Given this, we were curious to see whether the cardiac extracellular environment was disorganized in *MZtmem2* mutants. Whereas *Mtmem2* embryos display a normal pattern of polarized Fn deposition adjacent to the myocardium (Fig. 2.3D'), we observe abnormally abundant and disorganized Fn deposition around the *MZtmem2* mutant cardiomyocytes (Fig. 2.3E'). Strikingly, we find that the abnormal localization of Fn in *MZtmem2* mutants is reminiscent of the *hand2* mutant phenotype (Fig. 1.2B). Therefore, we hypothesized that excessive ECM deposition may be responsible for the cell movement defects seen in *MZtmem2* mutants.

We initially tested this hypothesis by observing whether alteration of the *MZtmem2* mutant ECM can rescue cardiac fusion. Genetic reduction of Fn was achieved by breeding female chimeras with *tmem2* mutant germlines (Ciruna et al., 2002; Totong et al., 2011) to males heterozygous for both *tmem2* and *natter (nat)*, a mutation in *fn1* (Trinh and Stainier, 2004). Interestingly, we found partial rescue of cardiac fusion in 13 out of 29

MZtmem2 embryos that were heterozygous for the *nat* mutation. (data not shown). Although decreasing Fn levels helped ameliorate *MZtmem2* cardiac fusion defects, it did not efficiently rescue them. These findings raise interesting questions about what underlies the partial rescue in this scenario.

Certainly, it is possible that reducing the levels of any single ECM component might not be adequate for complete rescue of cardiac fusion, especially if Tmem2 regulates multiple ECM components simultaneously. One way to address this issue would be through more comprehensive modification of the ECM, such as using two or more mutations to modulate levels of multiple ECM components simultaneously. Another possibility is that the defects in the *MZtmem2* mutant ECM relate more to its precise organization rather than simply to excess deposition. To begin to test this, we compared amounts of Fn present in embryonic lysate from *MZtmem2* mutants and from their wild-type siblings. Despite the observed disorganization of Fn deposition seen in *MZtmem2* mutants, they did not exhibit globally increased levels of Fn (data not shown). These preliminary data support the idea that Tmem2 functions within the context of cardiac fusion to coordinate the precise organization of Fn rather than as an upstream regulator of Fn production. In future studies, it will be helpful to confirm and extend these studies to examine the affect of Tmem2 on Fn and other ECM components during cardiac fusion. Excitingly, the Holley lab has created a transgenic zebrafish line that allows for live fluorescent imaging of Fn (Julich et al., 2015). Emerging tools like these

could help us move toward a better understanding of Fn organization and temporal dynamics during development.

Currently, it remains unclear precisely how Tmem2 impacts the ECM and whether ECM organization is the sole mechanism by which Tmem2 promotes cardiac fusion. Moving forward, it is helpful to consider the most likely models of Tmem2 function in this context. One possibility, as discussed above, is that Tmem2 could act primarily to govern ECM deposition and organization. Alternatively, Tmem2 could interact with upstream signaling pathways to promote cardiac fusion.

Does Tmem2 influence the EGF signaling pathway?

In selecting which pathways to investigate, we have become interested in considering the pathways that involve KIAA1199. KIAA1199 is structurally very similar to Tmem2; it contains a G8 domain, PbH1 repeats, and two Pander-like domains (Yoshida et al., 2013). Further, like Tmem2, KIAA1199 has been shown to depolymerize HA. However, KIAA1199 also has additional modes of activity. For example, studies of KIAA1199 have revealed an association between its G8 domain and the EGF receptor (EGFR) that activates downstream EGF signaling and promotes migration of cancer cells (Shostak et al., 2014). Because of the structural and functional similarities between KIAA1199 and Tmem2, we hypothesized that perhaps Tmem2 could

likewise bind EGFR and activate EGF signaling as a means of promoting cardiomyocyte migration during fusion. Our preliminary data, however, do not support this hypothesis. For example, we have found that chemical inhibition of EGF signaling does not hinder cardiac fusion (data not shown). Additionally, pulldowns of Tmem2-Gfp from transfected HEK cell lysate did not reveal a protein interaction between EGFR and Tmem2. Although these are only preliminary results, they do not support the hypothesis that Tmem2 functions through EGFR binding or activation of EGFR specifically.

It is possible that Tmem2 could activate EGF signaling in some alternative, indirect way. It is also plausible, however, that Tmem2 does not function to activate EGF signaling and, instead, influences a different signaling pathway entirely. Therefore, it would be valuable for us to extend our work to include the analysis of additional pathways known to influence cell movement. One potential pathway to examine is the non-canonical Wnt signaling pathway. Importantly, non-canonical Wnts have been shown to modulate cell movement during development and cardiogenesis (McEwen and Peifer, 2000; Pandur et al., 2002). For instance, in Xenopus, morpholino knockdown of the non-canonical Wnt ligand, Wnt11R, induces defects in heart tube fusion (Garriock et al., 2005). Alongside testing whether Tmem2 is involved with candidate pathways such as non-canonical Wnt signaling, another strategy for identifying alternative pathways to investigate is to determine Tmem2 protein binding partners.

What proteins does Tmem2 interact with?

To better understand the mechanisms of Tmem2 activity, we aim to identify which proteins Tmem2 interacts with in a functionally relevant context. In order to identify relevant potential Tmem2 protein interactors, our goal was to compare which proteins complex with full-length Tmem2 versus non-functional Tmem2 variants. Given that the functionality of specific Tmem2 variants is context-dependent, this approach could also potentially reveal context-dependent protein interactions. To achieve this, we transiently transfected HEK293T cells with Tmem2 and Tmem2 variant cDNA, immunoprecipitated Tmem2 from cell lysate, and submitted these samples for mass spectrometry analysis in collaboration with the Briggs Lab.

Pilot studies did not indicate any obviously compelling candidate proteins that interact with Tmem2. Further, our pulldown samples yielded single-digit spectral counts for nearly all identified proteins except Tmem2, limiting our ability to prioritize which candidates to investigate. This may be due to several factors. First, the procedural conditions for the pulldowns may not be optimized for the types of interactions we hope to uncover. Second, it is entirely plausible that we are performing these pulldowns in cells that don't provide the proper biochemical environment for Tmem2 function.

To achieve our goal of identifying Tmem2 protein interactors, it may be beneficial to do these analyses in either cardiac or muscle cell lines or, ideally,

in zebrafish embryos. Once the optimal conditions for Tmem2 pulldowns are established, it would be exciting to compare which proteins complex with full-length Tmem2 versus which proteins complex with the R267H variant. This particular experiment has the potential to provide novel information about the differential roles of Tmem2 across cardiac morphogenesis. Overall, determining Tmem2 binding partners is likely to provide valuable insight into Tmem2 activity, ECM regulation, and the pathways involved in cardiac morphogenesis.

What is the broader significance of this work?

Within the field of developmental biology, we are becoming more aware of the extensive impact that the ECM has on cell behavior during morphogenesis. Overall, our data provide valuable insight into Tmem2 function and support a model whereby Tmem2 coordinates cardiac and skeletal muscle morphogenesis through regulation of the ECM. While it is intriguing to consider how the orchestration of matrix by Tmem2 influences early development, it is still unknown how conserved these mechanisms of Tmem2 function are across species. In future studies, it will be beneficial to confirm and extend these findings in mammalian model systems.

Additionally, there remain many intriguing open questions regarding the role of the ECM in cardiac development, some of which I have discussed in this chapter. A more comprehensive understanding of Tmem2 activity will be instrumental to our grasp of the nature of ECM regulation as well as the interplay between matrix and developing organ systems. Ultimately, these insights will increase our comprehension of how cell behavior is coordinated during organogenesis and how the boundaries of tissue differentiation are established and maintained in the developing embryo.

Moreover, continuing investigation of Tmem2 has the potential to yield therapeutic strategies to address congenital heart disease as well as muscular dystrophies. Additionally, we stand to enhance our understanding of cell movement, a process that is frequently aberrant in a variety of diseases.

Overall, our work investigating the role of Tmem2 has the potential to enrich our awareness of the multiple processes, pathways, and physical cues that overlap to dictate embryonic development and disease.

Preliminary experiments described in Chapter 4 were designed and performed primarily by Lydia Hernandez. Lucile Ryckebüsch performed genetic reduction of Fn in *MZtmem2* mutants. Parthiv Sheth assisted with cell culture transfections and western blots. Arjana Pradhan and Prae Pongtornpipat examined pharmacological inhibition of EGFR in zebrafish embryos. Mass spectrometry analysis of Tmem2 immunoprecipitate was performed in collaboration with Zhouxin Shen of the Briggs laboratory.

REFERENCES

Abe, S., Usami, S., and Nakamura, Y. (2003). Mutations in the gene encoding KIAA1199 protein, an inner-ear protein expressed in Deiters' cells and the fibrocytes, as the cause of nonsyndromic hearing loss. Journal of human genetics *48*, 564-570.

Aleksandrova, A., Czirok, A., Kosa, E., Galkin, O., Cheuvront, T.J., and Rongish, B.J. (2015). The endoderm and myocardium join forces to drive early heart tube assembly. Developmental biology *404*, 40-54.

Alexander, J., Rothenberg, M., Henry, G.L., and Stainier, D.Y. (1999). casanova plays an early and essential role in endoderm formation in zebrafish. Developmental biology *215*, 343-357.

Armstrong, E.J., and Bischoff, J. (2004). Heart valve development: endothelial cell signaling and differentiation. Circulation research *95*, 459-470.

Arrington, C.B., and Yost, H.J. (2009). Extra-embryonic syndecan 2 regulates organ primordia migration and fibrillogenesis throughout the zebrafish embryo. Development *136*, 3143-3152.

Auman, H.J., Coleman, H., Riley, H.E., Olale, F., Tsai, H.J., and Yelon, D. (2007). Functional modulation of cardiac form through regionally confined cell shape changes. PLoS biology *5*, e53.

Bajanca, F., Luz, M., Raymond, K., Martins, G.G., Sonnenberg, A., Tajbakhsh, S., Buckingham, M., and Thorsteinsdottir, S. (2006). Integrin alpha6beta1-laminin interactions regulate early myotome formation in the mouse embryo. Development *133*, 1635-1644.

Bakkers, J., Verhoeven, M.C., and Abdelilah-Seyfried, S. (2009). Shaping the zebrafish heart: from left-right axis specification to epithelial tissue morphogenesis. Developmental biology *330*, 213-220.

Barresi, M.J., Stickney, H.L., and Devoto, S.H. (2000). The zebrafish slow-muscle-omitted gene product is required for Hedgehog signal transduction and the development of slow muscle identity. Development *127*, 2189-2199.

Bassett, D.I., Bryson-Richardson, R.J., Daggett, D.F., Gautier, P., Keenan, D.G., and Currie, P.D. (2003). Dystrophin is required for the formation of stable muscle attachments in the zebrafish embryo. Development *130*, 5851-5860.

Beis, D., Bartman, T., Jin, S.W., Scott, I.C., D'Amico, L.A., Ober, E.A., Verkade, H., Frantsve, J., Field, H.A., Wehman, A., Baier, H., Tallafuss, A., Bally-Cuif, L., Chen, J., Stainier, D., Jungblut, B. (2005). Genetic and cellular analyses of zebrafish atrioventricular cushion and valve development. Development *132*, 4193-4204.

Berdougo, E., Coleman, H., Lee, D.H., Stainier, D.Y., and Yelon, D. (2003). Mutation of weak atrium/atrial myosin heavy chain disrupts atrial function and influences ventricular morphogenesis in zebrafish. Development *130*, 6121-6129.

Berger, J., and Currie, P.D. (2012). Zebrafish models flex their muscles to shed light on muscular dystrophies. Disease models & mechanisms *5*, 726-732.

Bertini, E., D'Amico, A., Gualandi, F., and Petrini, S. (2011). Congenital muscular dystrophies: a brief review. Seminars in pediatric neurology *18*, 277-288.

Blagden, C.S., Currie, P.D., Ingham, P.W., and Hughes, S.M. (1997). Notochord induction of zebrafish slow muscle mediated by Sonic hedgehog. Genes & development *11*, 2163-2175.

Bloomekatz, J., Singh, R., Prall, O.W., Dunn, A.C., Vaughan, M., Loo, C.S., Harvey, R.P., and Yelon, D. (2017). Platelet-derived growth factor (PDGF) signaling directs cardiomyocyte movement toward the midline during heart tube assembly. eLife *6*.

Bouchet-Séraphin, C., Vuillaumier-Barrot, S., and Seta, N. (2015). Dystroglycanopathies: about numerous genes involved in glycosylation of one single glycoprotein. J Neuromuscular Dis *2*, 27-38.

Bourguignon, L.Y., Peyrollier, K., Gilad, E., and Brightman, A. (2007). Hyaluronan-CD44 interaction with neural Wiskott-Aldrich syndrome protein (N-WASP) promotes actin polymerization and ErbB2 activation leading to beta-catenin nuclear translocation, transcriptional up-regulation, and cell migration in ovarian tumor cells. The Journal of biological chemistry *282*, 1265-1280.

Brade, T., Pane, L.S., Moretti, A., Chien, K.R., and Laugwitz, K.L. (2013). Embryonic heart progenitors and cardiogenesis. Cold Spring Harb Perspect Med *3*, a013847.

Brand, T. (2003). Heart development: molecular insights into cardiac specification and early morphogenesis. Developmental biology *258*, 1-19.

Bryson-Richardson, R.J., and Currie, P.D. (2008). The genetics of vertebrate myogenesis. Nature reviews Genetics *9*, 632-646.

Buckingham, M., and Vincent, S.D. (2009). Distinct and dynamic myogenic populations in the vertebrate embryo. Current opinion in genetics & development *19*, 444-453.

Bussmann, J., Bakkers, J., and Schulte-Merker, S. (2007). Early endocardial morphogenesis requires Scl/Tal1. PLoS genetics *3*, e140.

Camenisch, T.D., Spicer, A.P., Brehm-Gibson, T., Biesterfeldt, J., Augustine, M.L., Calabro, A., Jr., Kubalak, S., Klewer, S.E., and McDonald, J.A. (2000). Disruption of hyaluronan synthase-2 abrogates normal cardiac morphogenesis and hyaluronan-mediated transformation of epithelium to mesenchyme. J Clin Invest *106*, 349-360.

Cao, X., Gao, Z., Robert, C.E., Greene, S., Xu, G., Xu, W., Bell, E., Campbell, D., Zhu, Y., Young, R., Trucco, M., Markmann, J.F., Naji, A., Wolf, B.A. (2003). Pancreatic-derived factor (FAM3B), a novel islet cytokine, induces apoptosis of insulin-secreting beta-cells. Diabetes *52*, 2296-2303.

Chang, C.P., Neilson, J.R., Bayle, J.H., Gestwicki, J.E., Kuo, A., Stankunas, K., Graef, I.A., and Crabtree, G.R. (2004). A field of myocardial-endocardial NFAT signaling underlies heart valve morphogenesis. Cell *118*, 649-663.

Charvet, B., Ruggiero, F., and Le Guellec, D. (2012). The development of the myotendinous junction. A review. Muscles, ligaments and tendons journal *2*, 53-63.

Ciruna, B., Weidinger, G., Knaut, H., Thisse, B., Thisse, C., Raz, E., and Schier, A.F. (2002). Production of maternal-zygotic mutant zebrafish by germ-line replacement. Proceedings of the National Academy of Sciences of the United States of America *99*, 14919-14924.

Crawford, B.D., Henry, C.A., Clason, T.A., Becker, A.L., and Hille, M.B. (2003). Activity and distribution of paxillin, focal adhesion kinase, and cadherin indicate cooperative roles during zebrafish morphogenesis. Molecular biology of the cell *14*, 3065-3081.

Cui, C., Cheuvront, T.J., Lansford, R.D., Moreno-Rodriguez, R.A., Schultheiss, T.M., and Rongish, B.J. (2009). Dynamic positional fate map of the primary heart-forming region. Developmental biology *332*, 212-222.

De Angelis, J.E., Lagendijk, A.K., Chen, H., Tromp, A., Bower, N.I., Tunny, K.A., Brooks, A.J., Bakkers, J., Francois, M., Yap, A.S., Simons, C., Wiking, C., Hogan, B., Smith, K. (2017). Tmem2 Regulates Embryonic Vegf Signaling by Controlling Hyaluronic Acid Turnover. Developmental cell *40*, 421.

Devoto, S.H., Melancon, E., Eisen, J.S., and Westerfield, M. (1996). Identification of separate slow and fast muscle precursor cells in vivo, prior to somite formation. Development *122*, 3371-3380.

Dunwoodie, S.L. (2007). Combinatorial signaling in the heart orchestrates cardiac induction, lineage specification and chamber formation. Seminars in cell & developmental biology *18*, 54-66.

Eisenberg, L.M., and Markwald, R.R. (1995). Molecular regulation of atrioventricular valvuloseptal morphogenesis. Circulation research *77*, 1-6.

Ekker, S.C., Ungar, A.R., Greenstein, P., von Kessler, D.P., Porter, J.A., Moon, R.T., and Beachy, P.A. (1995). Patterning activities of vertebrate hedgehog proteins in the developing eye and brain. Current biology : CB *5*, 944-955.

Ervasti, J.M., and Campbell, K.P. (1993). Dystrophin and the membrane skeleton. Current opinion in cell biology *5*, 82-87.

Erickson, S.L., O'Shea, K.S., Ghaboosi, N., Loverro, L., Frantz, G., Bauer, M., Lu, L.H., and Moore, M.W. (1997). ErbB3 is required for normal cerebellar and cardiac development: a comparison with ErbB2-and heregulin-deficient mice. Development *124*, 4999-5011.

Ervasti, J.M., and Campbell, K.P. (1993). Dystrophin and the membrane skeleton. Current opinion in cell biology *5*, 82-87.

Evans, S.M., Yelon, D., Conlon, F.L., and Kirby, M.L. (2010). Myocardial lineage development. Circulation research *107*, 1428-1444.

Evensen, N.A., Kuscu, C., Nguyen, H.L., Zarrabi, K., Dufour, A., Kadam, P., Hu, Y.J., Pulkoski-Gross, A., Bahou, W.F., Zucker, S., Cao, J. (2013). Unraveling the role of KIAA1199, a novel endoplasmic reticulum protein, in cancer cell migration. Journal of the National Cancer Institute *105*, 1402-1416.

Fishman, M.C., and Chien, K.R. (1997). Fashioning the vertebrate heart: earliest embryonic decisions. Development *124*, 2099-2117.

Fodde, R., Kuipers, J., Rosenberg, C., Smits, R., Kielman, M., Gaspar, C., van Es, J.H., Breukel, C., Wiegant, J., Giles, R.H., Clevers, H. (2001). Mutations in the APC tumour suppressor gene cause chromosomal instability. Nature cell biology *3*, 433-438.

Garavito-Aguilar, Z.V., Riley, H.E., and Yelon, D. (2010). Hand2 ensures an appropriate environment for cardiac fusion by limiting Fibronectin function. Development *137*, 3215-3220.

Garriock, R.J., D'Agostino, S.L., Pilcher, K.C., and Krieg, P.A. (2005). Wnt11-R, a protein closely related to mammalian Wnt11, is required for heart morphogenesis in Xenopus. Developmental biology *279*, 179-192.

Gee, S.H., Montanaro, F., Lindenbaum, M.H., and Carbonetto, S. (1994). Dystroglycan-alpha, a dystrophin-associated glycoprotein, is a functional agrin receptor. Cell *77*, 675-686.

George, E.L., Baldwin, H.S., and Hynes, R.O. (1997). Fibronectins are essential for heart and blood vessel morphogenesis but are dispensable for initial specification of precursor cells. Blood *90*, 3073-3081.

Gibbs, E.M., Horstick, E.J., and Dowling, J.J. (2013). Swimming into prominence: the zebrafish as a valuable tool for studying human myopathies and muscular dystrophies. The FEBS journal *280*, 4187-4197.

Gillies, A.R., and Lieber, R.L. (2011). Structure and function of the skeletal muscle extracellular matrix. Muscle & nerve *44*, 318-331.

Glickman, N.S., and Yelon, D. (2002). Cardiac development in zebrafish: coordination of form and function. Seminars in cell & developmental biology *13*, 507-513.

Godfrey, C., Foley, A.R., Clement, E., and Muntoni, F. (2011). Dystroglycanopathies: coming into focus. Current opinion in genetics & development *21*, 278-285.

Goody, M.F., Kelly, M.W., Lessard, K.N., Khalil, A., and Henry, C.A. (2010). Nrk2b-mediated NAD+ production regulates cell adhesion and is required for muscle morphogenesis in vivo: Nrk2b and NAD+ in muscle morphogenesis. Developmental biology *344*, 809-826.

Goody, M.F., Kelly, M.W., Reynolds, C.J., Khalil, A., Crawford, B.D., and Henry, C.A. (2012). NAD+ biosynthesis ameliorates a zebrafish model of muscular dystrophy. PLoS biology *10*, e1001409.

Goody, M.F., Sher, R.B., and Henry, C.A. (2015). Hanging on for the ride: adhesion to the extracellular matrix mediates cellular responses in skeletal muscle morphogenesis and disease. Developmental biology *401*, 75-91.

Gros, J., Scaal, M., and Marcelle, C. (2004). A two-step mechanism for myotome formation in chick. Developmental cell *6*, 875-882.

Gupta, V.A., Kawahara, G., Myers, J.A., Chen, A.T., Hall, T.E., Manzini, M.C., Currie, P.D., Zhou, Y., Zon, L.I., Kunkel, L.M., Beggs, A. (2012). A splice site mutation in laminin-alpha2 results in a severe muscular dystrophy and growth abnormalities in zebrafish. PLoS One *7*, e43794.

Habets, P.E., Moorman, A.F., Clout, D.E., van Roon, M.A., Lingbeek, M., van Lohuizen, M., Campione, M., and Christoffels, V.M. (2002). Cooperative action of Tbx2 and Nkx2.5 inhibits ANF expression in the atrioventricular canal: implications for cardiac chamber formation. Genes & development *16*, 1234-1246.

Hall, T.E., Bryson-Richardson, R.J., Berger, S., Jacoby, A.S., Cole, N.J., Hollway, G.E., Berger, J., and Currie, P.D. (2007). The zebrafish candyfloss mutant implicates extracellular matrix adhesion failure in laminin alpha2-deficient congenital muscular dystrophy. Proceedings of the National Academy of Sciences of the United States of America *104*, 7092-7097.

Harrelson, Z., Kelly, R.G., Goldin, S.N., Gibson-Brown, J.J., Bollag, R.J., Silver, L.M., and Papaioannou, V.E. (2004). Tbx2 is essential for patterning the atrioventricular canal and for morphogenesis of the outflow tract during heart development. Development *131*, 5041-5052.

Harvey, R.P. (2002). Patterning the vertebrate heart. Nature reviews Genetics *3*, 544-556.

He, Q.Y., Liu, X.H., Li, Q., Studholme, D.J., Li, X.W., and Liang, S.P. (2006). G8: a novel domain associated with polycystic kidney disease and non-syndromic hearing loss. Bioinformatics *22*, 2189-2191.

Henrissat, B., Heffron, S.E., Yoder, M.D., Lietzke, S.E., and Jurnak, F. (1995). Functional implications of structure-based sequence alignment of proteins in the extracellular pectate lyase superfamily. Plant Physiol *107*, 963-976.

Henry, C.A., and Amacher, S.L. (2004). Zebrafish slow muscle cell migration induces a wave of fast muscle morphogenesis. Developmental cell *7*, 917-923.

Henry, C.A., McNulty, I.M., Durst, W.A., Munchel, S.E., and Amacher, S.L. (2005). Interactions between muscle fibers and segment boundaries in zebrafish. Developmental biology *287*, 346-360.

Holt, K.H., Crosbie, R.H., Venzke, D.P., and Campbell, K.P. (2000). Biosynthesis of dystroglycan: processing of a precursor propeptide. FEBS letters *468*, 79-83.

Holtzman, N.G., Schoenebeck, J.J., Tsai, H.J., and Yelon, D. (2007). Endocardium is necessary for cardiomyocyte movement during heart tube assembly. Development *134*, 2379-2386.

Hori, Y.S., Kuno, A., Hosoda, R., Tanno, M., Miura, T., Shimamoto, K., and Horio, Y. (2011). Resveratrol ameliorates muscular pathology in the dystrophic mdx mouse, a model for Duchenne muscular dystrophy. The Journal of pharmacology and experimental therapeutics *338*, 784-794.

Hu, N., Sedmera, D., Yost, H.J., and Clark, E.B. (2000). Structure and function of the developing zebrafish heart. The Anatomical record *260*, 148-157.

Hurlstone, A.F., Haramis, A.P., Wienholds, E., Begthel, H., Korving, J., Van Eeden, F., Cuppen, E., Zivkovic, D., Plasterk, R.H., and Clevers, H. (2003). The Wnt/beta-catenin pathway regulates cardiac valve formation. Nature *425*, 633-637.

Ibraghimov-Beskrovnaya, O., Ervasti, J.M., Leveille, C.J., Slaughter, C.A., Sernett, S.W., and Campbell, K.P. (1992). Primary structure of dystrophin-associated glycoproteins linking dystrophin to the extracellular matrix. Nature *355*, 696-702.

Inamori, K., Yoshida-Moriguchi, T., Hara, Y., Anderson, M.E., Yu, L., and Campbell, K.P. (2012). Dystroglycan function requires xylosyl- and glucuronyltransferase activities of LARGE. Science *335*, 93-96.

Itano, N. (2008). Simple primary structure, complex turnover regulation and multiple roles of hyaluronan. Journal of biochemistry *144*, 131-137.

Jackson, H.E., and Ingham, P.W. (2013). Control of muscle fibre-type diversity during embryonic development: the zebrafish paradigm. Mechanisms of development *130*, 447-457.

Jacoby, A.S., Busch-Nentwich, E., Bryson-Richardson, R.J., Hall, T.E., Berger, J., Berger, S., Sonntag, C., Sachs, C., Geisler, R., Stemple, D.L., Currie, P.D. (2009). The zebrafish dystrophic mutant softy maintains muscle fibre viability despite basement membrane rupture and muscle detachment. Development *136*, 3367-3376.

Jenkins, M.H., Alrowaished, S.S., Goody, M.F., Crawford, B.D., and Henry, C.A. (2016). Laminin and Matrix metalloproteinase 11 regulate Fibronectin levels in the zebrafish myotendinous junction. Skeletal muscle *6*, 18.

Jiang, D., Liang, J., Fan, J., Yu, S., Chen, S., Luo, Y., Prestwich, G.D., Mascarenhas, M.M., Garg, H.G., Quinn, D.A., Homer, R.J., Goldstein, D.R., Bucala, R., Lee, P.J., Medzhitov, R., Noble, P.W. (2005). Regulation of lung injury and repair by Toll-like receptors and hyaluronan. Nature medicine *11*, 1173-1179.

Jing, S.Q., Spencer, T., Miller, K., Hopkins, C., and Trowbridge, I.S. (1990). Role of the human transferrin receptor cytoplasmic domain in endocytosis: localization of a specific signal sequence for internalization. The Journal of cell biology *110*, 283-294.

Johansson, P., Bernstrom, J., Gorman, T., Oster, L., Backstrom, S., Schweikart, F., Xu, B., Xue, Y., and Schiavone, L.H. (2013). FAM3B PANDER and FAM3C ILEI represent a distinct class of signaling molecules with a non-cytokine-like fold. Structure *21*, 306-313.

Julich, D., Geisler, R., Holley, S.A., and Tubingen Screen, C. (2005). Integrinalpha5 and delta/notch signaling have complementary spatiotemporal requirements during zebrafish somitogenesis. Developmental cell *8*, 575-586.

Julich, D., Mould, A.P., Koper, E., and Holley, S.A. (2009). Control of extracellular matrix assembly along tissue boundaries via Integrin and Eph/Ephrin signaling. Development *136*, 2913-2921.

Julich, D., Cobb, G., Melo, A.M., McMillen, P., Lawton, A.K., Mochrie, S.G., Rhoades, E., and Holley, S.A. (2015). Cross-Scale Integrin Regulation Organizes ECM and Tissue Topology. Developmental cell *34*, 33-44.

Kanagawa, M., Michele, D.E., Satz, J.S., Barresi, R., Kusano, H., Sasaki, T., Timpl, R., Henry, M.D., and Campbell, K.P. (2005). Disruption of perlecan binding and matrix assembly by post-translational or genetic disruption of dystroglycan function. FEBS letters *579*, 4792-4796.

Kawahara, A., Nishi, T., Hisano, Y., Fukui, H., Yamaguchi, A., and Mochizuki, N. (2009). The sphingolipid transporter spns2 functions in migration of zebrafish myocardial precursors. Science *323*, 524-527.

Kawahara, G., Guyon, J.R., Nakamura, Y., and Kunkel, L.M. (2010). Zebrafish models for human FKRP muscular dystrophies. Human molecular genetics *19*, 623-633.

Kikuchi, Y., Agathon, A., Alexander, J., Thisse, C., Waldron, S., Yelon, D., Thisse, B., and Stainier, D.Y. (2001). casanova encodes a novel Sox-related protein necessary and sufficient for early endoderm formation in zebrafish. Genes & development *15*, 1493-1505.

Kirschner, J. (2013). Congenital muscular dystrophies. Handbook of clinical neurology *113*, 1377-1385.

Kupperman, E., An, S., Osborne, N., Waldron, S., and Stainier, D.Y. (2000). A sphingosine-1-phosphate receptor regulates cell migration during vertebrate heart development. Nature *406*, 192-195.

Lackner, S., Schwendinger-Schreck, J., Julich, D., and Holley, S.A. (2013). Segmental assembly of fibronectin matrix requires rap1b and integrin alpha5. Developmental dynamics : an official publication of the American Association of Anatomists *242*, 122-131.

Lagendijk, A.K., Goumans, M.J., Burkhard, S.B., and Bakkers, J. (2011). MicroRNA-23 restricts cardiac valve formation by inhibiting Has2 and extracellular hyaluronic acid production. Circulation research *109*, 649-657.

Larson, J.D., Wadman, S.A., Chen, E., Kerley, L., Clark, K.J., Eide, M., Lippert, S., Nasevicius, A., Ekker, S.C., Hackett, P.B., Essner, J.J. (2004). Expression of VE-cadherin in zebrafish embryos: a new tool to evaluate vascular development. Developmental dynamics : an official publication of the American Association of Anatomists *231*, 204-213.

Lewis, K.E., Currie, P.D., Roy, S., Schauerte, H., Haffter, P., and Ingham, P.W. (1999). Control of muscle cell-type specification in the zebrafish embryo by Hedgehog signalling. Developmental biology *216*, 469-480.

Li, S., Zhou, D., Lu, M.M., and Morrisey, E.E. (2004). Advanced cardiac morphogenesis does not require heart tube fusion. Science *305*, 1619-1622.

Liebner, S., Cattelino, A., Gallini, R., Rudini, N., Iurlaro, M., Piccolo, S., and Dejana, E. (2004). Beta-catenin is required for endothelial-mesenchymal transformation during heart cushion development in the mouse. The Journal of cell biology *166*, 359-367.

Lin, Y.Y., White, R.J., Torelli, S., Cirak, S., Muntoni, F., and Stemple, D.L. (2011). Zebrafish Fukutin family proteins link the unfolded protein response with dystroglycanopathies. Human molecular genetics *20*, 1763-1775.

Linask, K.K., and Lash, J.W. (1988). A role for fibronectin in the migration of avian precardiac cells. II. Rotation of the heart-forming region during different stages and its effects. Developmental biology *129*, 324-329.

Lunardi, A., and Dente, L. (2002). Molecular cloning and expression analysis of dystroglycan during Xenopus laevis embryogenesis. Mechanisms of development *119 Suppl 1*, S49-54.

Mao, B., Wu, W., Li, Y., Hoppe, D., Stannek, P., Glinka, A., and Niehrs, C. (2001a). LDL-receptor-related protein 6 is a receptor for Dickkopf proteins. Nature *411*, 321-325.

Mao, J., Wang, J., Liu, B., Pan, W., Farr, G.H., 3rd, Flynn, C., Yuan, H., Takada, S., Kimelman, D., Li, L., Wu, D. (2001b). Low-density lipoprotein receptor-related protein-5 binds to Axin and regulates the canonical Wnt signaling pathway. Molecular cell *7*, 801-809.

Markwald, R.R., Fitzharris, T.P., and Manasek, F.J. (1977). Structural development of endocardial cushions. Am J Anat *148*, 85-119.

Mayans, O., Scott, M., Connerton, I., Gravesen, T., Benen, J., Visser, J., Pickersgill, R., and Jenkins, J. (1997). Two crystal structures of pectin lyase A from Aspergillus reveal a pH driven conformational change and striking divergence in the substrate-binding clefts of pectin and pectate lyases. Structure *5*, 677-689.

McEwen, D.G., and Peifer, M. (2000). Wnt signaling: Moving in a new direction. Current biology : CB *10*, R562-564.

Mendelson, K., Lan, Y., Hla, T., and Evans, T. (2015). Maternal or zygotic sphingosine kinase is required to regulate zebrafish cardiogenesis. Developmental dynamics : an official publication of the American Association of Anatomists *244*, 948-954.

Michele, D.E., Barresi, R., Kanagawa, M., Saito, F., Cohn, R.D., Satz, J.S., Dollar, J., Nishino, I., Kelley, R.I., Somer, H., Straub, V., Mathews, K.D., Moore, S.A., Campbell, K.P. (2002). Post-translational disruption of dystroglycan-ligand interactions in congenital muscular dystrophies. Nature *418*, 417-422.

Miquerol, L., and Kelly, R.G. (2013). Organogenesis of the vertebrate heart. Wiley Interdiscip Rev Dev Biol *2*, 17-29.

Molkentin, J.D., Lin, Q., Duncan, S.A., and Olson, E.N. (1997). Requirement of the transcription factor GATA4 for heart tube formation and ventral morphogenesis. Genes & development *11*, 1061-1072.

Moore, C.J., and Winder, S.J. (2012). The inside and out of dystroglycan post-translational modification. Neuromuscular disorders : NMD *22*, 959-965.

Moorman, A.F., and Christoffels, V.M. (2003). Cardiac chamber formation: development, genes, and evolution. Physiol Rev *83*, 1223-1267.

Moreau, N., Alfandari, D., Gaultier, A., Cousin, H., and Darribere, T. (2003). Cloning and expression patterns of dystroglycan during the early development of Xenopus laevis. Development genes and evolution *213*, 355-359.

Moreno-Rodriguez, R.A., Krug, E.L., Reyes, L., Villavicencio, L., Mjaatvedt, C.H., and Markwald, R.R. (2006). Bidirectional fusion of the heart-forming fields in the developing chick embryo. Developmental dynamics : an official publication of the American Association of Anatomists *235*, 191-202.

Moro, E., Ozhan-Kizil, G., Mongera, A., Beis, D., Wierzbicki, C., Young, R.M., Bournele, D., Domenichini, A., Valdivia, L.E., Lum, L., Chen, C., Amatruda, J.F., Tiso, N., Weidinger, G., Argenton, F. (2012). In vivo Wnt signaling tracing through a transgenic biosensor fish reveals novel activity domains. Developmental biology *366*, 327-340.

Muntoni, F., Torelli, S., and Brockington, M. (2008). Muscular dystrophies due to glycosylation defects. Neurotherapeutics : the journal of the American Society for Experimental NeuroTherapeutics *5*, 627-632.

Nelson, W.J., and Nusse, R. (2004). Convergence of Wnt, beta-catenin, and cadherin pathways. Science *303*, 1483-1487.

Nord, H., Burguiere, A.C., Muck, J., Nord, C., Ahlgren, U., and von Hofsten, J. (2014). Differential regulation of myosin heavy chains defines new muscle domains in zebrafish. Molecular biology of the cell *25*, 1384-1395.

Osborne, N., Brand-Arzamendi, K., Ober, E.A., Jin, S.W., Verkade, H., Holtzman, N.G., Yelon, D., and Stainier, D.Y. (2008). The spinster homolog, two of hearts, is required for sphingosine 1-phosphate signaling in zebrafish. Current biology : CB *18*, 1882-1888.

Pandur, P., Lasche, M., Eisenberg, L.M., and Kuhl, M. (2002). Wnt-11 activation of a non-canonical Wnt signalling pathway is required for cardiogenesis. Nature *418*, 636-641.

Parsons, M.J., Campos, I., Hirst, E.M., and Stemple, D.L. (2002a). Removal of dystroglycan causes severe muscular dystrophy in zebrafish embryos. Development *129*, 3505-3512.

Parsons, M.J., Pollard, S.M., Saude, L., Feldman, B., Coutinho, P., Hirst, E.M., and Stemple, D.L. (2002b). Zebrafish mutants identify an essential role for laminins in notochord formation. Development *129*, 3137-3146.

Peal, D.S., Burns, C.G., Macrae, C.A., and Milan, D. (2009). Chondroitin sulfate expression is required for cardiac atrioventricular canal formation. Developmental dynamics : an official publication of the American Association of Anatomists *238*, 3103-3110.

Pereira, N.A., Pu, H.X., Goh, H., and Song, Z. (2014). Golgi phosphoprotein 3 mediates the Golgi localization and function of protein O-linked mannose beta-1,2-N-acetlyglucosaminyltransferase 1. The Journal of biological chemistry *289*, 14762-14770.

Ragkousi, K., Beh, J., Sweeney, S., Starobinska, E., and Davidson, B. (2011). A single GATA factor plays discrete, lineage specific roles in ascidian heart development. Developmental biology *352*, 154-163.

Rampoldi, E., Meola, G., Conti, A.M., Velicogna, M., and Larizza, L. (1986). A comparative analysis of collagen III, IV, laminin and fibronectin in Duchenne muscular dystrophy biopsies and cell cultures. European journal of cell biology *42*, 27-34.

Rodgers, L.S., Lalani, S., Hardy, K.M., Xiang, X., Broka, D., Antin, P.B., and Camenisch, T.D. (2006). Depolymerized hyaluronan induces vascular endothelial growth factor, a negative regulator of developmental epithelial-to-mesenchymal transformation. Circulation research *99*, 583-589.

Runyan, R.B., and Markwald, R.R. (1983). Invasion of mesenchyme into three-dimensional collagen gels: a regional and temporal analysis of interaction in embryonic heart tissue. Developmental biology *95*, 108-114.

Ryckebusch, L., Hernandez, L., Wang, C., Phan, J., and Yelon, D. (2016). Tmem2 regulates cell-matrix interactions that are essential for muscle fiber attachment. Development *143*, 2965-2972.

Schauerte, H.E., van Eeden, F.J., Fricke, C., Odenthal, J., Strahle, U., and Haffter, P. (1998). Sonic hedgehog is not required for the induction of medial floor plate cells in the zebrafish. Development *125*, 2983-2993.

Schleich, J.M., Abdulla, T., Summers, R., and Houyel, L. (2013). An overview of cardiac morphogenesis. Arch Cardiovasc Dis *106*, 612-623.

Schoenebeck, J.J., and Yelon, D. (2007). Illuminating cardiac development: Advances in imaging add new dimensions to the utility of zebrafish genetics. Seminars in cell & developmental biology *18*, 27-35.

Schofield, J.N., Gorecki, D.C., Blake, D.J., Davies, K., and Edwards, Y.H. (1995). Dystroglycan mRNA expression during normal and mdx mouse embryogenesis: a comparison with utrophin and the apo-dystrophins. Developmental dynamics : an official publication of the American Association of Anatomists *204*, 178-185.

Schroeder, J.A., Jackson, L.F., Lee, D.C., and Camenisch, T.D. (2003). Form and function of developing heart valves: coordination by extracellular matrix and growth factor signaling. Journal of molecular medicine *81*, 392-403.

Sciandra, F., Bozzi, M., Bigotti, M.G., and Brancaccio, A. (2013). The multiple affinities of alpha-dystroglycan. Current protein & peptide science *14*, 626-634.

Shirai, M., Imanaka-Yoshida, K., Schneider, M.D., Schwartz, R.J., and Morisaki, T. (2009). T-box 2, a mediator of Bmp-Smad signaling, induced hyaluronan synthase 2 and Tgfbeta2 expression and endocardial cushion formation. Proceedings of the National Academy of Sciences of the United States of America *106*, 18604-18609.

Shostak, K., Zhang, X., Hubert, P., Goktuna, S.I., Jiang, Z., Klevernic, I., Hildebrand, J., Roncarati, P., Hennuy, B., Ladang, A., Somja, J., Gothot, A., Close, P., Delvenne, P., Chariot, A. (2014). NF-kappaB-induced KIAA1199 promotes survival through EGFR signalling. Nature communications *5*, 5232.

Smith, K.A., Lagendijk, A.K., Courtney, A.D., Chen, H., Paterson, S., Hogan, B.M., Wicking, C., and Bakkers, J. (2011). Transmembrane protein 2 (Tmem2) is required to regionally restrict atrioventricular canal boundary and endocardial cushion development. Development *138*, 4193-4198.

Snow, C.J., Goody, M., Kelly, M.W., Oster, E.C., Jones, R., Khalil, A., and Henry, C.A. (2008a). Time-lapse analysis and mathematical characterization elucidate novel mechanisms underlying muscle morphogenesis. PLoS genetics *4*, e1000219.

Snow, C.J., and Henry, C.A. (2009). Dynamic formation of microenvironments at the myotendinous junction correlates with muscle fiber morphogenesis in zebrafish. Gene expression patterns : GEP *9*, 37-42.

Snow, C.J., Peterson, M.T., Khalil, A., and Henry, C.A. (2008b). Muscle development is disrupted in zebrafish embryos deficient for fibronectin. Developmental dynamics : an official publication of the American Association of Anatomists *237*, 2542-2553.

Song, W.K., Wang, W., Foster, R.F., Bielser, D.A., and Kaufman, S.J. (1992). H36-alpha 7 is a novel integrin alpha chain that is developmentally regulated during skeletal myogenesis. The Journal of cell biology *117*, 643-657.

Staal, F.J., and Clevers, H.C. (2005). WNT signalling and haematopoiesis: a WNT-WNT situation. Nature reviews Immunology *5*, 21-30.

Stemple, D.L. (2005). Structure and function of the notochord: an essential organ for chordate development. Development *132*, 2503-2512.

Tamai, K., Semenov, M., Kato, Y., Spokony, R., Liu, C., Katsuyama, Y., Hess, F., Saint-Jeannet, J.P., and He, X. (2000). LDL-receptor-related proteins in Wnt signal transduction. Nature *407*, 530-535.

Termeer, C., Benedix, F., Sleeman, J., Fieber, C., Voith, U., Ahrens, T., Miyake, K., Freudenberg, M., Galanos, C., and Simon, J.C. (2002). Oligosaccharides of Hyaluronan activate dendritic cells via toll-like receptor 4. The Journal of experimental medicine *195*, 99-111.

Thorsteinsdottir, S., Deries, M., Cachaco, A.S., and Bajanca, F. (2011). The extracellular matrix dimension of skeletal muscle development. Developmental biology *354*, 191-207.

Toole, B.P. (2004). Hyaluronan: from extracellular glue to pericellular cue. Nature reviews Cancer *4*, 528-539.

Totong, R., Schell, T., Lescroart, F., Ryckebusch, L., Lin, Y.F., Zygmunt, T., Herwig, L., Krudewig, A., Gershoony, D., Belting, H.G., Affolter, M., Torres-Vazquez, J., Yelon, D. (2011). The novel transmembrane protein Tmem2 is essential for coordination of myocardial and endocardial morphogenesis. Development *138*, 4199-4205.

Trinh, L.A., and Stainier, D.Y. (2004). Fibronectin regulates epithelial organization during myocardial migration in zebrafish. Developmental cell *6*, 371-382.

Trinh, L.A., Yelon, D., and Stainier, D.Y. (2005). Hand2 regulates epithelial formation during myocardial diferentiation. Current biology : CB *15*, 441-446.

Valiente-Alandi, I., Schafer, A.E., and Blaxall, B.C. (2016). Extracellular matrix-mediated cellular communication in the heart. Journal of molecular and cellular cardiology *91*, 228-237.

van Eeden, F.J., Granato, M., Schach, U., Brand, M., Furutani-Seiki, M., Haffter, P., Hammerschmidt, M., Heisenberg, C.P., Jiang, Y.J., Kane, D.A., Kelsh, R.N., Mullins, M.C., Odenthal, J., Warga, R.M., Allende, M.L., Weinberg, E.S., Nusslein-Volhard, C. (1996). Mutations affecting somite formation and patterning in the zebrafish, Danio rerio. Development *123*, 153-164.

Varner, V.D., and Taber, L.A. (2012). Not just inductive: a crucial mechanical role for the endoderm during heart tube assembly. Development *139*, 1680-1690.

Verhoeven, M.C., Haase, C., Christoffels, V.M., Weidinger, G., and Bakkers, J. (2011). Wnt signaling regulates atrioventricular canal formation upstream of BMP and Tbx2. Birth Defects Res A Clin Mol Teratol *91*, 435-440.

Walsh, E.C., and Stainier, D.Y. (2001). UDP-glucose dehydrogenase required for cardiac valve formation in zebrafish. Science *293*, 1670-1673.

Wells, L. (2013). The o-mannosylation pathway: glycosyltransferases and proteins implicated in congenital muscular dystrophy. The Journal of biological chemistry *288*, 6930-6935.

Xie, H., Ye, D., Sepich, D., and Lin, F. (2016). S1pr2/Galpha13 signaling regulates the migration of endocardial precursors by controlling endoderm convergence. Developmental biology *414*, 228-243.

Yamada, H., Shimizu, T., Tanaka, T., Campbell, K.P., and Matsumura, K. (1994). Dystroglycan is a binding protein of laminin and merosin in peripheral nerve. FEBS letters *352*, 49-53.

Yamamoto, H., Tobisawa, Y., Inubushi, T., Irie, F., Oyama, C., and Yamaguchi, Y. (2017). A Mammalian Homolog of the Zebrafish Transmembrane Protein 2 (TMEM2) Is the Long-sought-after Cell Surface Hyaluronidase. The Journal of biological chemistry.

Ye, D., and Lin, F. (2013). S1pr2/Galpha13 signaling controls myocardial migration by regulating endoderm convergence. Development *140*, 789-799.

Ye, D., Xie, H., Hu, B., and Lin, F. (2015). Endoderm convergence controls subduction of the myocardial precursors during heart-tube formation. Development *142*, 2928-2940.

Yelon, D., Horne, S.A., and Stainier, D.Y. (1999). Restricted expression of cardiac myosin genes reveals regulated aspects of heart tube assembly in zebrafish. Developmental biology *214*, 23-37.

Yelon, D., Ticho, B., Halpern, M.E., Ruvinsky, I., Ho, R.K., Silver, L.M., and Stainier, D.Y. (2000). The bHLH transcription factor hand2 plays parallel roles in zebrafish heart and pectoral fin development. Development *127*, 2573-2582.

Yoshida, H., Nagaoka, A., Kusaka-Kikushima, A., Tobiishi, M., Kawabata, K., Sayo, T., Sakai, S., Sugiyama, Y., Enomoto, H., Okada, Y., Inoue, S. (2013). KIAA1199, a deafness gene of unknown function, is a new hyaluronan binding protein involved in hyaluronan depolymerization. Proceedings of the National Academy of Sciences of the United States of America *110*, 5612-5617.

Zacharias, U., Purfurst, B., Schowel, V., Morano, I., Spuler, S., and Haase, H. (2011). Ahnak1 abnormally localizes in muscular dystrophies and contributes to muscle vesicle release. Journal of muscle research and cell motility *32*, 271-280.